University of BRISTOL

NRC

IAC

Welcome

On behalf of the Bristol-Oxford Nuclear Research Centre (NRC), I would like to warmly welcome you to the vibrant city of Bristol for the 42èmes Journées des Actinides (JdA) conference. Continuing the long tradition of the JdA we sincerely hope that you will enjoy the conference and take time to explore the historic dockside and sample our famous West Country cider!

Bristol is an academic centre of expertise for research on actinide materials and, given the current UK nuclear renaissance, the University and wider city is ideally situated to provide the role of a nuclear research hub, surrounded regionally by nuclear sites, companies and regulatory bodies. Correspondingly, a key objective for the Bristol-Oxford NRC is to build upon existing collaborative relationships with other research bodies and companies, home and abroad, to become an internationally recognised flagship for nuclear research. We sincerely hope that this year's JdA will prove fruitful for instigating new research collaborations and reaffirming existing partnerships.

In such a busy year for nuclear conferences we would also like to thank you for supporting the JDA.

Best wishes for an enjoyable conference.

Dr Thomas Scott
University of Bristol

JdA School

All activity in the NSQI unless stated otherwise

Monday 16th	Activity
09.00 - 10.00	Registration and refreshments
10.00 - 11.30	School overview: Introduction to the nuclear fuel cycle **T Scott (University of Bristol)**
11.30 - 13.00	Nuclear fuels and cladding corrosion **C Younes (University of Bristol)**
13.00 - 14.00	Lunch break
14.00 - 15.30	Geological disposal of nuclear waste **C Padovani (Nuclear Decommissioning Authority)**
15.30 - 17.00	Actinides in the environment **T Scott (University of Bristol)**
17.00 - onwards	Refreshments and socialising

Tuesday 17th	Activity
09.00 - 12.00	Actinide physics **R Springell (University of Bristol)**
12.00 - 13.00	Actinide modelling **A Willetts (Atomic Weapons Establishment)**
13.00 - 14.00	Lunch break
14.00 - 15.00	Radiation damage modelling **N Allan (University of Bristol)**
15.00 - 17.00	The UK nuclear renaissance - how is it going? **W Nuttall (University of Cambridge)** Old Council Chamber, Wills Memorial Building
17.00 - onwards	Refreshments and socialising Old Council Chamber, Wills Memorial Building

Wednesday 18th	Activity
09.00 - 17.00	UK nuclear scoping workshop
09.00 - 11.00	Uranium oxide physiochemistry *Parallel School session to UK workshop **G Allen (University of Bristol)**
11.00 - 15.00 Including 'working' lunch	New aspects in nuclear forensics *Parallel School session to UK workshop Aerial radiological event monitoring First responders in radiological events An experimental study of indoor dispersion of radioactive material Outdoor dispersion of radioactive material (radiological terrorism study) **I Halevy (Nuclear Research Center - Negev)** Analytical techniques for nuclear safeguards **A Pidduck (Atomic Weapons Establishment)**
15.00 - 17.00	Surface and materials analysis of nuclear materials (including laboratory tour/demonstration) *Parallel School session to UK workshop **P Heard, C Jones (University of Bristol**
17.00 - 17.30	Closing address **T Scott (University of Bristol)**
17.30 - 18.00	Break
18.00 - 19.00	JdA registration M-Shed
19.00 - 22.00	Welcome party M-Shed

JdA Conference

All activity in the M-Shed unless stated otherwise

Wednesday 18th	Activity
18.00 - 19.00	JdA registration
19.00 - 22.00	Welcome party

Thursday 19th	Activity
09.00 - 09.30	Refreshments
	Introduction
09.30 - 09.35	Welcome and housekeeping **T Scott**
09.35 - 09.55	Bristol-Oxford Nuclear Research Centre **D Smith**
	Physics 1
09.55 - 10.20	Variations of actinide magnetism in uranium-base hydrides **A Adamska, L Havela, A Andreev, Y Skourski**
10.20 - 10.45	Magnetic properties of epitaxial UO_2 thin films **Z Bao, R Springell, R Caciuffo, T Gouder, S Langridge, G Nisbet, G Lander**
10.45 - 11.05	Refreshments
	Materials
11.05 - 11.30	Modelling of uranium hydride reaction site initiation **J Glascott, J Petherbridge, S Bazley, T Scott, C Jones**
11.30 - 11.55	Controlled conversion of uranium carbide fission targets using water vapour **T Scott, N Harker, C Jones,K Hallam, P Heard, R Catherall**
11.55 - 12.20	Preparation and characterisation of thin actinide layers **G Sibbens, A Moens, R Eykens, D Vanleeuw**
12.20 - 12.45	Corrosion of uranium in mixed environments of water vapour and oxygen **N Harker, T Scott, C Jones, P Heard, K Hallam, J Petherbridge, J Glascott**
12.45 - 13.10	Investigation of oxide growth and structure on the surface of uranium **C Jones, T Scott, P Heard, K Hallam, J Petherbridge, J Glascott**
13.10 - 14.10	Lunch break
	Physics 2
14.10 - 14.35	Magnetic and electronic properties of NpCoGe **E Colineau, R Eloirdi, J-C Griveau, P Gaczynski, A Shick**
14.33 - 15.00	Studies on the UFe_3B_2 uranium boride **A Gonçalves, M Dias, P Carvalho, L Pereira, I Santos, O Tougait, V Tran**
15.00 - 15.25	Crystal structure and physical properties of RBeGe (R = La-Nd, Th, U) **R Gumeniuk, A Leithe-Jasper, H Borrmann, U Burkhardt, W Schnelle, Yu Grin**
15.25 - 15.45	Refreshments
	Oral presentations of posters
15.45 - 17.15	A series of five minute presentations of each poster
17.15 - 19.00	Break
19.00 - 22.00	Poster session with refreshments

Friday 20th	Activity
09.00 - 09.30	Refreshments
	Physics 3
09.30 - 09.55	Strengthening of magnetic interactions in UGa_2 under pressure **L Havela, A Kolomiets, J Prchal, A Andreev**
09.55 - 10.20	Progress in the magnetic study of Np_2Co_{17} **A Hen, I Halevy, I Orion, E Colineau, R Eloirdi, J-C Griveau, P Gaczyński, F Wilhelm, A Rogalev, J-P Sanchez, M Winterrose, N Magnani, A Shick, R Caciuffo**
10.20 - 10.45	Progress in the magnetic study of Np_2Ni_{17} and $NpNi_5$ **I Halevy, A Hen, I Orion, E Colineau, R Eloirdi, J-C Griveau, P Gaczyński, M Winterrose, N Magnani, A Shick, R Caciuffo**
10.45 - 11.05	Refreshments
	Chemistry
11.05 - 11.30	Actinide-ligand multiple bond linkages: Recent progress in uranium carbene and nitride chemistry **S Liddle**
11.30 - 11.55	Polymorphism in salts of tetraalkylammoniumhexanitratothorium **G Soldani, C Renard, S Grandjean, E Welcomme, F Abraham**
11.55 - 12.20	Sorption preconcentration of radionuclides using detonation nanodiamonds **Y Buchatskaya, A Romanchuk, A Shiryaev, I Kulakova, S Kalmykov**
12.20 - 12.45	Nanoscale zero-valent iron particles for the remediation of uranium contaminated groundwater **R Crane, I-C Popescu, K Hallam, T Scott**
12.45 - 13.10	New ammonium thorium oxalates **F Blanchard, M Rivenet, N Vigier, I Hablot, S Grandjean, F Abraham**
13.10 - 14.10	Lunch break
	Physics 4
14.10 - 14.35	Superconductivity in the cubic γ-phase uranium molybdenum alloys synthesised by ultrafast cooling **I Tkach, N-TH Kim-Ngan, S Mašková, L Havela, A Warren, C Stitt, T Scott**
14.35 - 15.00	Development of new generation of radio-luminescence emitters based on durable actinide-doped crystals **J Ipatova, B Burakov, M Petrova, V Zirlin, Y Kuznetsova, M Zamoryanskaya**
15.00 - 15.25	Time-resolved laser induced chemiluminescence spectroscopy and detection of actinides in solutions **I Izosimov, N Gorshkov, V Mikhalev, S Nekhoroshkov, Yu Trifonov, N Firsin**
15.25 - 15.45	Refreshments
	Fuels
15.45 - 16.35	Plenary lecture **G Allen**
16.35 - 17.00	Stabilisation of cubic γ-phase uranium molybdenum alloys by splat-cooling technique **N-T Kim-Ngan, I Tkach, S Mašková, L Havela, A Warren, C Stitt, T Scott**
17.00 - 17.25	Thermodynamic investigations of the $(Th, U)O_2$ solid solution **O Vălu, O Beneš, R Konings**
17.25 - 17.50	The study of thermal cycling effect on the stability of a δ-stabilised Pu-Ga alloy **M Ling**
17.50 - 19.00	Break
19.00 - 23.00	Conference dinner SS Great Britain

Saturday 21st	**Activity**
09.00 - 09.30	Refreshments
	Forensics
09.30 - 09.55	New aspects in nuclear forensics **I Halevy, A Hen, A Sharon**
09.55 - 10.20	Nuclear forensics analytical approaches and simulations **I Halevy, A Hen, A Sharon**
10.20 - 10.45	Mikro-kopter, chopper and mini UAV system for monitoring a radioactive dispersion scene in RDD scenario **A Hen, I Halevy, A Sharon, E Boublil, M Ghelman, T Ridnik, I Yaar**
10.45 - 11.10	Nuclear terrorism: A brief review of threats and responses **I Halevy, A Hen, A Sharon**
11.10 - 11.30	Refreshments
	Physics 5
11.30 - 11.55	Suppression of magnetic order in $U_2(Ni_{1-x}Fe_x)_2Sn$ **S Mašková, L Havela, A Kolomiets, J Peterson, H Nakotte, K Miliyanchuk, A Andreev**
11.55 - 12.20	Focused ion beams in actinides research **P Heard, C Jones, T Scott**
12.20 - 12.45	XMCD in magnetic properties research **A Hen, I Halevy**
12.45 - 13.10	Mössbauer and SQUID under high pressure in actinides research **I Halevy, A Hen, M Pasternak**
13.10 - 13.35	Atom probe in materials science research **O Beeri**
13.35 - 14.45	Lunch break
	Concluding remarks
14.45 - 15.10	Conference summary: Chemistry **To be confirmed**
15.10 - 15.35	Conference summary: Physics **To be confirmed**
15.35 - 15.50	JdA43, Sestri Levante, Italy **M Giovannini**
15.50 - 16.05	Closing address **T Scott**

Locations

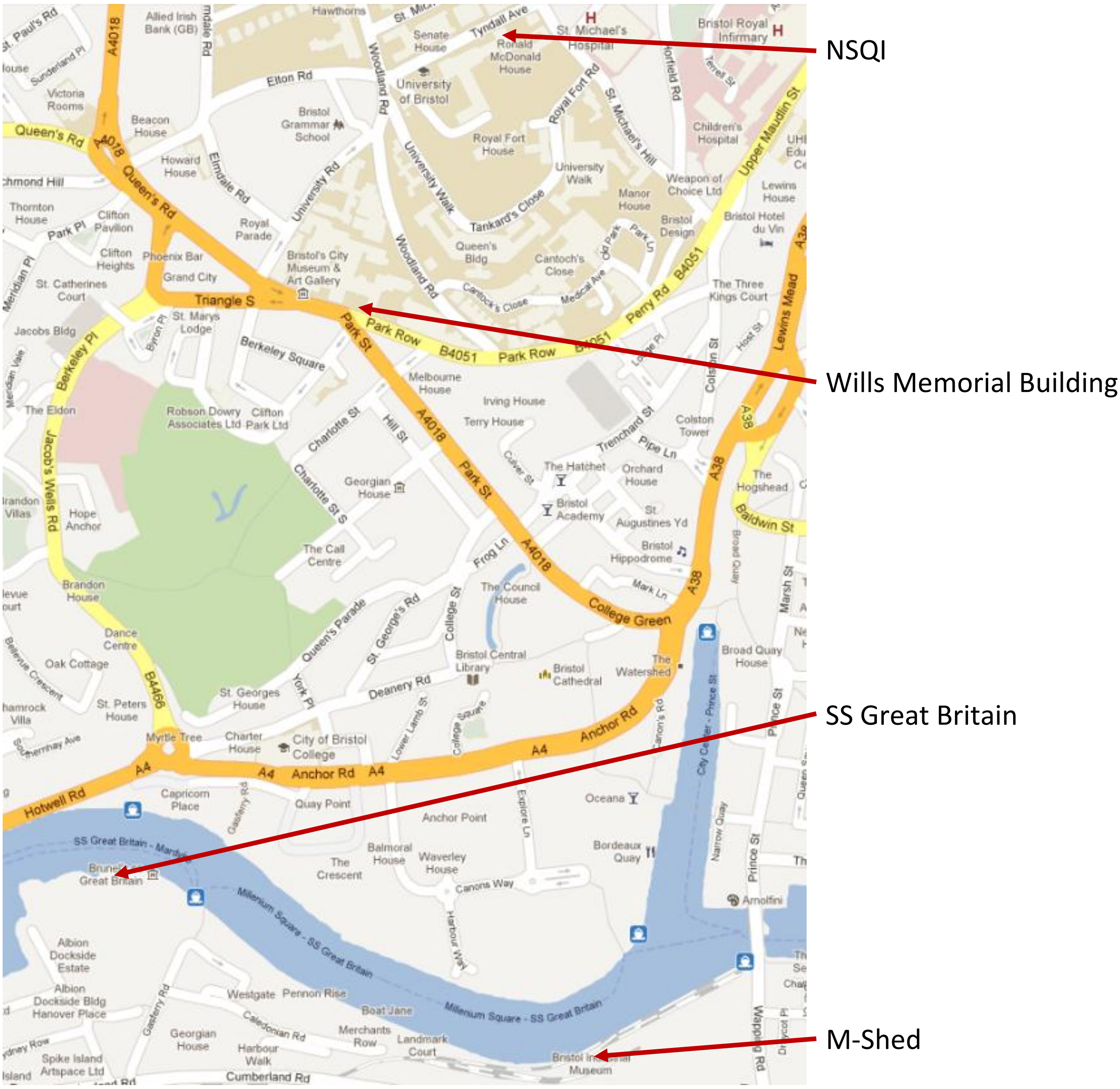

Delegate List

A Adamska	University of Bristol
N Allan	University of Bristol
G Allen	University of Bristol
Z Bao	European Commission, Joint Research Centre, Institute for Transuranium Elements
O Beeri	Nuclear Research Center - Negev
F Blanchard	Université Lille Nord de France Areva
A Bram	Ben-Gurion University of the Negev
Y Buchatskaya	Moscow State University
E Butcher	Sellafield
R Catherall	CERN - European Organization for Nuclear Research
C Coe	Atomic Weapons Establishment
E Colineau	European Commission, Joint Research Centre, Institute for Transuranium Elements
G Cook	Health and Safety Executive
M Cooper	Imperial College
R Crane	University of Bristol
B Egorova	Moscow State University
D Geeson	Atomic Weapons Establishment
A Gheorghe	University Politehnica of Bucharest
M Giovannini	Università di Genova
H Godfrey	National Nuclear Laboratory
A Gonçalves	Instituto Tecnológico e Nuclear
A Gottberg	CERN - European Organization for Nuclear Research
R Gumeniuk	Max-Planck-Institut für Chemische Physik fester Stoffe
I Halevy	Nuclear Research Center - Negev Ben-Gurion University of the Negev California Institute of Technology
K Hallam	University of Bristol
C-E Haralambie	University Politehnica of Bucharest
E Hargreaves	University of Bristol
N Harker	University of Bristol
R Harrison	Imperial College
L Havela	Charles University
P Heard	University of Bristol
A Hen	European Commission, Joint Research Centre, Institute for Transuranium Elements Ben-Gurion University of the Negev
Z Hiezl	Imperial College
J Ipatova	VG Khlopin Radium Institute
I Izosimov	VG Khlopin Radium Institute
C Jones	University of Bristol
A Kayrov	State Scientific Center
A Keatley	University of Bristol
N-T Kim-Ngan	Pedagogical University
M Kuzin	State Scientific Center
A Leith-Jasper	Max-Planck Gesellschaft
S Liddle	University of Nottingham

M Ling	Atomic Weapons Establishment
J Macfarlane	University of Bristol
D Maltsev	Ural Federal University
S Mašková	Charles University
B Negulici	University Politehnica of Bucharest
M Nodilo	Ruer Boškovi and Institute
W Nuttall	University of Cambridge
R Orr	National Nuclear Laboratory
C Padovani	Nuclear Decommissioning Authority
L Payne	University of Bristol
J Petherbridge	Atomic Weapons Establishment
A Pidduck	Atomic Weapons Establishment
I-C Popescu	R&D National Institute for Metals and Radioactive Resources
T Prußmann	Karlsruhe Institute of Technolog
M Reiffers	Institute of Experimental Physics
G Rule	Atomic Weapons Establishment University of Nottingham
T Scott	University of Bristol
A Sharon	Nuclear Research Center - Negev
A Shiryaev	Frumkin Institute of Physical Chemistry and Electrochemistry of RAS
G Sibbens	European Commission, Joint Research Centre, Institute for Reference Materials and Measurements
D Smith	University of Bristol
G Soldani	CEA Marcoule/DRCP/SCPS UCCS UMR CNRS 8181
R Springell	University of Bristol
C Stitt	University of Bristol
S Tesh	University of Bristol
I Tkach	Charles University
Y Totskiy	Karlsruhe Institute of Technology
O Vălu	European Commission, Joint Research Centre, Institute for Transuranium Elements Delft University of Technology
D Vanleeuw	European Commission, Joint Research Centre, Institute for Reference Materials and Measurements
A Warren	University of Bristol
A Willetts	Atomic Weapons Establishment
C Younes	University of Bristol

Introduction
Welcome and housekeeping **T Scott**
Bristol-Oxford Nuclear Research Centre **D Smith**

Bristol-Oxford Nuclear Research Centre

D Smith

Department of Mechanical Engineering, University of Bristol, Queen's Building, University Walk, Bristol, BS8 1TR, United Kingdom
e-mail: david.smith@bristol.ac.uk

The NRC is a joint venture between the University of Bristol and the University of Oxford, creating a centre of national and international importance in nuclear research.

Aims and purpose
Our purpose is to provide leading edge and innovative research to support the safe operation of current and future generation nuclear systems. This centre builds on the advantages of our existing strategic alliances with EDF-Energy, Rolls-Royce and AWE, the firm plans for new nuclear build in the South of England; our geographical focus on nuclear research, and the co-location of key nuclear stakeholders in the region. The centre provides a highly professional team of scientists, engineers and external experts in the South of England that underpins future developments in nuclear safety and economic operation, seeks to ensure continuity of the nuclear community and safeguard the expert knowledge base, and importantly provides leading edge research to support the nuclear business community.

The history of the two universities in working to advance fundamental understanding and the applications of nuclear research is the key to the NRC contribution to industry, government and the research community. It is based on the collective experience of a large, research active community at the two institutions with direct experience of the nuclear sector:

- Helping to solve problems in the operation of nuclear facilities
- Advancing the thinking on technical operations and future research needs
- Building a strong platform of pre-eminent world class researchers in nuclear research
- Providing access to geographically accessible, world class research facilities and expertise relevant to the nuclear sector developing the advanced skills needed for those who will work in the nuclear facilities of the future
- Responding to needs in an effective, professional way in partnership with Industry, Government and the wider nuclear Research Community
- Cost effective research that adds value to the operation of nuclear facilities
- A research platform to help government and the regulatory authorities develop policy and make informed decisions ensuring the UK has a strong nuclear research sector in the South and South West of England
- Maintaining the UK's reputation for the quality of its international research, partnerships and competitiveness in the nuclear sector

A community of over 100 key research personnel in nuclear research
The centre assembles underpinning research groups at Bristol and Oxford, involving the Safety Systems Research Centre in Civil Engineering at Bristol, Chemistry, Physics and Materials Research in the Oxford Division of Mathematical, Physical and Life Sciences, the Oxford Martin School, and in the Bristol Faculty of Science and the Interface Analysis Centre, Mechanics of Materials and Structural Integrity, Seismic Research in the Departments of Engineering at Bristol and Oxford and expert groups in Social Science and Law examining social policy and public perceptions.

As well as our research focus we will be developing new researchers, capturing, sustaining and transferring skills related to the safe and extended operation of current and future nuclear systems and facilitating, via a neutral network environment, discussion on all aspects of nuclear futures.

Physics 1
Variations of actinide magnetism in uranium-base hydrides **A Adamska, L Havela, A Andreev, Y Skourski**
Magnetic properties of epitaxial UO_2 thin films **Z Bao, R Springell, R Caciuffo, T Gouder, S Langridge, G Nisbet, G Lander**

Variations of actinide magnetism in uranium-base hydrides

A Adamska[1], L Havela[2], A Andreev[3], Y Skourski[4]

[1]*Interface Analysis Centre, University of Bristol, Oldbury House, 121 St. Michaels Hill, Bristol, BS2 8BS, United Kingdom*
e-mail: anna_adamska@interia.eu
[2]*Department of Condensed Matter Physics, Charles University, 12116 Prague 2, Czech Republic*
[3]*Institute of Physics, Academy of Sciences, 18221 Prague, Czech Republic*
[4]*Dresden High Magnetic Field Laboratory, Helmholtz-Zentrum Dresden-Rossendorf, 01314 Dresden, Germany*

Magnetic properties of uranium-based intermetallics are intimately related to the character of the 5*f* electronic states, ranging between a localised character, similar to lanthanides, and itinerancy, which is reminiscent of magnetism emerging in transition metals. One of specific characteristics of the 5*f* electron magnetism is its high sensitivity to external variations, such as pressure, magnetic field, composition, hydrogen absorption etc. For purely band systems, the actinide-actinide spacing is a crucial parameter, which determines the magnetic properties. However, for uranium compounds with the U-U spacing large enough the principal controlling parameter is the 5*f*-ligand hybridisation.

Hydrogenation in general leads to changes/modifications of both crystal and electronic structure of intermetallic compounds. It brings a relatively small perturbation to the system, namely a lattice expansion and the hydrogen bonding with other atoms in the lattice.

Our detailed study of the UTGe (T = late transition metal) hydrides underlines the general tendency of strengthening of magnetic properties of U compounds due to hydrogenation [1]. In this particular case, there is also a primary impact on the crystal structure. For compounds with the 3*d* transition metals (T = Fe, Co, Ni) the orthorhombic TiNiSi-type of structure (or its monoclinic variant) was transformed into the the hexagonal ZrBeSi-type, expanding even up to 10.7 % for $UCoGeH_{1.7}$. In the case of compounds with the 4*d* and 5*d* transition metals (T = Rh, Pd and T = Ir), the structure type was not changed upon hydrogenation, only a weak expansion of the unit cell (e.g. up to 1.3 % in $URhGeH_{0.3}$) was observed. The variations of magnetism upon hydrogenation can be really significant. H absorption can induce a change of the type of magnetic order (e.g. from AF to F as in $UNiGeH_{1.2}$ and $UIrGeH_{0.1}$), an additional phase transition (e.g. in $UNiGeH_{0.3\text{-}1.0}$), or a shift of the magnetic ordering temperature (e.g. from 3 K in UCoGe up to 50 K in $UCoGeH_{1.7}$ or from 9 K in URhGe up to 17 K in $URhGeH_{0.3}$). All those effects reported for hydrogenated UTGe are shown in Figure 1.

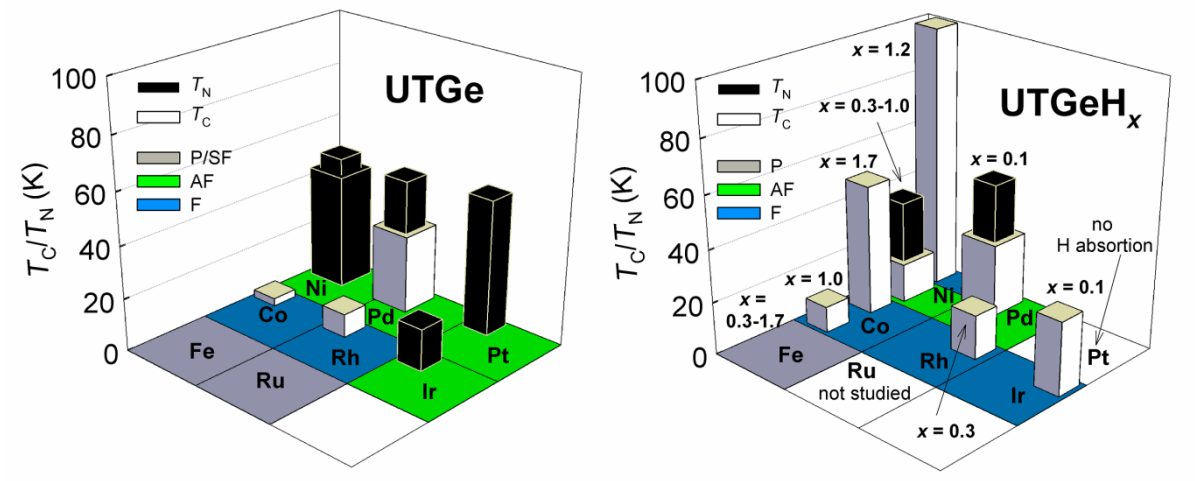

Figure 1. Summary of magnetic properties of UTGe hydrides (right panel) compared to the parent UTGe compounds (left panel). The type of ground state of the initial compounds is indicated: P/SF - paramagnetic/spin fluctuator; AF - antiferromagnetic; F - ferromagnetic. The column-height shows the values of ordering temperatures (the white-coloured column shows T_C and black one shows T_N).

In general, observed changes in magnetism of UTGe compounds can be attributed to an enhancement of the U-U spacing and reducing the 5*f*-5*f* overlap.

The most prominent example of variations of magnetic properties caused by the H absorption is UNiGe-H system [2]. All UNiGe hydrides, namely $UNiGeH_{1.2}$, $UNiGeH_{1.0}$ and $UNiGeH_{0.3}$, synthesised under p_{H2} = 156, 2 bar, and by a controlled decomposition of $UNiGeH_{1.0}$, crystallise in the ZrBeSi structure type. This points to a largely variable H concentration within the same β-hydride phase, with a respective volume expansion of 7.6, 5.8, and 4.4 %, with reference to pure UNiGe. The shortest U-U distances ($d_{U\text{-}U}$) increase by about 11, 8.4, and 6.7 %, respectively. An attempt to obtain an α-hydride by applying quite low H_2 pressure of 0.6 bar resulted in phase-mixed material. No expansion is observed for the orthorhombic phase, thus we can conclude that no α-hydride exists.

Magnetic susceptibility of $UNiGeH_{1.2}$ exhibits the F-type of behaviour below $T_C \approx 100$ K (Figure 2(a)) in contrast to UNiGe (an antiferromagnet below 44 and 50 K [3]). Two intermediate hydrides: $UNiGeH_{1.0}$ and $UNiGeH_{0.3}$ undergo two phase transitions, the first one around $T_N \approx$ 38-35 K and the second one at $T_C \approx$ 7-15 K seen in Figure 2(b)-(c). The magnetisation of UNiGe has no remanence and exhibits a hysteretic metamagnetic behaviour in the range of 3-5 T (Figure 3). At 60 T it reaches approx. 1.6 μ_B/f.u. and has clearly still an increasing tendency. The magnetisation of the UNiGe hydrides reveals μ_S and approaches the saturation faster.

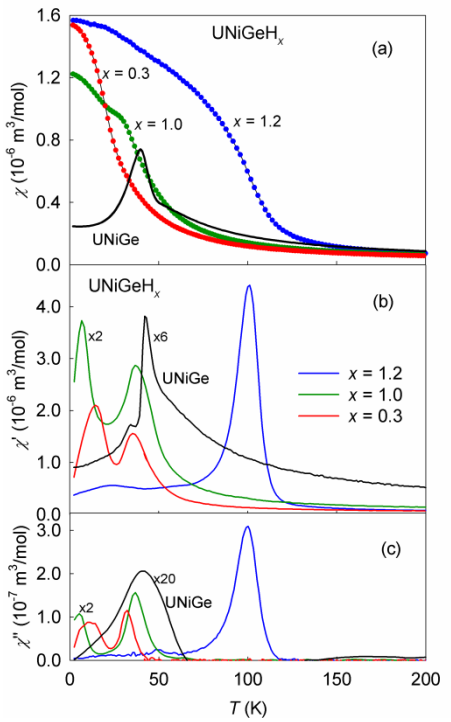

Figure 2. (a) Temperature dependence of *dc* susceptibilities for $UNiGeH_x$ and UNiGe measured in $\mu_0 H$ = 2 T. (b) Real and (c) imaginary part of *ac* susceptibilities for $UNiGeH_x$ and UNiGe measured in zero *dc* field and *ac* field of 1 mT and frequency 80 Hz.

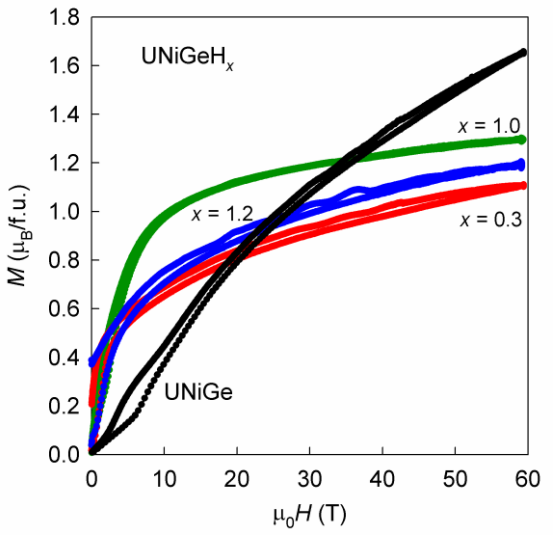

Figure 3. Comparison of magnetisation curves of $UNiGeH_x$ and UNiGe measured in pulsed magnetic field swept up and down up to 60 T at T = 1.5 K.

References

[1] A Adamska et al., J. Alloys Compds. 515, 171-179 (2012)
[2] A Adamska et al., J. Magn. Magn. Mater. 323, 3217-3222 (2011)
[3] A Purwanto et al., Phys. Rev. B 53, 758 (1996)

Magnetic properties of epitaxial UO_2 thin films

Z Bao[1], R Springell[2], R Caciuffo[1], T Gouder[1], S Langridge[3], G Nisbet[4], G Lander[1]

[1]European Commission, Joint Research Centre, Institute for Transuranium Elements, Postfach 2340, D-76125 Karlsruhe, Germany
e-mail: zhaohui.bao@ec.europa.eu
[2]HH Wills Physics Laboratory, Tyndall Avenue, Bristol, BS8 1TL, United Kingdom
[3]ISIS, Harwell Science and Innovation Campus, STFC, Oxfordshire, OX11 0QX, United Kingdom
[4]Diamond Light Source, Chilton, Didcot, Oxfordshire, OX11 0DE, United Kingdom

The low-temperature magnetic properties of uranium dioxide have raised the attention of experimentalists and theoreticians for several decades and continue to be a central issue in the investigation of actinide compounds [1, 2]. The peculiar 3-***k*** antiferromagnetic structure of UO_2, combined with a 3-***k*** internal distortion of the oxygen sublattice and long-range order of the uranium electric quadruple moments, have called for extensive investigations based on neutron and x-ray scattering techniques. In bulk samples, the transition to the ordered state is discontinuous at T_N = 30.8 K [1]. In contrast to that, the surface layers order continuously, as revealed by resonant x-ray scattering experiments performed on a single-crystal sample with an exposed (001) surface [3]. These experiments showed that a magnetically disordered region exists at the surface below T_N, separated from the magnetically ordered bulk by a diffuse magnetic interface. The width of the magnetic interface is temperature dependent, and appears to diverge as the sample temperature approaches T_N, leading to a continuous variation of the surface magnetic scattering [3]. The observed behaviour was attributed to surface induced disorder phenomena [3].

In order to understand the surface effect comprehensively, we have performed resonant x-ray scattering at the uranium M_{IV} edge on a series of UO_2 thin films, with thickness ranging from about 100 to 2000 Å. The UO_2 thin films were prepared by reactive sputtering from a 99.9% depleted uranium metallic target in an oxygen-rich environment. By appropriate controlling the substrate temperature, UO_2 films were grown on a $LaAlO_3$ substrate inside the UHV chamber of an XPS spectrometer at ITU. In order to prevent oxidation while exposed in air, the films were capped by a protective Mg layer. Various techniques including XPS and XRD confirmed the stoichiometry and the epitaxial nature of the UO_2 thin films. The x-ray scattering experiments were performed at the ID20 beamline of the European Synchrotron Radiation facility, Grenoble, France, and at the I16 beamline of the Diamond Light Source, Chilton, UK.

Due to the large resonance-enhanced scattering cross-section at the M_{IV} uranium edge, we measured a strong magnetic scattering intensity for all the films studied. As an example, Figure 1 shows the temperature dependence of the intensity of the (001) magnetic Bragg peak observed in a film with a thickness of 482 Å. The intensity is normalised to the value measured at 15 K, the lowest temperature achievable with the experimental setup that we used for this experiment. The continuous changing of the scattering intensity is a signature of the second-order nature of the phase transition. For a second-order phase transition near the critical temperature, where a correlation length can be defined, the spontaneous magnetisation shows a power-law dependence on the reduced temperature, $\tau = (T-T_N)T_N$, being $M(\tau) \sim \beta|\tau|^{\beta}$. Typical values for β are 0.365 for a 3D Heisenberg model, 0.325 for a 3D Ising model, and 0.5 in mean-field approximation. A power law fitting near the Néel temperature T_N of the intensity (proportional to $M^{2}\sim|\tau|^{2B}$) reported in Figure 1 provides a critical exponent β = 0.21(1).

The Jahn-Teller distortion of the oxygen sublattice accompanying to the magnetic phase transition, is revealed by superlattice reflections forbidden in the Space Group of the disordered phase. Figure 1 also shows the temperature dependence of the (014) Jahn-Teller peak intensity. In this case, the corresponding critical exponent is β_{JT} = 0.55(1) about two times higher than the one of magnetic scattering. This suggests that the Jahn-Teller distortion, in the case of UO_2, is driven by the magnetic ordering.

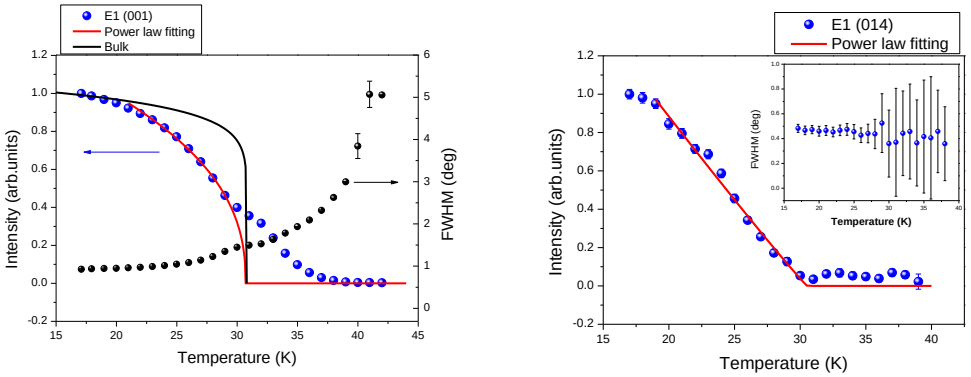

Figure 1. X-ray diffraction results obtained for a UO_2 thin film with a thickness of 482 Å. (Left panel) Temperature dependence of the intensity of the (001) magnetic Bragg peak measured by resonant x-ray scattering at the uranium M_{IV} edge. (Right panel) Temperature dependence of the (014) superlattice Bragg reflection associated to the internal Jahn-Teller distortion, measured with 5.1 KeV incident photons.

References

[1] P Santini et al., Rev. Mod. Phys. 81, 807 (2009)
[2] R Caciuffo et al., Phys. Rev. B 84, 104409 (2011)
[3] G Watson et al., Phys. Rev. B 61, 8966 (2000)

Materials
Modelling of uranium hydride reaction site initiation **J Glascott, J Petherbridge, S Bazley, T Scott, C Jones**
Controlled conversion of uranium carbide fission targets using water vapour **T Scott, N Harker, C Jones,K Hallam, P Heard, R Catherall**
Preparation and characterisation of thin actinide layers **G Sibbens, A Moens, R Eykens, D Vanleeuw**
Corrosion of uranium in mixed environments of water vapour and oxygen **N Harker, T Scott, C Jones, P Heard, K Hallam, J Petherbridge, J Glascott**
Investigation of oxide growth and structure on the surface of uranium **C Jones, T Scott, P Heard, K Hallam, J Petherbridge, J Glascott**

Modelling of uranium hydride reaction site initiation

J Glascott[1], J Petherbridge[1], S Bazley[1], T Scott[2], C Jones[2]

[1]Atomic Weapons Establishment, Aldermaston, Reading, Berkshire, RG7 4PR, United Kingdom
[2]Interface Analysis Centre, University of Bristol, Oldbury House, 121 St. Michael's Hill, Bristol, BS2 8BS, United Kingdom

The interaction of hydrogen with uranium is of particular interest in the nuclear industry. This reaction is characterised by initial spot-wise pitting attack followed by site agglomeration to form a continuous hydride surface layer, which then propagates through the uranium sample. Although the kinetics of the later bulk reaction are well established, the rate (and mechanism) of initiation of the initial reaction sites is poorly understood.

It has been proposed that site initiation is controlled by the diffusion of hydrogen species through the surface oxide layer to the underlying metal. To test this hypothesis, a mathematical model has been constructed and then compared to experimental data.

Specifically, experiments have been carried out in which uranium samples bearing a "standard" oxide film were exposed to hydrogen gas at a constant pressure (0.06-1.0 bar) and temperature (75, 100 and 130°C). The increase in the number of reaction sites (*N)* was measured as a function of time. Care was taken to prepare samples with well controlled oxide characteristics to allow parameterisation of the initiation model. Model and experimental *N* vs *t* curves were compared and it was concluded that the model used was applicable to the experimental dataset and was also self consistent.

Controlled conversion of uranium carbide fission targets using water vapour

T Scott[1], N Harker[1], C Jones[1], K Hallam[1], P Heard[1], R Catherall[2]

[1]*Interface Analysis Centre, University of Bristol, Oldbury House, 121 St Michaels Hill, Bristol, BS2 8BS, United Kingdom*
e-mail: t.b.scott@bristol.ac.uk
[2]*CERN - European Organization for Nuclear Research, CH-1211 Genève 23, Switzerland*

Abstract

The safe disposal of radioactive waste arising from experimental fission studies at CERN is a key objective for the organisation. The current work has sought to determine a repeatable, reliable and safe method of converting UC_2 fission targets into an acceptable uranium oxide waste form for subsequent disposal by the Swiss authorities.

Research has drawn upon the experimental and analytical capabilities of the Interface Analysis Centre (IAC), a group specialising in nuclear materials research at the University of Bristol, England. Pills of UC_2+C supplied by the ISOLDE group at CERN were oxidised in the presence of water vapour in a specialist gas exposure system at temperatures from 100 to 600°C. In all experiments the controlled oxidation of UC_2 to a uranium oxide powder was observed, with x-ray diffraction analyses indicating an oxide composition between UO_2 and U_4O_7 as the principal oxidation product. The evolving gas composition of the reaction cells indicated that two reactions occurred during water vapour exposure: (1) oxidation of UC_2 to U-oxide and (2) oxidation of graphitic carbon to form CO_2. The reaction rates of these two processes were observed to be significantly different, with carbide oxidation proceeding more rapidly than graphite oxidation. At elevated temperatures (≥300°C) the rate of carbide oxidation was controlled by the rate of water vapour diffusion, allowing for a controlled conversion of the target material.

Stemming from the current work we will seek to upscale the experimental method and apparatus for waste conversion on a larger scale.

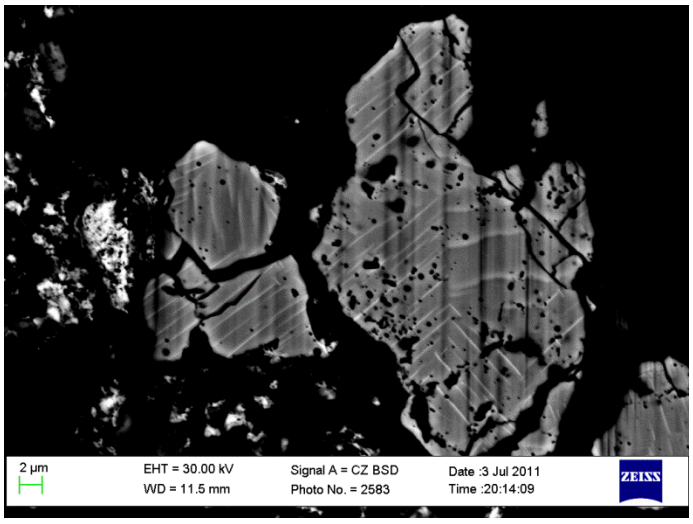

Figure 1. A high contrast and high resolution backscattered electron image of a region of the carbide pill surface showing twinning throughout the carbide grains.

Preparation and characterisation of thin actinide layers

G Sibbens, A Moens, R Eykens, D Vanleeuw

European Commission, Joint Research Centre, Institute for Reference Materials and Measurements (IRMM), Retieseweg 111, B- 2440 Geel, Belgium
e-mail: goedele.sibbens@ec.europa.eu

The Institute for Reference Materials and Measurements (IRMM) has a long experience in the development of isotopic reference materials and is one of the very few providers of well characterised targets for measurements in nuclear physics for studies on reactor safety and waste transmutation. Thin layers of U, Pu, Np, and Am are prepared in the IRMM Target Preparation Laboratory for neutron-induced reaction cross-section measurements performed at the IRMM's linear electron accelerator (GELINA) and Van de Graaff accelerator. Occasionally, under respective collaboration agreements thin layers prepared at IRMM are used for measurements at other renown nuclear research institutes, such as the commissariat à l'énergie atomique (CEA) or CERN.

The actinide deposits are prepared by molecular plating and for ^{235}U also by vacuum deposition. The total activity of the actinide layer, and for larger deposits also the homogeneity of the layer, are determined by low-geometry alpha-particle counting. The atomic abundances of the actinide material are measured by thermal ionisation mass spectrometry In case the ingrowth of a daughter nuclide would interfere with the characterisation and cross-section measurements, a radiochemical separation by ion exchange is done prior to the preparation of the layer.

The vacuum deposition of $^{235}UF_4$ is done by fluoride sublimation from a resistance-heated Ta crucible. Therefore the original triuranium octoxide is first converted into uranium fluoride by a wet chemical precipitation method. The area of the active layer on the backings is defined by masks mounted in a planetary rotating system in the vacuum deposition set-up (Figure 1.)

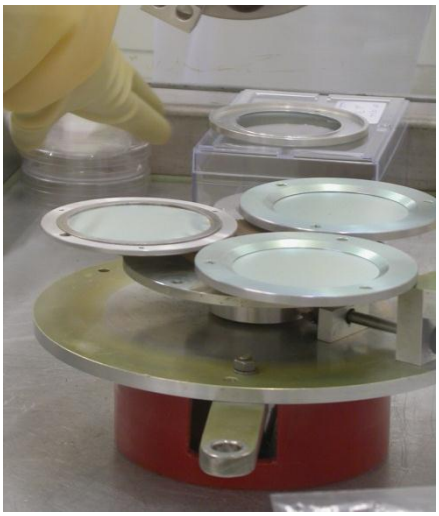

Figure 1. Rotating system holding the backings with the vacuum deposited $^{235}UF_4$ layers and the masks.

The molecular plating method is based on the cathodic deposition of the actinides onto metallic backings using an organic solvent as electrolyte. The anode is a rotating platinum grid to mix the electrolyte without disturbing the deposition.

In addition to the general presentation about the preparation and characterisation techniques, an overview will be given of the actinide targets that can be prepared in the Target Preparation Laboratory at IRMM, illustrated with some examples.

Corrosion of uranium in mixed environments of water vapour and oxygen

N Harker[1], T Scott[1], C Jones[1], P Heard[1], K Hallam[1], J Petherbridge[2], J Glascott[2]

[1]Interface Analysis Centre, University of Bristol, Oldbury House, 121 St Michaels Hill, Bristol, BS2 8BS, United Kingdom
e-mail: n.j,harker@bristol.ac.uk
[2]Atomic Weapons Establishment, Aldermaston, Reading, Berkshire, RG7 4PR, United Kingdom

Investigation of oxide growth and structure on the surface of uranium

C Jones[1], T Scott[1], P Heard[1], K Hallam[1], J Petherbridge[2], J Glascott[2]

[1]Interface Analysis Centre, University of Bristol, Oldbury House, 121 St Michaels Hill, Bristol, BS2 8BS, United Kingdom
e-mail: cj0810@bristol.ac.uk
[2]Atomic Weapons Establishment, Aldermaston, Reading, Berkshire, RG7 4PR, United Kingdom

Physics 2
Magnetic and electronic properties of NpCoGe **E Colineau, R Eloirdi, J-C Griveau, P Gaczynski, A Shick**
Studies on the UFe_3B_2 uranium boride **A Gonçalves, M Dias, P Carvalho, L Pereira, I Santos, O Tougait, V Tran**
Crystal structure and physical properties of RBeGe (R = La-Nd, Th, U) **R Gumeniuk, A Leithe-Jasper, H Borrmann, U Burkhardt, W Schnelle, Yu Grin**

Magnetic and electronic properties of NpCoGe

E Colineau, R Eloirdi, J-C Griveau, P Gaczyński, A Shick

European Commission, Joint Research Centre, Institute for Transuranium Elements, Postfach 2340, 76125 Karlsruhe, Germany
e-mail: eric.colineau@ec.europa.eu

The orthorhombic isostructural series AnTGe (An = actinide; T = transition metal), with the TiNiSi-type structure presenting U zig-zag chains along the a-axis, offers a unique opportunity to observe and investigate detailed properties and systematic trends in a system where ferromagnetism and superconductivity coexist at ambient pressure in URhGe (T_C = 9.5K, T_{SC} = 0.26K) [1] and UCoGe (T_C = 3K, T_{SC} = 0.7K) [2].

However, due to the difficulty to handle them, transuranium systems are much less documented. In an effort to bridge this gap, we have undertaken the study of the neptunium analogues NpRhGe and NpCoGe. NpRhGe orders antiferromagnetically below $T_N \approx 21$K with an ordered moment $\mu_{Np} = 1.14\mu_B$ and no hint of superconductivity has been found down to 1.8 K. The specific heat indicates a high Sommerfeld coefficient value γ = 195 mJ mol^{-1} K^{-2} [3].

In the present work, we have investigated NpCoGe by dc magnetisation, ac susceptibility, specific heat, electrical resistivity, ^{237}Np Mössbauer spectroscopy and electronic structure calculations. We find that NpCoGe orders antiferromagnetically at T_N=13K with an average ordered moment $\langle m_{Np} \rangle = 0.8\ \mu_B$. The weak antiferromagnetic interactions (θ_p = -5.5K) are overcome by the application of a moderate magnetic field (B ~ 3T) that induces a metamagnetic phase of, if not pure, dominant ferromagnetic character. The magnetic structure in zero-field is probably complex and intermediate between a pure sine and a squared modulation. NpCoGe appears as a more delocalised antiferromagnet than NpRhGe, which is consistent with the trend observed in UTGe analogues. The proximity of NpCoGe to a quantum critical point and its implications will be discussed.

Acknowledgements
The high purity Np metals required for the fabrication of the compound were made available through a loan agreement between Lawrence Livermore National Laboratory and ITU, in the frame of a collaboration involving LLNL, Los Alamos National Laboratory and the US Department of Energy.

References
[1] D Aoki et al., Nature 413, 613 (2001)
[2] N Huy et al., Phys. Rev. Lett. 99, 067006 (2007)
[3] E Colineau et al., J. Phys.: Condens. Matter 20, 255234 (2008)

Studies on the UFe_3B_2 uranium boride

A Gonçalves[1], M Dias[1,2], P Carvalho[2], L Pereira[1], I Santos[1], O Tougait[3], V Tran[4]

[1]Dept. Química, IST-ITN/CFMC-UL, P-2686-953 Sacavém, Portugal
e-mail: apg@itn.pt
[2]Dept. Engenharia de Materiais, IST, Av. Rovisco Pais, 1049-001 Lisboa, Portugal
[3]Sciences Chimiques de Rennes, UMR CNRS 6226, Université de Rennes 1, Avenue de Général Leclerc, 35042 Rennes, France
[4]Institute of Low Temperature and Structure Research, Polish Academy of Sciences, 50-950 Wroclaw, Poland

Ternary uranium borides generally do not show magnetic ordering. The reported exceptions to this trend are URh_3B_x (x ~ 1) and UNi_4B, the magnetism emergence being due to the particular characteristics of their crystal structures and interatomic distances [1, 2].

UFe_3B_2, the only RFe_3B_2 (R = f-element) compound described up to now, has been previously reported as crystallising with the hexagonal $CeCo_3B_2$-type structure [3, 4] and probably not being magnetically ordered [5]. However, no detailed magnetic studies on this compound were published. In fact, our work on the U-Fe-B phase diagram indicates that UFe_3B_2 cannot be easily prepared as single phase, as it is formed by peritectic reaction, samples usually having significant amounts of iron-rich phases. Here we present the synthesis and detailed crystallographic and magnetic studies on UFe_3B_2, with the objective of determine and refine its crystal structure and clarify its magnetic ground state.

Almost single phase samples (UFe_3B_2 >92% vol., α-Fe <7 % vol. and UO_2 ~1 % vol.) were prepared by Czochralski pulling from the 23B:62Fe:15U alloy that belongs to the primary crystallisation zone of UFe_3B_2. Single crystal x-ray diffraction studies confirmed that UFe_3B_2 crystallises in the $CeCo_3B_2$ type-structure (P6/mmm S.G. no.191, Z = 1, ρ = 10.79 g/cm^3), with *a* = 0.5052(1) nm, *c* = 0.3002(1) nm and V = 0.664(1) nm^3 at room temperature.

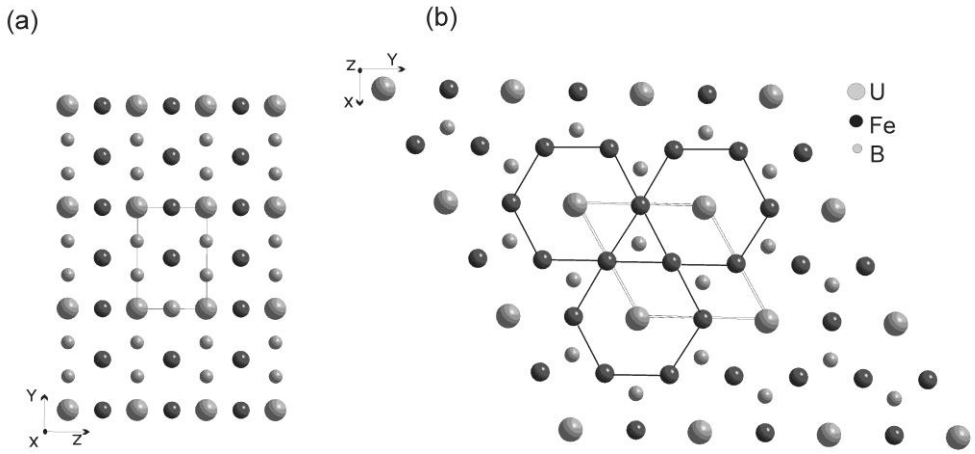

Figure 1. UFe3B2 unit cell projections along (a) [100] and (b) [001].

The U-U distance (0.300 nm) is lower than the sum of the metallic radii (0.308 nm, for a coordination number of 12), being below the Hill limit, which would predict a delocalisation via direct 5f-5f orbital overlap and a non-magnetic behaviour of the uranium atoms. The U-Fe distance (0.294 nm) is only slightly higher than the sum of the respective metallic radius (0.279 nm) and a non-negligible hybridisation between the 5f-3d orbitals can exist. The Fe-B distance (0.209 nm) is shorter than the sum of the two radii (0.217 nm), pointing to significant interactions between these two elements. Therefore, only small iron magnetic moments are expected in this compound.

Magnetic susceptibility measurements as a function of the temperature, χ(T) = M/H, were made between 2 K and 800 K. The χ(T) curve exhibits a broad maximum at T_{max} = ~370 K and monotonically decreases with lowering temperature. No other magnetic transitions were observed down to the lowest studied temperature.

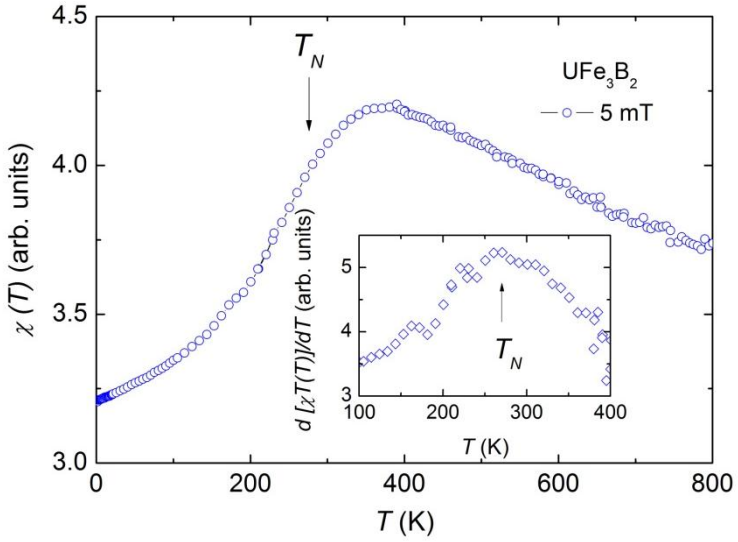

Figure 2. Temperature dependence of dc-magnetic susceptibility of UFe_3B_2 measured under 0.5 mT. Inset shows the temperature derivative of the product [**χ**(T)T] as as function of temperature. The maximum of d**χ**(T)T/dT is taken as the Néel temperature of UFe_3B_2.

Using Fisher's method for itinerant antiferromagnets [6], the Néel temperature can be determined as the maximum of the derivative of the product [χ(T)T], which suggests that UFe_3B_2 is an antiferromagnet with a rather high Néel temperature, T_N = 268(5) K. Measurements made under different magnetic fields corroborate this assumption, with the maximum shifting down with increasing fields. Albeit small, the quantity of ferromagnetic impurities is significant enough to disturb the magnetic behaviour of the studied compound, and therefore proper UFe_3B_2 magnetic parameters, like the effective magnetic moment, paramagnetic Curie temperature, ordered magnetic moment, etc… cannot be determined at the present stage. However, this study indicates that UFe_3B_2 is an itinerant antiferromagnet, with the magnetic ordering most probably coming from the interactions between the iron atoms.

References

[1] Z Zolnierek, D Kaczorowski, J. Magn. Magn. Mater. 63-4 (1987) 178
[2] Y Haga, A Oyamada, T Matsuda, S Ikeda, Y Ounki, Physica B, 403 (2008) 900
[3] I Valyovka, Yu Kuzma, Dop. Akad. Nauk Ukr. RSR, A: Fiz.-Tekhn. Mat. Nauki (1975) 652
[4] I Valyovka, Yu Kuzma, Dop. Akad. Nauk Ukr. RSR, A: Fiz.-Tekhn. Mat. Nauki (1974) 1029
[5] S Yushuk, Y Kuzma, A Kamzin, I Valovka, M Zakharko, I Adamenko, Fizika Tverdogo Tela, 22 (1980) 612
[6] M Fisher, Philos. Mag. 7 (1962) 1731

Crystal structure and physical properties of *R*BeGe (*R* = La-Nd, Th, U)

R Gumeniuk, A Leithe-Jasper, H Borrmann, U Burkhardt, W Schnelle, Yu Grin

Max-Planck-Institut für Chemische Physik fester Stoffe, Nöthnitzer Str. 40, 01187 Dresden, Germany
e-mail: gumeniuk@cpfs.mpg.de

New ternary germanides with composition *R*BeGe (where *R* = La-Nd, Th, U) have been synthesised. They crystallise with ZrBeSi structure type (space group $P6_3/mmc$) [1]. The dependence of unit cell volume of *R*BeGe *vs* ionic radii of R^{n+} (Figure 1) indicates 3^+ oxidation states for rare-earth metals and 4^+ for Th. These findings are complemented by preliminary physical properties measurements as well as by electronic structure calculations.

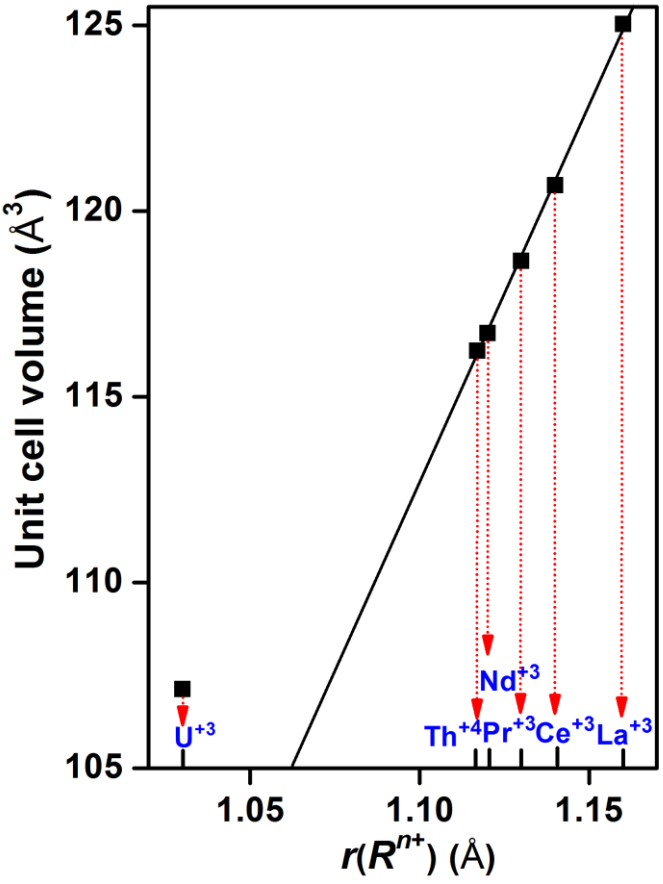

Figure 1. Unit cell volume of *R*BeGe *vs* ionic radii of R^{n+}.

References

[1] J Nielsen, N Baenziger, Acta Crystallogr. 7, 132 (1954)

Physics 3
Strengthening of magnetic interactions in UGa_2 under pressure **L Havela, A Kolomiets, J Prchal, A Andreev**
Progress in the magnetic study of Np_2Co_{17} **A Hen, I Halevy, I Orion, E Colineau, R Eloirdi, J-C Griveau, P Gaczyński, F Wilhelm, A Rogalev, J-P Sanchez, M Winterrose, N Magnani, A Shick, R Caciuffo**
Progress in the magnetic study of Np_2Ni_{17} and $NpNi_5$ **I Halevy, A Hen, I Orion, E Colineau, R Eloirdi, J-C Griveau, P Gaczyński, M Winterrose, N Magnani, A Shick, R Caciuffo**

Strengthening of magnetic interactions in UGa_2 under pressure

L Havela[1], A Kolomiets[1,2], J Prchal[1], A Andreev[3]

[1]*Department of Condensed Matter Physics, Charles University, Ke Karlovu 5, 12116 Prague 2, Czech Republic*
e-mail: havela@mag.mff.cuni.cz
[2]*Department of Physics, Lviv Polytechnic National University, 12 Bandera Str., 79013 Lviv, Ukraine*
[3]*Institute of Physics, ASCR, Na Slovance 2, 18221 Prague 8, Czech Republic*

UGa_2, crystallising in the hexagonal structure (AlB_2 type), has quite exceptional position among U-based intermetallics. For a compound with the U-U spacing exceeding 4 Å, it is common to have a magnetic ground state, but typically it is antiferromagnet with ordering temperatures well below 100 K. But UGa_2 is ferromagnet with T_C = 126 K. After many years of both theoretical and experimental studies there is still no consensus about the character of the 5*f* states. In particular, $5f^2$ localised, $5f^3$ localised, and 5*f* band-like states were considered, none of those is able to explain all the features observed [1]. A photoelectron spectroscopy study reveals a high 5*f* density at the Fermi level, which excludes any purely localised model [2].

Response of magnetic properties to the lattice compression is an important indicator of the situation of the 5*f* states. While band systems tend to a general suppression of magnetic moments and their ordering, magnetism based on localised states has insensitive size of moments while their ordering temperatures can weakly increase. Previous experiments [3] indicated a quite rapid increase (approx. 3 K/GPa) of the Curie temperature monitored by a SQUID magnetometry up to p = 0.8 GPa, while the magnetisation is practiaclly invariable. Such increase can be perhaps understood in the framework of a two-band model, in which the compression leads to a stronger hybridisation of the 5*f* and other conduction-electron states, which supports the specific exchange interaction. To explore the tendency to higher pressures, we have applied a different technique, a resistivity measurement on Bridgman-type clamped pressure cells with a solid pressure-transmitting medium (steatite). So far we achived pressures over 7 GPa.

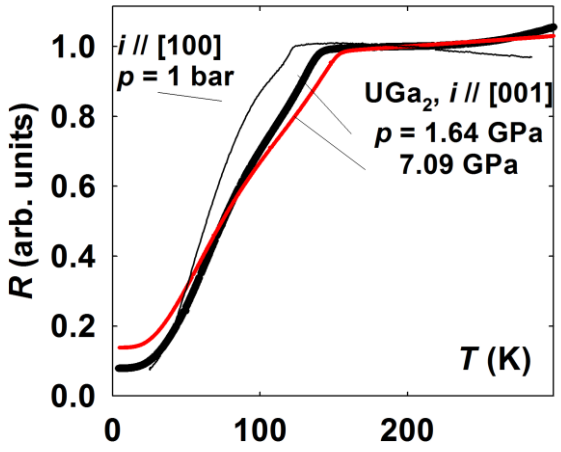

Figure 1. Temperature dependences of electrical resistivity of UGa_2 single crystal with *I* // [100] at ambient pressure and *I* // [001] for selected pressures.

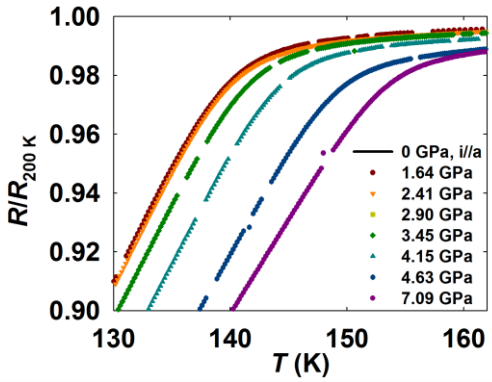

Figure 2. Detail of electrical resistivity around T_C shows more pressure points. Increasing pressure shifts the knee to higher temperatures.

A single crystal of UGa_2 was grown by a tri-arc Czochralski method. It was oriented by the Laue method and a bar for electrical resistivity was cut for the current direction *i* // [100]. Figure 1 reveals basic features of electrical resistivity of UGa_2, namely a very large spin-disorder scattering, which reaches 150-200 μΩcm for *I* // [100] and almost twice as much for [001] [1, 3]. Such situation makes the Curie temperature very well pronounced in the resistivity, which becomes a convenient tool to see the variations of magnetic ordering.

Resistivity measurements in the pressure cell were performed on a small needle with *i* // [001]. The data do not give reliable absolute values, the contacts can be somewhat displaced under pressure. Therefore we normalised the resistivities at T = 200 K. The fact that the effective residual resistivity on the relative scale increases as a function of pressure (seen in Figure 1) most probably means that the spin-disorder resistivity decreases. Our data exhibit also the shoulder observed below 100 K in earlier studies [1, 3]. It was attributed to a distortion within the hexagonal plane [1]. Figure 1 shows that its temperature does not change.

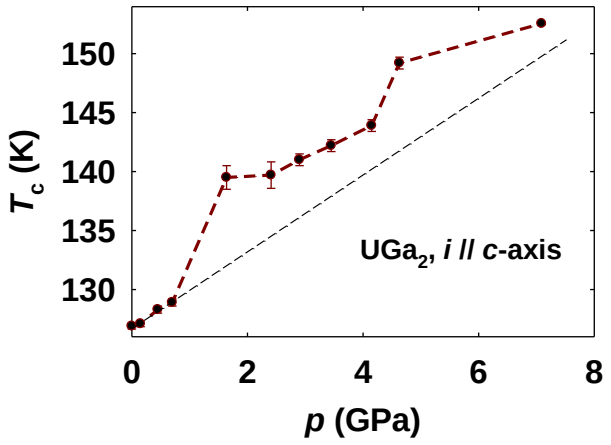

Figure 3. Pressure dependence of T_C of UGa_2 obtained from electrical resistivity measurements, plotted together with the data from [3] (the points below 1 GPa). The scatter of individual data points can be due to a difference between the pressure at the sample and manometer (Pb), but the global increasing tendency is without any doubt.

Figure 3 reveals a monotonous increase of T_C up to the highest pressure applied, i.e. above 7 GPa, reaching almost 160 K. Such dramatic effect can be attributed only to a situation, in which the 5*f* states do not interact directly, but only via the hybridisation with non-*f* states. Strengthening such hybridisation by the lattice compression (low bulk modulus of 100 GPa [5] leads to a large lattice compression at given pressures) can first increase the exchange coupling without suppressing the moments. Eventually the moments have to be affected (washed out), and their reduction has to lead to a decrease of T_C. In the case of UGa_2 apparently higher pressures are needed to reach the descending part. Analogous behaviour is rather seldom. A best example is UTe with the slope od 13 K/GPa. In this case, however, the increase of T_C saturates at 7.5 GPa and then decreases, marking the 5*f* instability.

Acknowledgements
This work was supported by the Grant Agency of the Czech Republic under the grant No. P204/10/0330 and by the Grant Agency of the Academy of Sciences under the grant No. IAA100100912.

References
[1] T Honma et al., J. Phys. Soc. Japan 69, 2647 (2000)
[2] T Gouder et al., J. Alloys Comp. 314, 7 (2001)
[3] A Kolomiets et al., Physica B 259-261, 238 (1999)
[4] P Link et al., J.Phys.: Condens. Matter 4, 5585 (1992)
[5] N Sanjay Kumar et al., Phil.Mag.Letters 84, 791 (2004)

Progress in the magnetic study of Np_2Co_{17}

A Hen[1,2], I Halevy[2,3,4], I Orion[2], E Colineau[1], R Eloirdi[1], J-C Griveau[1], P Gaczyński[1], F Wilhelm[5], A Rogalev[5], J-P Sanchez[6], M Winterrose[4], N Magnani[7], A Shick[1,8], R Caciuffo[1]

[1]European Commission, Joint Research Centre, Institute for Transuranium Elements, Postfach 2340, DE-76125 Karlsruhe, Germany
e-mail: amir.hen@mail.huji.ac.il
[2]Nuclear Engineering Department, Ben-Gurion University, IL84105 Beer-Sheva, Israel
[3]Physics Department, Nuclear Research Center - Negev, P.O. Box 9001, IL84190 Beer-Sheva, Israel
[4]California Institute of Technology, W. M. Keck Laboratory 138-78, Pasadena, California 91125, USA
[5]European Synchrotron Radiation Facility (ESRF), Boîte Postale 220, FR-38043 Grenoble, France
[6]SPSMS, UMR-E CEA/UJF-Grenoble 1, INAC, FR-38054 Grenoble, France
[7]Lawrence Berkeley National Laboratory, Chemical Sciences Division, 1 Cyclotron Road, Berkeley, California 94720, USA
[8]Institute of Physics, Academy of Sciences of the Czech Republic, Na Slovance 2, CZ-182 21 Prague, Czech Republic

A neptunium-transition-metal binary compound Np_2Co_{17} has been synthesised and characterised by means of powder x-ray diffraction, ^{237}Np Mössbauer spectroscopy (Figure 1), superconducting-duantum-interference-device magnetometry (SQUID, see Figure 2), and x-ray magnetic circular dichroism (XMCD, see Figure 3).

The compound crystallises in a Th_2Ni_{17}-type hexagonal structure with room-temperature lattice parameters a = 8.3107(1) Å and c = 8.1058(1) Å.

Magnetisation curves indicate the occurrence of ferromagnetic order below $T_C > 350$ K.

Mössbauer spectra suggest a Np^{3+} oxidation state and give an ordered moment of $\mu_{Np} = 1.57(4)\ \mu_B$ and $\mu_{Np} = 1.63(4)\ \mu_B$ for the Np atoms located, respectively, at the 2b and 2d crystallographic positions of the $P6_3/mmc$ space group.

Combining these values with a sum-rule analysis of the XMCD spectra measured at the neptunium $M_{4,5}$ absorption edges, one obtains the spin and orbital contributions to the site-averaged Np moment [$\mu_S = -1.88(9)\ \mu_B$, $\mu_L = 3.48(9)\ \mu_B$].

The ratio between the expectation value of the magnetic-dipole moment and the spin magnetic moment ($m_{md}/\mu_S = +1.36$) is positive as predicted for localised 5*f* electrons and lies between the values calculated in intermediate-coupling (IC) and *jj* approximations.

The expectation value of the angular part of the spin-orbit-interaction operator is in excellent agreement with the IC estimate.

The ordered moment averaged over the four inequivalent Co sites, as obtained from the saturation value of the magnetisation, is $\mu_{Co} \approx 1.6\ \mu_B$.

The experimental results are discussed against the predictions of first-principles electronic-structure calculations (Table 1) based on the spin-polarised local-spin-density approximation plus the Hubbard interaction [1].

Acknowledgements
The high purity Np metals required for the fabrication of the compound were made available through a loan agreement between Lawrence Livermore National Laboratory and ITU, in the frame of a collaboration involving LLNL, Los Alamos National Laboratory and the US Department of Energy.

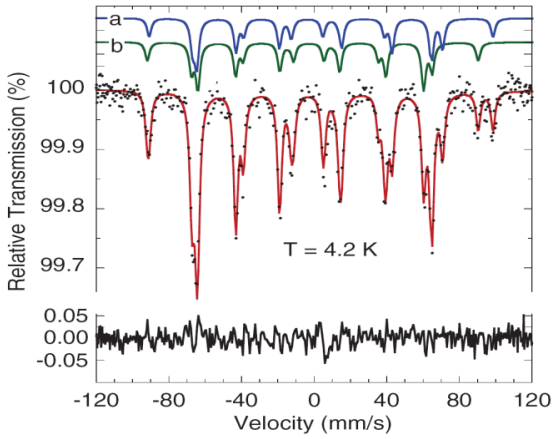

Figure 1. ^{237}Np Mössbauer spectrum of Np_2Co_{17} taken at 4.2 K in the ferromagnetic state, red line - best fit to the data, given by the superposition of component spectra (blue and green lines) conditions.

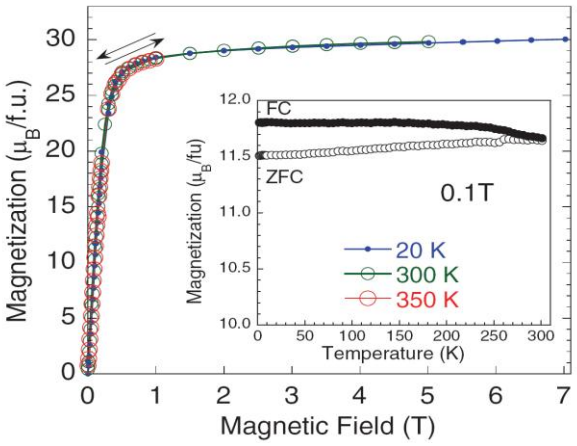

Figure 2. Magnetic field dependence of Np_2Co_{17} magnetisation measured in the range of 20-350 K. Inset - magnetisation temperature dependence measured up to 300 K in a field μ_0H = 0.1 T in field cooled (FC) and zero-field cooled (ZFC).

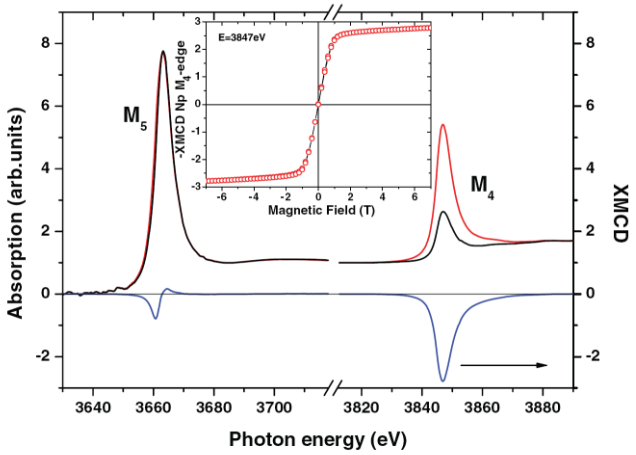

Figure 3. X-ray absorption spectra $\mu^{+,-}$ measured at 50 K at the $M_{4,5}$ Np absorption edges in Np_2Co_{17}. Red line - photon helicity parallel. Black line - antiparallel with respect to a 7T magnetic field applied along the beam direction. Blue line - The XMCD signal, given by $\mu^+ - \mu^-$. Inset - field dependence of the XMCD signal at the M_4 edge.

		LSDA(+SOC)			AMF−LSDA+U			
Atom	Site	μ_S	μ_L	μ	μ_S	μ_L	μ	$\mu_{expt.}$
Np_1	2*b*	−3.15	1.97	−1.18	−1.96	3.50	1.54	1.57(4)
Np_2	2*d*	−3.14	1.87	−1.27	−2.09	3.94	1.85	1.63(4)
Co_1	4*f*	1.58	0.05	1.63	1.59	0.05	1.64	1.58
Co_2	6*g*	1.50	0.08	1.58	1.50	0.09	1.59	1.58
Co_3	12*j*	1.38	0.10	1.48	1.37	0.13	1.50	1.58
Co_4	12*k*	1.50	0.09	1.59	1.51	0.08	1.59	1.58
Total		17.56	5.26	22.82	20.14	9.12	29.26	30.0(5)

Table 1. Spin (μ_S), orbital (μ_L), and total ($\mu = \mu_S + \mu_L$) magnetic moments in the "muffin-tin" spheres around the Np and Co atoms (in μ_B units) together with total values (including interstitial contributions) per formula unit of μ_S , μ_L, and μ. Experimental values obtained from the Np Mössbauer spectra and SQUID-magnetisation measurements are given in the last column.

References

[1] I Halevy et al. Phys. Rev. B. 85, 014434 (2012)

Progress in the magnetic study of Np_2Ni_{17} and $NpNi_5$

I Halevy[1,2,3], A Hen[2,4], I Orion[2], E Colineau[4], R Eloirdi[4], J-C Griveau[4], P Gaczyński[4], M Winterrose[3], N Magnani[5], A Shick[4,6], R Caciuffo[4]

[1]*Physics Department, Nuclear Research Center - Negev, P.O. Box 9001, IL84190 Beer-Sheva, Israel*
e-mail: ihalevyi@caltech.edu
[2]*Nuclear Engineering Department, Ben-Gurion University, IL84105 Beer-Sheva, Israel*
[3]*California Institute of Technology, W. M. Keck Laboratory 138-78, Pasadena, California 91125, USA*
[4]*European Commission, Joint Research Centre, Institute for Transuranium Elements, Postfach 2340, DE-76125 Karlsruhe, Germany*
[5]*Lawrence Berkeley National Laboratory, Chemical Sciences Division, 1 Cyclotron Road, Berkeley, California 94720, USA*
[6]*Institute of Physics, Academy of Sciences of the Czech Republic, Na Slovance 2, CZ-182 21 Prague, Czech Republic*

A neptunium-transition-metal binary compound Np_2Ni_{17} has been synthesised and characterised by means of powder x-ray diffraction (Figure 1), superconducting-quantum-interference-device magnetometry (SQUID, see Figure 2 left), and Cp (see Figure 2 right), ^{237}Np Mössbauer spectroscopy (Figure 3).

The compound crystallises in a Th_2Ni_{17}-type hexagonal structure with room-temperature lattice parameters a = 8.2830(5) Å and c = 8.0403(5) Å.

A minor phase of $NpNi_5$ was identified. A new sample of $NpNi_5$ crystallises in the hexagonal structure with room-temperature lattice parameters a = 4.8397(7) Å and c = 3.9895(7) Å.

Magnetisation and Cp curves of the Np_2Ni_{17} sample indicate the occurrence of magnetic ordering below T_m > 17 K. The homologous Np_2Co_{17} is magnetic near room temperature [1].

Mössbauer spectra suggest a complex magnetic structure in two different isomeric shifts as expected at the 2b and 2d crystallographic positions of the $P6_3/mmc$ space group.

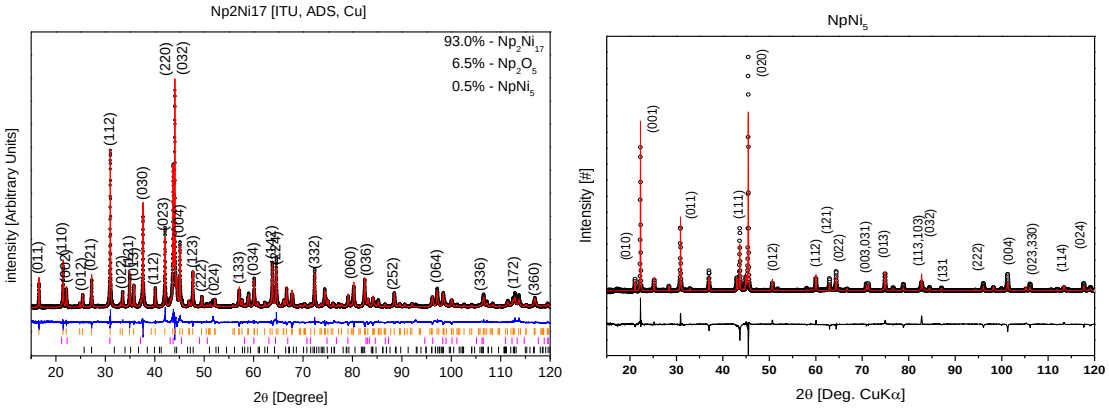

Figure 1. X-ray diffraction spectrum with Rietveld fitting of Np_2Ni_{17} and $NpNi_5$, to the hexagonal structure.

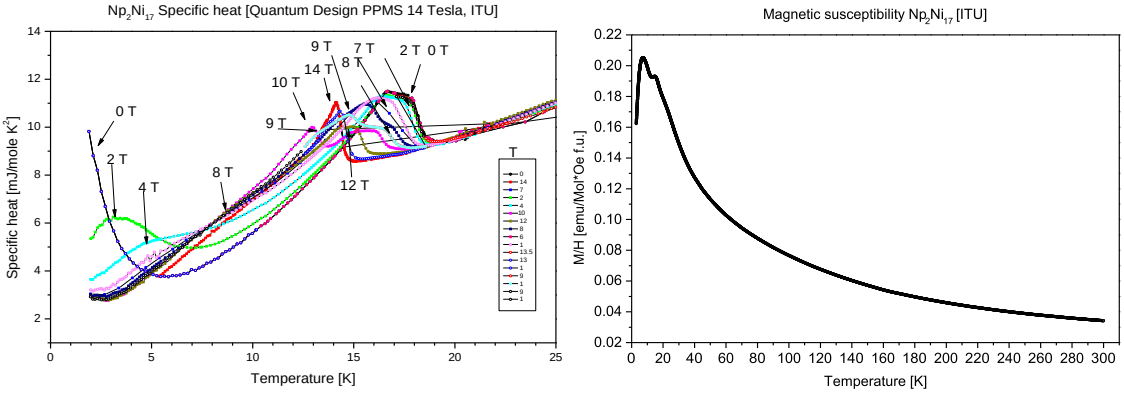

Figure 2. Magnetic susceptibility (right) and Specific heat (left) spectrum of Np_2Ni_{17} sample.

The results obtained suggest a ground state with modulated magnetic moments and the occurrence of spin-flop transitions. Schottky anomaly at 0 field and T < 5 K: presence of low-energy electronic levels. Spin reorientation above T_N, (17K as it was found at the Mössbauer spectrum) at a T for which the Zeeman energy is comparable to the AF exchange energy (3d and 5f moments become parallel).

We are re-measuring the samples trying to avoid oxidation or minor phases to get a clear picture and solve the puzzle.

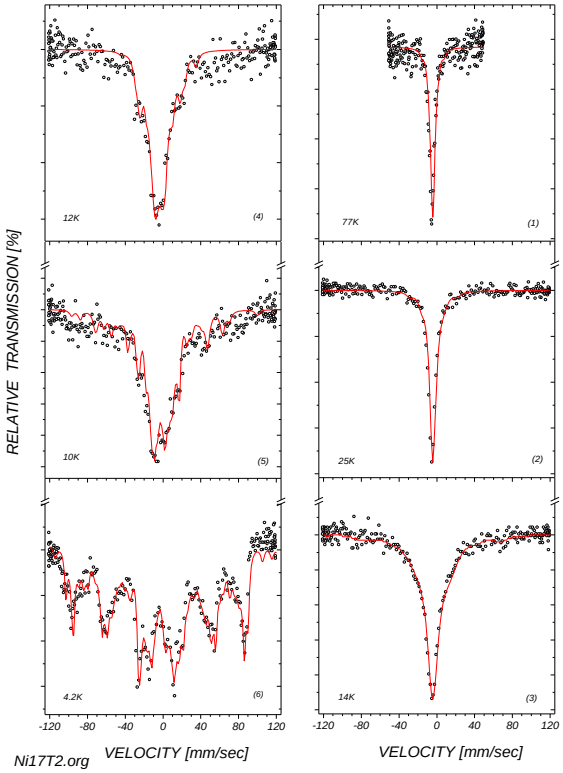

Figure 3. ^{237}Np Mössbauer spectrum of Np_2Ni_{17}, measured in the range of 77-4.2 K. Red line - best fit to the data by five different fields it two different isomer shifts.

References

[1] I Halevy, A Hen, I Orion, E Colineau, R Eloirdi, J-C Griveau, P Gaczy´nski, F Wilhelm, A Rogalev, J-P Sanchez, M Winterrose, N Magnani, A Shick, R Caciuffo Physical Review B 85, 014434 (2012)

Chemistry
Actinide-ligand multiple bond linkages: Recent progress in uranium carbene and nitride chemistry **S Liddle**
Polymorphism in salts of tetraalkylammoniumhexanitratothorium **G Soldani, C Renard, S Grandjean, E Welcomme, F Abraham**
Sorption preconcentration of radionuclides using detonation nanodiamonds **Y Buchatskaya, A Romanchuk, A Shiryaev, I Kulakova, S Kalmykov**
Nanoscale zero-valent iron particles for the remediation of uranium contaminated groundwater **R Crane, I-C Popescu, K Hallam, T Scott**
New ammonium thorium oxalates **F Blanchard, M Rivenet, N Vigier, I Hablot, S Grandjean, F Abraham**

Actinide-ligand multiple bond linkages: Recent progress in uranium carbene and nitride chemistry

S Liddle

School of Chemistry, University of Nottingham, University Park, Nottingham, NG7 2RD, United Kingdom
e-mail: stephen.liddle@nottingham.ac.uk

There is currently great interest in the nature and reactivity of actinide-ligand multiple bond linkages in a molecular context. This is because molecular routes enable mild syntheses of these functional groups, thus avoiding difficult to remove impurities generated by high temperature methods. Uranium carbenes and nitrides are of particular interest because of their relevance to uranium carbides and nitrides which may form the basis for alternative nuclear fuel cycles. In particular, uranium nitride is often cited as providing materials with improved melting points, densities, and thermal conductivities in comparison to uranium oxides. Furthermore, uranium-ligand multiple bond linkages are of interest in terms of the extent of 5f/6d orbital participation and covalency and, by extension, applications in atom efficient catalysis and small molecule activation. However, little is known of the intrinsic nature of U=C and U≡N bonds, and the latter is yet to be reported, yet this information is crucial to understanding the inherent physicochemical properties of these linkages.

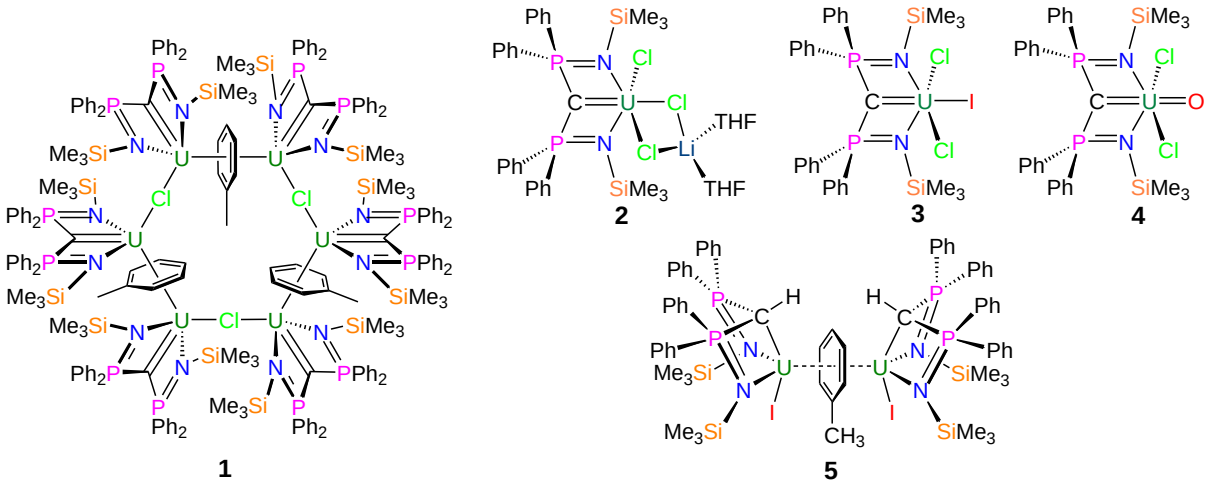

We will present our recent work on uranium carbenes which exhibit U=C double bonds over all commonly accessible oxidation states of uranium (**1**-**4**) [1, 2]. This has enabled us to uniquely probe the nature of these linkages as a function of the oxidation state of uranium and to compare their reactivity to rare earth congeners [3]. Some of these compounds show fascinating magnetism, including single molecule magnetism mediated by a covalent bridge (**5**) [4].

More recent work describing our efforts to isolate a terminal uranium nitride via photolytic and redox routes will be presented; this has resulted in the isolation and characterisation of the first terminal uranium nitride linkage [5].

References

[1] S Liddle et al., Angew. Chem. Int. Ed. 50, 2383 (2011)
[2] S Liddle et al., submitted
[3] S Liddle et al., J. Am. Chem. Soc. 132, 14379 (2010)
[4] S Liddle et al., Nat. Chem. 3, 454 (2011)
[5] S Liddle et al., submitted

Polymorphism in salts of tetraalkylammoniumhexanitratothorium

G Soldani[1,2], C Renard[2], S Grandjean[1], E Welcomme[1], F Abraham[2]

[1]Laboratoire de Chimie et Conversion des Actinides, CEA MARCOULE/DRCP/SCPS, Bat.399, CEA Marcoule, BP 17171, 30207 Bagnols sur Cèze cedex, France
e-mail: guillaume.peter@cea.fr
[2]Unité de Catalyse et de Chimie du Solide, UCCS UMR CNRS 8181, Univ. Lille Nord de France, ENSCL-USTL, B.P. 90108, 59652 Villeneuve d'Ascq Cedex, France

Tetraalkylammonium hexanitratothorium $[Et_4N]_2[Th(NO_3)_6]$, $[Pr_4N]_2[Th(NO_3)_6]$, $[Bu_4N]_2[Th(NO_3)_6]$ were synthesised by mixing the corresponding alkylammonium nitrate with thorium nitrate in nitric acid solution.

The structure of the three compounds was determined using single-crystal x-ray diffraction data. These salts are isostructural to the uranium based compounds [1-2], however a second phase was identified on the x-ray pattern of the as-synthesised powder of $[Pr_4N]_2[Th(NO_3)_6]$. Thermal analyses (TGA-TDA and temperature-dependent x-ray diffraction) demonstrate that the second phase is an intermediate temperature polymorph of the first one (Fig1), the corresponding irreversible phase transition occurring at about 120°C and being succeeded by a reversible phase transition at about 155°C.

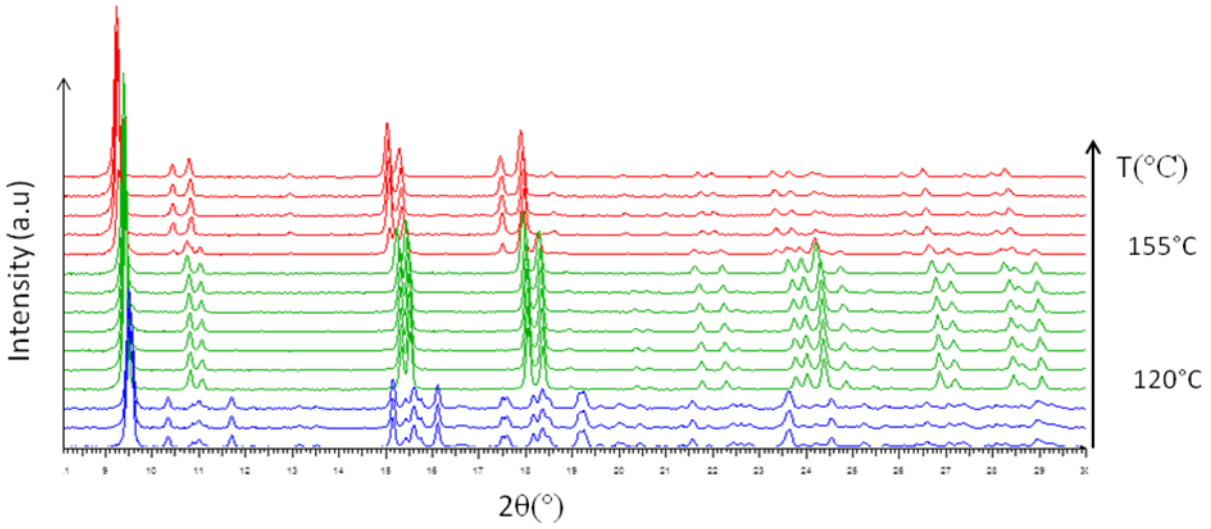

Figure 1. Temperature-dependent x-ray diffraction patterns for $[Pr_4N]_2[Th(NO_3)_6]$ in air atmosphere (heating rate: 5°C.min^{-1}) showing the two phase transitions.

$[Bu_4N]_2[Th(NO_3)_6]$ melts above the irreversible phase transition. The structure of the monotropic systems ($[Pr_4N]_2[Th(NO_3)_6]$, $[Bu_4N]_2[Th(NO_3)_6]$) were determined from x-ray powder diffraction data collected at ambient temperature.

For $[Et_4N]_2[Th(NO_3)_6]$ two reversible phase transitions are observed at 77 and 94°C.

The thermal behaviours of the thorium and uranium analogues are compared.

References

[1] J Rebizant et al., Acta Crystallogr. C 44, 2098 (1988)
[2] M Crawford et al., Inorg. Chem. 48, 10877 (2009)

Sorption preconcentration of radionuclides using detonation nanodiamonds

Y Buchatskaya[1], A Romanchuk[1], A Shiryaev[2], I Kulakova[1], S Kalmykov[1]

[1]Lomonosov Moscow State University, Department of Chemistry, Moscow, 119991, Russia
[2]Frumkin Institute of Physical Chemistry and Electrochemistry of RAS, Moscow, 119071, Russia
e-mail: shiryaev@phyche.ac.ru

Wastewater and groundwater treatment in areas of processing of spent nuclear fuel is one of the most serious actual problems of nuclear energy. To solve this problem in recent years more and more attention is paid to carbon nanomaterials. Nanodiamonds are potentially promising candidate for sorption applications due to their unique properties: high surface area, highly developed surface, low weight, chemical and radiation resistance.

Nanodiamonds (ND) are commercially synthesised by detonation of explosives (for example a mix of 60 wt% trinitrotoluene and 40 wt% hexogen with a negative oxygen balance) in a closed volume. The primary particle size is 4-5 nm. It has a quasispherical shape and a high surface areas (250-300 m^2/g or more). To remove non-carbon and non-diamond impurities the detonation soot undergoes gas- and liquid-phase treatment, which forms various oxygen-containing functional groups on its surface (e.g., [1]). Various types of chemical and physical processes are known and continuously being developed to modify the surface chemistry according to specific applications ([2]). These groups are responsible for the cation-exchange properties of ND. The primary ND particles are prone to aggregation into very stable agglomerates having sizes of several tens nanometers. Such behaviour must be accounted for in all studies and applications involving nanodiamonds.

The purpose of this work is to establish the sorption behaviour of radionuclides (Tc(VII), U(VI), Np(V), Th(IV), Pu(IV), Am(III), Eu(III) and Sr(II)) on detonation ND. In our experiments different types of ND were used: treated with hydrogen, ozone, oxygen and ND with various groups attached to its surface (glycine, imino- and hydroxyl group). ND surfaces were characterised by IR spectroscopy. The values of ζ-potential at different pH of the suspensions and the particle size were measured using dynamic light scattering.

Kinetics of sorption shows that steady state conditions are achieved within first 30 minutes of interaction. Figure 1 shows dependence of actinide sorption on pH suspension. The sorption Is very high for U(VI), Th(IV), Am(III) and Pu(IV) even in the range of pH 1-3.

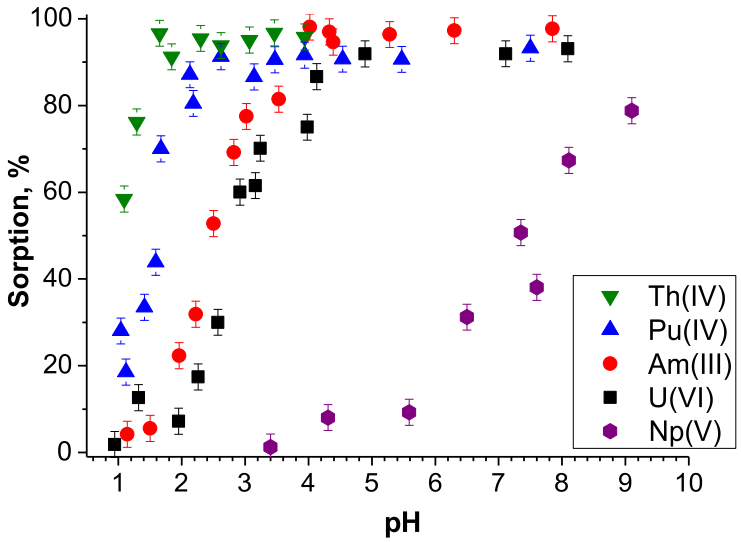

Figure 1. pH-dependence of actinide sorption on non-modified ND.

For Tc(VII), which present in solution in the form of an pertechnetate ion TcO_4^- high sorption was observed only in the strongly acidic pH of 0-1, where ND surface is protonated.

Various methods of purification and modification of ND affect the composition and quantity of surface groups, which may influence the sorption properties. However it was observed that sorption U(VI) on non-modified ND is higher than on modified ND at the same pH.

Efficiency of Tc(VII) sorption onto ND functionalised by different groups is very similar. This effect can be explained by resistance of effective sorption sites to modification. Such similarity contrasts the results reported in [3], where type of the surface treatment was shown to be important.

The role of various surface groups and of aggregate sizes on sorption properties of nanodiamonds will be discussed in detail.

References

[1] V Dolmatov, Russian Chemical Reviews, 70 607 (2001)
[2] I Kulakova, Physics of the Solid State, 46 636 (2004)
[3] Ya Obruchnikova et al., Proc. of 7th Int. Symp. on Technetium and Rhenium - Science and Utilization, Moscow, 439 (2011)

Nanoscale zero-valent iron particles for the remediation of uranium contaminated groundwater

R Crane[1], I-C Popescu[2], K Hallam[1], T Scott[1]

[1]*Interface Analysis Centre, University of Bristol, Oldbury House, 121 St Michaels Hill, Bristol, BS2 8BS, United Kingdom*
e-mail: richard.crane@bristol.ac.uk
[2]*Laboratory of Environment Protection Techniques and Technologies, R&D National Institute for Metals and Radioactive Resources, B-dul Carol I no.70, sector 2, Bucharest 020917, Romania*

Abstract
The increased development and use of engineered nanomaterials has the potential to offer great benefits to society through their exploitation within numerous products developed by diverse industries. Some applications of nanomaterials have the potential to afford environmental benefits and of particular interest is the use of nanoscale particles of zerovalent iron for the *in-situ* cleanup of contaminated land and groundwater.

The current presentation describes a comparative and site specific study for the application of zero-valent iron nanoparticles, zero-valent iron-nickel nanoparticles and magnetite nanoparticles for the remediation of uranium contaminated groundwater taken from the Lişava valley, Banat, Romania. Nanoparticles were introduced to the Lişava groundwater under surface (bench top) and deep (anoxic) aquifer oxygen conditions and synthetic solutions containing uranyl-only and uranyl-carbonate were also tested as simple-system analogues. The batch systems were analysed over a 28 day reaction period during which the liquid samples were tested for changes in Eh/pH/DO and dissolved metal concentrations were determined using ICP-AES and ICP-MS. Extracted solid samples were also tested using Raman spectroscopy, XPS and XRD to determine the mechanism of uranium sorption and nanoparticle corrosion product evolution.

The results provide clear evidence that both zero-valent iron nanoparticles and zero-valent iron-nickel nanoparticles are highly effective for the rapid removal of uranium from the Lişava groundwater despite the presence of appreciable concentration of complexing agents (namely carbonate) within the water. In comparison, the nanoscale magnetite particles were recorded to have limited ability to remove uranium from the Lişava groundwater, which is attributed to the presence of Fe^0 within both the zero-valent iron nanoparticles and the zero-valent iron-nickel nanoparticles, providing an additional and active source of electrons for aqueous reaction and associated contaminant removal. Despite high uranium removal recorded in the early stages of the reaction period (timescales less than approximately 1 week) for both the zero-valent iron nanoparticles and the zero-valent iron-nickel nanoparticles, for longer timescales, significant uranium re-release was recorded for systems under surface aquifer oxygen conditions. In comparison, minimal uranium re-release was recorded for all systems containing deep aquifer oxygen conditions. Results demonstrate that for waters containing appreciable concentrations of complexing agents, namely dissolved carbonate, this re-release of uranium following a period of "apparent remediation" is driven by the ingress of atmospheric oxygen and other associated gases (including CO_2) back into the experimental solutions, facilitating the reformation of thermodynamically stable uranyl carbonate complexes.

The results presented in the current work demonstrate that, in principle, iron nanoparticles can be applied as a highly efficient tool for the remediation of uranium contaminated groundwater. However, with complexing agents such as carbonate ubiquitous in the natural environment, clear evidence is presented that further work is required in order to develop suitable nanoparticle physico-chemical modifications and/or deployment strategies to prevent uranium remobilisation during the *in-situ* treatment of uranium contaminated groundwater in the vadose (oxygenated) zone.

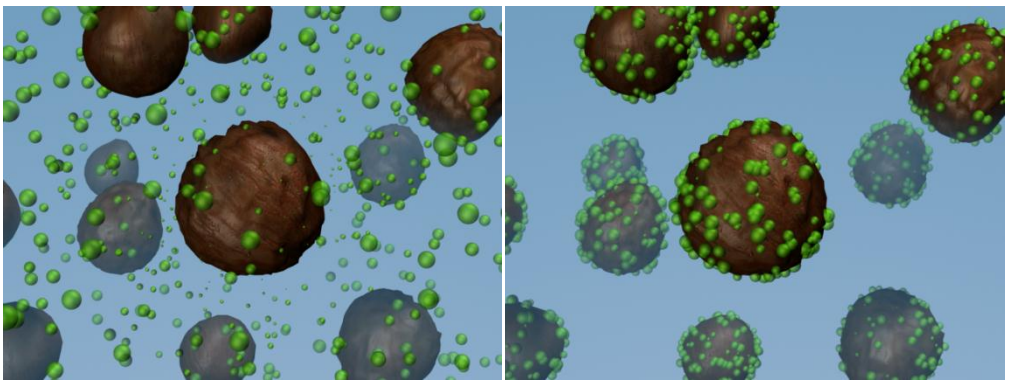

Figure 1. Graphic representation of the uptake of aqueous uranium onto the surface of iron nanoparticles.

New ammonium thorium oxalates

F Blanchard[1,2], M Rivenet[1], N Vigier[2], I Hablot[2], S Grandjean[3], F Abraham[1]

[1]Univ. Lille Nord de France, Unité de Catalyse et de Chimie du Solide, UCCS - UMR CNRS 8181, ENSCL-USTL, BP 90108, 59652 Villeneuve d'Ascq Cedex, France
E-mail: florent.blanchard@ed.univ-lille1.fr
[2]AREVA,1 Place Jean Millier, 92084 Paris La Défense, France
[3]CEA, Nuclear Energy Division, RadioChemistry & Processes Department, Laboratoire de Chimie et Conversion des Actinides, Bat.399, BP 17171, 30207 Bagnols sur Cèze cedex, France

Thermal decomposition of oxalate precursors is largely used to prepare various oxides such as porous stabilised zirconium dioxide, piezoelectric $BaZrO_3$ or $PbZrO_3$ ceramics, high temperature YBCO superconductors, rare-earth doped zirconia for SOFC solid electrolytes, actinide dioxide for Gen. IV mixed oxide-based nuclear fuels…

In this last application, the behaviour of actinides in oxalic acid is very important. If a lot of academic studies have been dedicated to U(VI), those concerning U(IV) oxalates are rarer due to the oxidation of U(IV) to U(VI) in nitric medium using dedicated laboratory synthesis methods. So, to obtain new actinide (IV) oxalates, in a first step, we favoured synthesis of Th(IV) oxalates in various conditions.

Three different Th-oxalate based compounds were synthesised by dissolving thorium nitrate in water and adding ammonium oxalate (until the amount of oxalate/Th is above 4). The solution was let to evaporate in order to initialise crystallisation.

When hydrogen peroxide is added to the mixture, the first compound which forms is $(NH_4)_3CaTh(C_2O_4)_{4,5}.xH_2O$. As no calcium was preliminary added to the solution, it shows that this compound precipitates the calcium cations initially present as traces in thorium nitrate. The crystal structure of two $(NH_4)_3CaTh(C_2O_4)_{4,5}.xH_2O$ isomorphs could be determined by single crystal x-ray diffraction.

By further evaporation, a second compound formed as a powder of composition $(NH_4)_2Th_2(C_2O_4)_5.nH_2O$, isomorphic to $(NH_4)_2U_2(C_2O_4)_5.nH_2O$ [1].

Finally, $(NH_4)_4Th(C_2O_4)_4.4H_2O$ is obtained. Crystals were harvested just before complete evaporation in order to determine their structure by single-crystal x-ray diffraction. It is a chain-like compound ever found with potassium [2] or guanidinium [3].

A summary of the different compounds forming during the progressive evaporation of solution is shown in Figure 1.

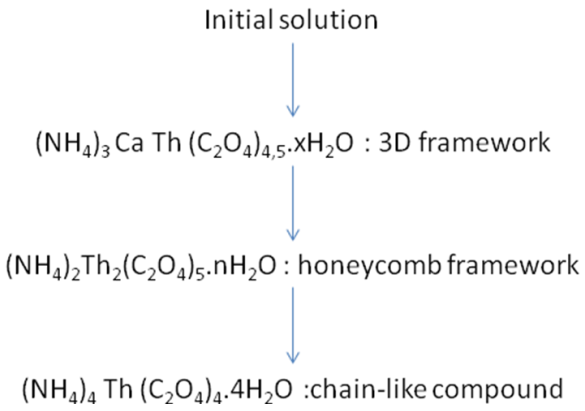

Figure 1. Crystallisation sequence during evaporation of the initial thorium-oxalate solution.

References

[1] B Chapelet-Arab, G Nowogrocki, F Abraham, S Grandjean, Journal of Solid State Chemistry, 178, 3046-3054 (2005)
[2] M Akhtar, A Smith, Acta Cryst., B31, 1361-1366 (1975)
[3] G Andreev, N Budantseva, A Fedoseev, P Moisy., Inorg. Chem., 50, 11481-11486 (2011)

Physics 4
Superconductivity in the cubic γ-phase uranium molybdenum alloys synthesised by ultrafast cooling **I Tkach, N-TH Kim-Ngan, S Mašková, L Havela, A Warren, C Stitt, T Scott**
Development of new generation of radio-luminescence emitters based on durable actinide-doped crystals **J Ipatova, B Burakov, M Petrova, V Zirlin, Y Kuznetsova, M Zamoryanskaya**
Time-resolved laser induced chemiluminescence spectroscopy and detection of actinides in solutions **I Izosimov, N Gorshkov, V Mikhalev, S Nekhoroshkov, Yu Trifonov, N Firsin**

Superconductivity in the cubic γ-phase uranium molybdenum alloys synthesised by ultrafast cooling

I Tkach[1], N-T Kim-Ngan[1,2], S Mašková[1], L Havela[1], A Warren[3], C Stitt[3], T Scott[3]

[1]*Faculty of Mathematics and Physics, Charles University, Ke Karlovu 5, 12116, Prague, Czech Republic*
e-mail: ilimp@yandex.ru
[2]*Institute of Physics, Pedagogical University, Podchorazych 2, 30-084 Krakow, Poland*
[3]*Interface Analysis Centre, University of Bristol, Oldbury House, 121 St Michael's Hill, Bristol, BS2 8BS, United Kingdom*

Uranium can exists in three allotropic phases, namely α - (orthorhombic), β - (tetragonal) and γ - (body-centred cubic). γ-uranium phase is thermodynamically stable in the temperature range 1048-1408 K. The metastable γ-phase can be retained at room temperature by doping 0-35 at.% of Mo and fast cooling (from the high-temperature solid solution to room temperature) [1].

To prepare samples with various Mo concentrations (0-15 at.%) we use splat cooling technique with cooling rate of 10^6 K/sec. X-ray diffraction (XRD) and electron backscattering diffraction (EBSD) analysis indicated that ultrafast cooling has a clear tendency to yield more γ-phase comparing to conventional quenching. Small amount of it was preserved even in pure U specimen (i.e. without Mo doping). With 11-12 at.% Mo, the sample revealed the modified tetragonal structure of the cubic phase (the γ^o phase). A pure γ-phase was stabilised by alloying with 15 at.% Mo [2, 3]. In this work we present the electrical resistivity, magnetic susceptibility and specific-heat of the γ-phase U-Mo alloys. As superconductivity had been detected at such phases [4], we focus on superconducting phase transitions.

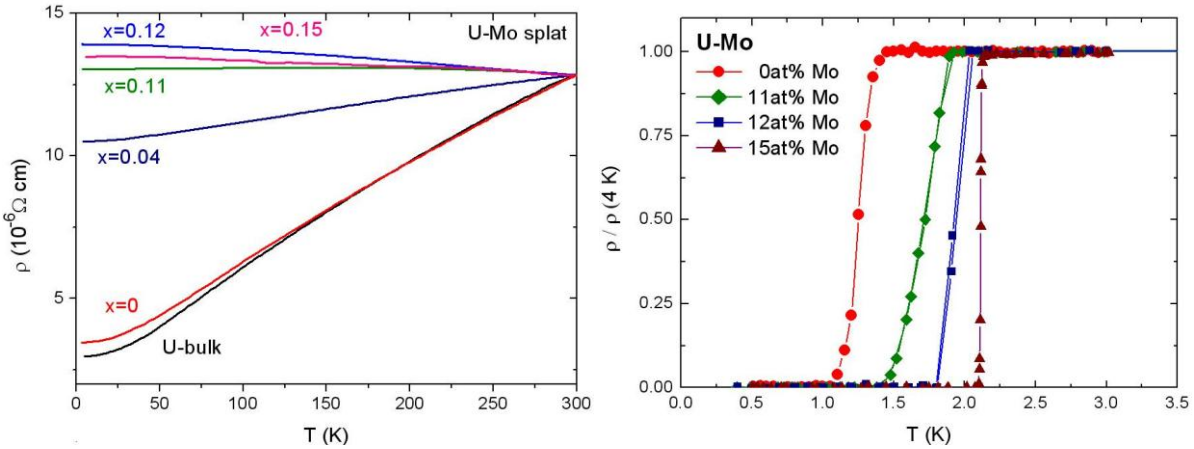

Figure 1. a) Temperature dependence of electrical resistivity (normalised to the value for pure U bulk sample at 300 K). b) Low-temperature dependence of resistivity (normalised to the value in the normal state at 4 K).

Electrical resistivity in the normal state increases with increasing Mo concentration, which can be attributed to an atomic disorder and/or disorder imposed by ultrafast cooling. The disorder also leads to progressive flattening of $\rho(T)$, amounting even into a negative slope ($d\rho/dT < 0$) for alloys with $x \geq 11$ at.% Mo. (Figure 1a), which is regularly observed in alloys with very strong scattering. Low-T resistivity exhibits superconductivity at all samples, from T_c=1.24 K (pure U splat) to 2.11 K (x = 0.15) with a quite sharp transition (Figure 1b). We also observed the shift of T_c to lower temperatures in applied magnetic fields (see Figure 2a). The H_c(T) dependence for the U-Mo alloys revealed neither a quadratic dependence as the temperature approaches 0 K expected for type-I superconductors, nor a linear dependence typically exhibited by strongly interacting Fermi liquid superconductors e.g. U_6Fe. We can tentatively conclude that we observe two different types of superconductivity, one type in α-U, not necessarily intrinsic, which has lower T_c and critical field. The other type, belonging to the *bcc* phase, has a higher T_c and much higher critical field. It would be interesting to follow the development of the two types of superconductivity in mixed-phase samples. This cannot be performed by resistivity studies - the phase with lower T_c remains

invisible in a two-phase material. That is why we turned to specific-heat measurements, which were performed down to 400 mK (Figure 2b). The most pronounced anomaly appears for 15% Mo. Its temperature coincides with T_c from el. resistivity. The size of the step ΔC even exceeds the BCS prediction $1.43*\gamma_e T_c$. Although the U-12 at.% Mo alloy exhibits the mixed ($\gamma^o + \gamma$) phase, we observed only one broad, the shape of which indicates possible inhomogeneities. 11% Mo exhibits clearly two broad anomalies, at 1.7 K and 1.0 K, respectively. Before more detailed structure characterisation we cannot decide whether they belong to coexisting $\gamma^o + \gamma$ phases (with variable Mo concentrations) or if □-U type of superconductivity enters the game. Only a weak and broad shoulder around 0.7 K, i.e. much below the resistivity T_c = 1.3 K, indicates that here the superconductivity is inhomogeneous and probably not intrinsic.

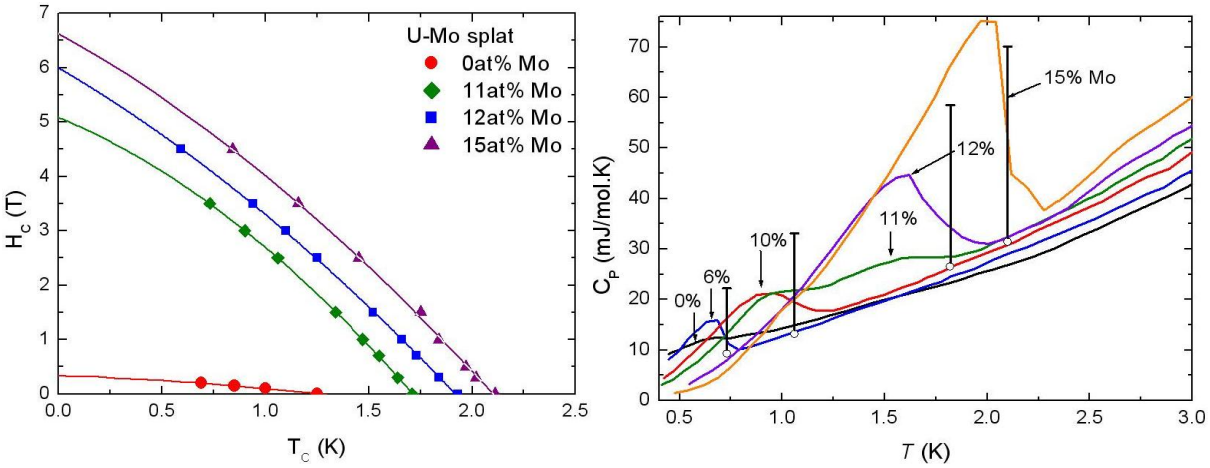

Figure 2. a) Field dependence of the critical magnetic field H_c. b) Superconducting phase transitions seen in specific heat. The vertical bars indicate the theoretical BCS values $1.43*\gamma_e T_c$, calculated using the experimental Sommerfeld coefficients γ_e.

Specific heat measured in the temperature range of 4-300 K shows no anomalies related to charge density wave transitions (observed in pure uranium single crystal) [5]. The Sommerfeld coefficient of electronic specific heat (γ_e) and Debye temperature was estimated from the linear fit of C_p/T vs. T^2 (in the range 16 - 100 K^2). For pure U splat γ_e = 11.0 mJ/mol K^2, in a good agreement with data for the bulk sample (11.2 mJ/mol K^2), but higher than that for uranium single crystal (9.13 mJ/mol K^2) [5]. For sample U-15 at.% Mo γ_e = 16.0 mJ/mol K^2 (i.e. 18.8 mJ/mol U K^2) which is a clear evidence of an increase of density of states at the Fermi level for γ-U. That can be ascribed to the increasing atomic volume (meaning U-U spacing), and consequently a narrower 5*f*-band.

Magnetic susceptibility was measured in temperatures from 4 K to 300 K. It does not reveal any anomalies. A weak paramagnetic behaviour was observed for all splat samples with values of magnetic susceptibility approximately $5*10^{-9}$ m^3/mol.

References

[1] V Sinha et al., J. Alloys Comp. 253-262, 506 (2010)
[2] I Tkach et al., submitted to J. Alloys Comp
[3] N-T Kim-Ngan et al., abstract at this conference
[4] B Chandrasekhar, J.K. Hulm, J. Phys. Chem. Solids. 7 259-267 (1958)
[5] J Lashley et al., Phys.Rev. B 63, 224510 (2001)

Development of new generation of radio-luminescence emitters based on durable actinide-doped crystals

J Ipatova[1], B Burakov[1], M Petrova[1], V Zirlin[1], Y Kuznetsova[2], M Zamoryanskaya[2]

[1]V.G. Khlopin Radium Institute, 28, 2-nd Murinskiy Ave., St. Petersburg, 194021, Russia
ipatova-julia@yandex.ru
[2]Ioffe Physico-Technical Institute, Russian Academy of Sciences, 26, Polytechnicheskaya Street, St. Petersburg, 194021, Russia

Introduction

Some solids may emit luminescence under external or internal ionising irradiation. This effect used to apply in first generation of radio-luminescence emitters consisted of separate parts: non-radioactive solid material doped with luminescence ion(s) and radionuclide in the form of sintered powder, ceramic or film [1]. Main disadvantage of regular light emitters is their short-term use (10-20 years) related to low resistance of luminescence material to radiation damage. Crystalline materials with high chemical resistance, mechanical durability, and stability under self-irradiation are very promising for development of new generation of radio-luminescence emitters. The most important requirement to such emitters is their durability in environment. In order to create environmentally friendly long-lived light-emitters we have suggested incorporating the actinides and non-radioactive luminescence ions in common durable crystalline matrix in the form of solid solution [2-6]. Durable crystals, which intensively glow in the dark, are advanced materials for use in optical couplers, robotics, medicine and other fields. Intensive radio-luminescence might be converted into electric current that allows development of reliable "nuclear" batteries. Such nuclear batteries can potentially be used in aggressive chemical media as well as for applications in space for dozens to hundreds of years. The main difficulty related to development of self-glowing crystals is to determine the optimal balance between the amounts of actinides initiating the glowing process and the non-radioactive luminescence ion supporting intensive scintillation [2-6]. Too high an admixture of luminescence ion can suppress scintillation. Similar behaviour is also found for excessive admixture of actinides. In addition, a high content of radionuclides may cause more rapid radiation damage of crystalline structure that has a negative effect not only on glowing but also on the chemical and mechanical durability of crystal matrix. It was suggested that content of ^{238}Pu and ^{241}Am in self-glowing crystals in any case should not exceed 0.1 wt. %. Admixture of ^{239}Pu and ^{237}Np can be accepted at the level of several wt. %. Well known durable actinide host phases initially proposed for actinide immobilisation [5] such as zircon, (Zr,…)SiO_4; zirconia, (Zr,…)O_2; monazite, (Ln,…)PO_4 and xenotime, (Y,…)PO_4, were selected for our research. It was demonstrated [2-6] that non-radioactive crystals doped with an optimal amount of luminescence ions can be used as starting precursors for the synthesis of self-glowing crystals. The use of cathodoluminescence (CL) method allows for the identification of the optimal amount and type of luminescence ion(s) incorporated in any non-radioactive crystals [2]. This paper summarises results on synthesis and study of different single crystals such as zircon, monoclinic zirconia, monazite and xenotime doped with different amount of actinides (^{239}Pu, ^{238}Pu, ^{241}Am, ^{237}Np) and non-radioactive luminescence ions (Tb and Eu).

Experimental details, results and discussion

All single crystal samples of zircon were synthesised by the flux method [7]. Some crystals were selected for electron microprobe analysis and CL investigations. Actinide contents in the crystals were measured by precise gamma-spectroscopy. The relative self-glowing intensity of the different radioactive samples was evaluated visually (Figure 1). Principal features of crystals synthesised are shown in Figure 2.

Conclusions

1. Intensively glowing crystals of zircon, xenotime and monazite doped with ^{238}Pu or ^{241}Am were successfully obtained. Actinide contents in these crystals did not exceed 0.1 wt.%. Crystals doped with ^{237}Np or ^{239}Pu were not characterised with self-glowing.
2. Study of optimal balance between actinide content and amount of non-radioactive luminescence ion(s) should allow obtaining relatively low radioactive crystals with intensive radioluminescence.

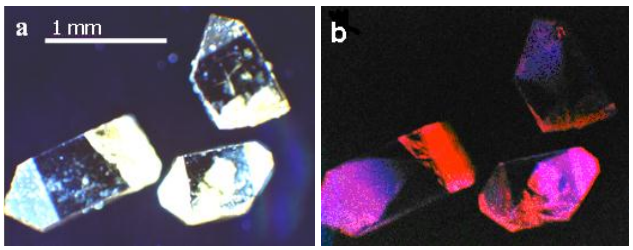

Figure 1. Crystals of zircon (Zr,^{238}Pu,Eu)(Si,P)O_4: a) in the light and b) self-glowing in the dark.

Crystal	Formula	Average content of luminescence ion, wt. %	Content of actinide, wt. %	Relative intensity of self-glowing
zircon	(Zr,Tb,Pu)(Si,P)O_4	Tb – 0.2-0.3	^{238}Pu – 0.02	very high
	(Zr,Eu,Pu)(Si,P)O_4	Eu – 0.1	^{238}Pu – 0.02	weak
		Eu – 0.1	^{238}Pu – 0.01	weak
		Eu – 0.3	^{238}Pu – 0.01	high
	(Zr,Eu,Pu)(Si,P)O_4	Eu – 0.1	^{238}Pu – 0.01	weak
	(Zr,Eu,Pu)(Si,P)O_4	Eu – less 0.01	^{239}Pu – 8-10	no
	(Zr,Am,Np)SiO_4	no	^{237}Np – 0.35; ^{241}Am – 0.01	weak
	(Zr,Np)SiO_4	no	^{237}Np – 1.9	no
	(Zr,Tb,Eu,Am)(Si,P)O_4	Tb – 0.2-0.3 Eu – less 0.1	^{241}Am – 0.002	weak
zirconia	(Zr,Tb,Pu)O_2	Tb – 0.02	^{238}Pu – 0.03	weak
	(Zr,Eu,Pu)O_2	Eu – 0.4	^{238}Pu – 0.01	weak
xenotime	(Y,Eu,Pu)PO_4	Eu – 1.8	^{238}Pu – 0.1	very high
	(Y,Eu,Pu)PO_4	Eu – 0.03	^{238}Pu – 0.002	weak
monazite	(Eu,Am)PO_4	Eu – main element	^{241}Am – 0.04	high
	(Eu,Pu)PO_4		^{238}Pu – 4.9	weak
	(Eu,Am)PO_4		^{241}Am – 0.39	high

Figure 2. Principal features of self-glowing crystals.

References

[1] G Mihalchenko (1988) Radio-luminescence emitters, Energoatomizdat, Moscow (in Russian)

[2] B Burakov, V Garbuzov, A Kitsay, V Zirlin, M Petrova, Ya Domracheva, M Zamoryanskaya, E Kolesnikova, M Yagovkina, M Orlova (2007) Semiconductors, 41, # 4, 427-430

[3] B Burakov, Ya Domracheva, M Zamoryanskaya, M Petrova, V Garbuzov, A Kitsay, V Zirlin (2009) J. Nucl. Mater. 385, 134-136

[4] B Burakov, M Zamoryanskaya, Ya Domracheva (2009) Mat. Res. Soc. Symp. Proc. Scientific Basis for Nuclear Waste Management XXXIII, 1193, 3-8

[5] B Burakov, M Ojovan, W Lee (2010) Crystalline materials for actinide immobilization. Imperial College Press, Materials for Engineering, Vol. 1

[6] B Burakov, J Ipatova, M Petrova, M Zamoryanskaya, Y Kuznetsova (2012), Mat. Res. Soc. Symp. Proc. Scientific Basis for Nuclear Waste Management XXXV (in press)

[7] J Hanchar, B Burakov, E Anderson, M Zamoryanskaya (2003) Mat. Res. Soc. Symp. Proc. Scientific Basis for Nuclear Waste Management XXVI, 757, 215-225

Time-resolved laser induced chemiluminescence spectroscopy and detection of actinides in solutions

I Izosimov, N Gorshkov, V Mikhalev, S Nekhoroshkov, Yu Trifonov, N Firsin

Khlopin Radium Institute, 2nd Murinscii avn. 28, St. Petersburg, 194021, Russia
e-mail: izig@mail.ru

Recently a new procedure of detection of lanthanides and actinides in solutions based on laser induced chemiluminescence was proposed [1, 2]. Chemiluminescence of luminol was initiated by excited actinides species. Pulsed laser radiation was used for actinides excitation. Appropriate selectivity in detection of actinides in solutions can be reached when absorption bands of ions in visible range caused by transitions of the inner 5f electrons are used for initiation of chemiluminescence. However, absorption of one quantum of visible light cannot impart the energy sufficient for chemiluminescence initiation. This energy can be reached when actinide complex absorbs two or more quanta of laser radiation in visible range.

Experiments on two-quantum excitation of chemiluminescence with participation of U(IV) and Pu(IV) species in solutios were performed on an installation consisting of a pulse nitrogen laser OBB 1010 with pulse length of 1 ns and pulse power approximately 1.4 MW and two dye lasers OBB 1012 and OBB 1011. Radiation generated by nitrogen laser came through a beam splitter to two dye lasers. This scheme allowed synchronisation of laser pulses in a cuvette within an accuracy of 10 ps at a pulse length of 0.8 ns generated by laser OBB 1012 and 1 ns for radiation generated by laser OBB 1011. Laser beams from two dye lasers were directed into a cuvette 1cm in thickness in the opposite direction to each other. Chemiluminescence radiation of luminol was collected with a lens whose optical axis was aligned to an angle of approximately 39° to the direction of laser beams and through flexible optical fibre was transferred to the entrance aperture of double prismatic monochromator DMR-4. Chemiluminescence was detected at a wavelength of 460 nm in the mode of quantum counting with the use of strobe technique. The strobe duration was 10 μs, delay time, 2 μs.

The spectrum of chemiluminescence excitation by the scheme two steps-two colours for a solution containing U(IV) and luminol is presented in Figure 1. Laser OBB 1011 operated at a fixed wavelength of 500 nm. Wavelength of radiation generated by laser OBB 1012 was varied in the limits of analytical absorption band of U(IV) with a maximum at 650 nm. The spectrum of chemiluminescence excitation obtained in retuning of generation wavelength of the second laser is similar to the absorption spectrum of uranium. The presence of absorption band of U(IV) in the range of retuning of the second laser results in appearance of a peak of luminol chemiluminescence. One can see (Figure 1) that the selectivity of chemiluminescence excitation reached in our experiments is caused by the features of absorption spectra of U(IV). This fact allows using highly sensitive chemiluminescence procedure for selective detection of various valence actinide species in solutions based on individual features of their absorption spectra.

A possibility of chemiluminescence initiation as a result of excitation of Pu(IV) with two dye lasers was studied for a solution containing 3.6 M CsF, luminol, and Pu(IV) as an example. A choice of this solution composition was caused by an effort to provide favorable conditions for chemiluminescence of luminol since pH of fluoride medium is sufficiently high and colloidal hydrolysed species of Pu(IV) are not formed. The first laser OBB 1011 operated at radiation wavelength of 490 nm. The wavelength of the second dye laser was varied from 630 to 660 nm (dye PLD-640). This choice of the wavelength range of the second laser was caused by the fact that Pu(IV) has strong absorption band in this range. When the mechanism two steps-two colour is realised the dependence of chemiluminescence intensity on wavelength reproduces the counter of absorption band of Pu(IV), i.e. we realised selective excitation of chemiluminescence and this selectivity is caused by the features of absorption spectra of Pu(IV) solutions.

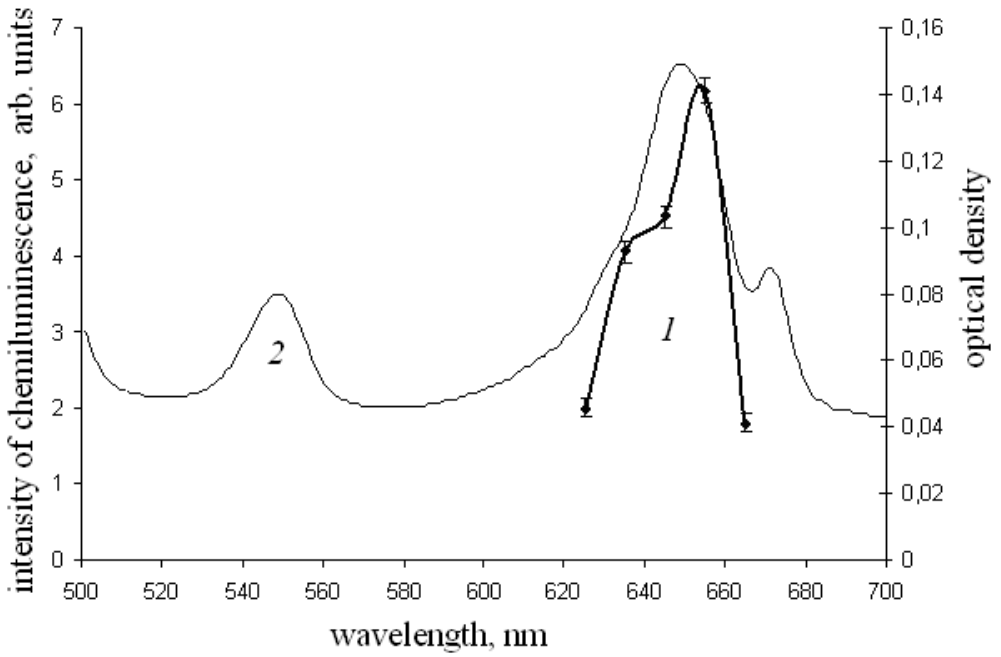

Figure 1. Two-step excitation of chemiluminescence in a solution containing luminol, U(IV), and 0.3 M HCl. (1) Spectrum of chemiluminescence excitation. Wavelength of generation of the first laser 490 nm, wavelength of generation of the second laser is varied. (2) Absorption spectrum of U(IV) solution in 0.3 M HCl.

Selective excitation of chemiluminescence excitation allows us to use chemiluminescence procedure as a method for selective detection of actinides in various valent states and molecular forms in solutions.

This work was financially supported by the ISTC (project no. 3694).

References

[1] I Izosimov, Phys. Part. Nucl., 38, 177 (2007)
[2] I Izosimov et al., Proc. Int. Conf. Actinides 2005, Manchester, UK, 2005, p.779

Fuels
Plenary lecture **G Allen**
Stabilisation of cubic γ-phase uranium molybdenum alloys by splat-cooling technique **N-T Kim-Ngan, I Tkach, S Mašková, L Havela, A Warren, C Stitt, T Scott**
Thermodynamic investigations of the (Th, U)O_2 solid solution **O Vălu, O Beneš, R Konings**
The study of thermal cycling effect on the stability of a δ-stabilised Pu-Ga alloy **M Ling**

Plenary lecture

G Allen

Interface Analysis Centre, University of Bristol, Oldbury House, 121 St. Michael's Hill, Bristol, BS2 8BS, United Kingdom

Stabilisation of cubic γ-phase uranium molybdenum alloys by splat-cooling technique

N-T Kim-Ngan[1], I Tkach[2], S Mašková[2], L Havela[2], A Warren[3], C Stitt[3], T Scott[3]

[1]Institute of Physics, Pedagogical University, Podchorazych 2, 30-084 Krakow, Poland
e-mail: tarnawsk@mag.mff.cuni.cz
[2]Faculty of Mathematics and Physics, Charles University, Ke Karlovu 5, 12116 Prague, Czech Republic
[3]Interface Analysis Centre, University of Bristol, Oldbury House, 121 St. Michael's Hill, Bristol, BS2 8BS, United Kingdom

U-Mo alloys with Mo concentration in the range 0 - 5 at.% Mo (x = 0 - 0.15) were synthesised using a splat-cooling technique with a cooling rate of the order of 10^6 K/s. Phase analysis using x-ray diffraction (XRD) indicated the presence of a small amount of (cubic) γ-U phase retained at room temperature alongside the majority (orthorhombic) α-U phase in the splat-cooled pure-U specimen (x = 0). The double-phase (α+γ) structure with predominance of the α-phase was obtained in the alloys with $x \leq 0.10$. Increasing further Mo doping leads to the transformation to the (body centred tetragonal) γ^o phase for x = 0.11 - 0.12 and pure (cubic) γ phase for x = 0.15 [1]. Scanning electron microscopy (SEM) and electron back-scatter diffraction (EBSD) analysis performed on the samples with x = 0, 0.15 corroborated the XRD results. Namely, the splat-cooled pure uranium (x = 0) revealed a predominantly α-U structure with rare, isolated grains of γ-U typically no more than 1 μm in maximum dimension, while the data for U-15 at.% Mo alloy (x = 0.15) clearly indicated the presence of a γ-U phase structure with no evidence for α or α-related phases. EBSD maps recorded and highlighting the unusual microstructures of these two samples are shown in Figure 1.

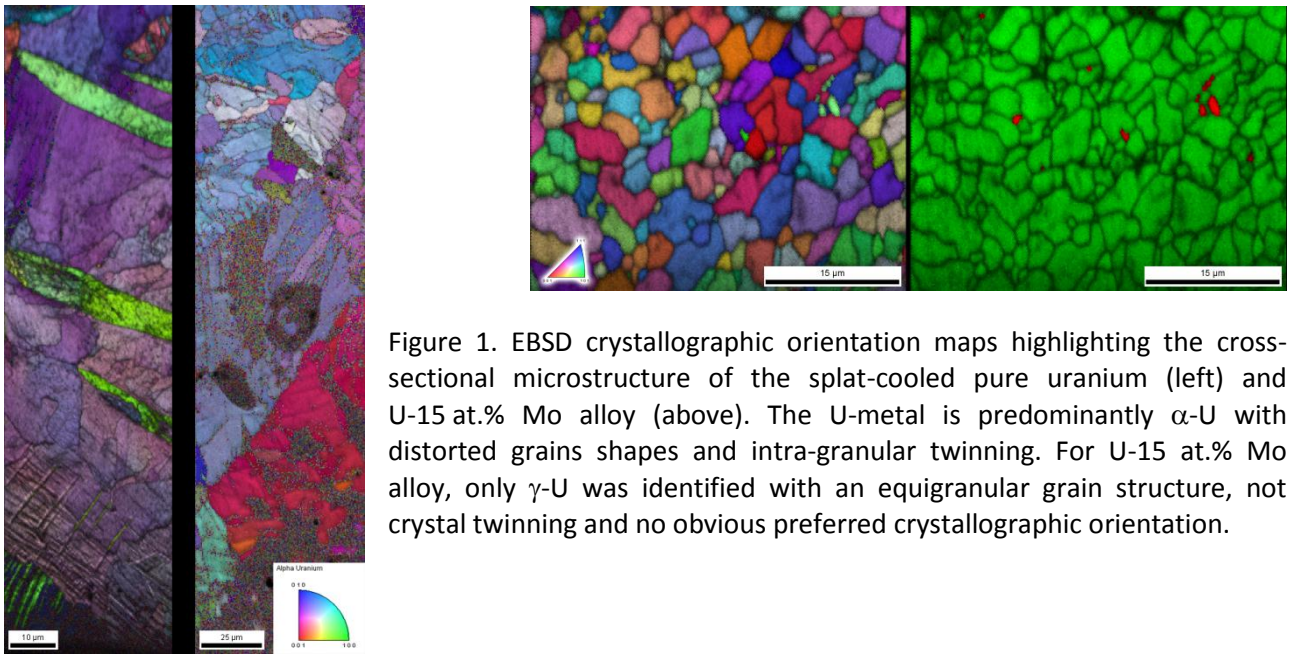

Figure 1. EBSD crystallographic orientation maps highlighting the cross-sectional microstructure of the splat-cooled pure uranium (left) and U-15 at.% Mo alloy (above). The U-metal is predominantly α-U with distorted grains shapes and intra-granular twinning. For U-15 at.% Mo alloy, only γ-U was identified with an equigranular grain structure, not crystal twinning and no obvious preferred crystallographic orientation.

The U-Mo splats become superconducting with T_c ranging from 1.24 K (for pure U-specimen) to 2.11 K (for 15 at.% Mo) [1, 2]. The $H_{c2}(T)$ dependence for the U-Mo alloys revealed neither a quadratic dependence as the temperature approaches 0 K expected for type-I superconductors, nor a linear dependence typically exhibited by strongly interacting Fermi liquid superconductors e.g. U_6Fe.

No change in the XRD patterns of the pure-U splat was observed upon annealing at 500°C up to annealing time (t) of 144 h. Namely, all the γ reflections are preserved upon annealing (Figure 2a). For both U-12 at.% and 15-at.% Mo alloy, the reflections of the orthorhombic α-phase (e.g. α(021) and α(002)) already appeared upon annealing for 4 h at 500°C. Increasing the annealing time (t = 10, 72, 144 h) leads to increase of intensities of all α-U reflections. For U-12 at.% Mo alloy, the double γ peak (γ(110) and γ(101) assigned to the γ^o phase) became one broad peak and shifted towards a higher reflection angle (t = 10 h). Upon further annealing such a peak was split into two separated peaks (Figure 2b) assigned as γ'(110) and

γ'(110) reflection of the ordered body centred tetragonal phase (U_2Mo intermetallic). In the case of U-15 at.% Mo alloy, only a small broadening of the γ(110) reflection appears, although a similar shift towards higher angles was also observed (Figure 2c). Further annealing leads to increase of the α-U reflections and appearance of the ordered body centred tetragonal phase (U_2Mo intermetallic).

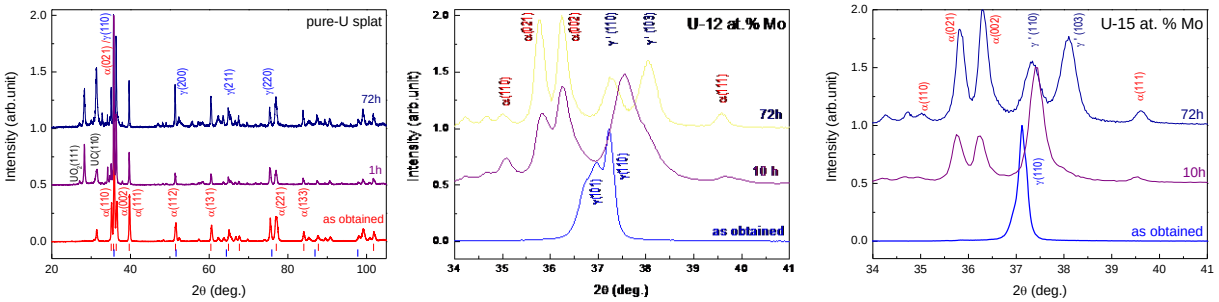

Figure 2. Comparison the x-ray diffraction patterns of splat-cooled U-Mo alloys in the as-obtained state with those upon annealing at 500°C for different time: (a) pure-U (all reflections), (b) U-12 at.%Mo and (c) U-15 at.% Mo (low angle reflections). The (colour) vertical lines indicate the main peak positions for the orthorhombic (red) and cubic (blue) structures.

Besides annealing, H absorption at room temperature was tested. Unlike α-U, the *bcc* phase does not absorb any H at pressures below 1 bar.

Our study opens a new possibility of stabilising the γ-phase at room temperature in uranium by ultrafast cooling. Moreover, it has demonstrated stabilisation of the γ°-phase and the pure cubic γ-phase in uranium alloys contained 11-12 at.% Mo and 15 at.% Mo respectively in the as-obtained state and without any reversion to an α-phase.

References

[1] I Tkach, N-T Kim-Ngan, S Mašková, M Dzevenko, L Havela, A Warren, C Stitt , T Scott, submitted to J. Nucl. Mat. (Dec. 2011)
[2] I Tkach, N-T Kim-Ngan, S Mašková, M Dzevenko, L Havela, A Warren, C Stitt , T Scott, at this conference

Thermodynamic investigations of the (Th, U)O_2 solid solution

O Vălu[1,2], O Beneš[1], R Konings[1]

[1]*European Commission, Joint Research Centre, Institute for Transuranium Elements, Karlsruhe, 76125, Germany*
e-mail: sorin.valu@ec.europa.eu
[2]*Delft University of Technology, Faculty of Applied Sciences, Mekelweg 15, 2629 JB Delft, The Netherlands*

Studies on oxides and mixed oxides of actinide elements such as thorium, uranium and plutonium are of great interest in nuclear industry since some of the oxides are used or are planned to be used as nuclear fuels in various types of reactors [1]. The thermodynamic properties such as enthalpy and heat capacity of these materials are needed for reactor design and safety calculations.

The main objective of this study is to investigate the (Th, U)O_2 solid solution system. In this purpose we are using a multi detector high temperature calorimeter (MDHTC), operated in drop mode in order to obtain the heat capacity by derivation of the enthalpy increments over temperature [2], and an adiabatic calorimeter for the low temperature heat capacity measurements [3]. The results of this study will be used to clarify if thorium and uranium dioxides that form a continuous solid solution show an ideal behaviour of the heat capacity or if some excess contributions appear.

Using a Setaram MDHTC, the enthalpy increments of (Th_{1-y}, U_y)O_2 solid solutions, with y = 0.4, 0.6 and 0.8, were measured in the temperature range 400 - 1800 K (shown in Figure 1) and the preliminary results of the heat capacity of these compositions was derived.

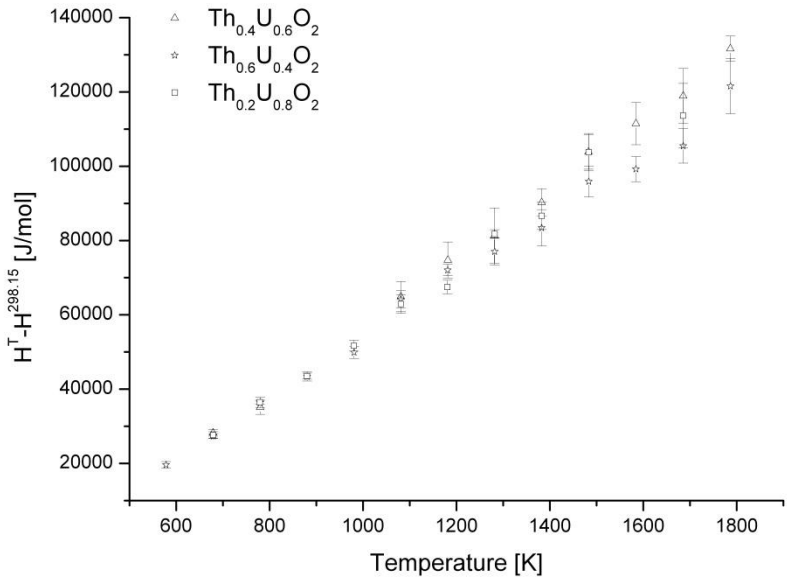

Figure 1. The enthalpy increments of the ($Th_{0.6}U_{0.4}$)O_2, ($Th_{0.4}U_{0.6}$)O_2 and ($Th_{0.8}U_{0.2}$)O_2 intermediate compositions, measured in this study.

The C_P fit of the intermediate compositions was made by simultaneous linear regression taking into account the measured enthalpy data and the low temperature C_P values which were estimated by Neumann-Kopp rule. The preliminary results of the thus obtained C_P curves of (Th_{1-y}, U_y)O_2 solid solutions, in the temperature range 298 - 1800 K, obey the Neumann-Kopp's molar additivity rule.

First results of the low temperature heat capacity of the ($Th_{1-y}U_y$)O_2 intermediate composition, were measured using the low temperature adiabatic calorimeter. The temperature range covered by this technique was from 77.7 K to 350 K. To describe the temperature region from the very low temperature

region we have used a PPMS technique and measured the heat capacity from 2 K up to 100 K obtaining a good agreement between adiabatic results and the ones from the PPMS in the region of overlap.

References

[1] C Ganguly IAEA-TECDOC 107-127, 352 (1985)
[2] O Beneš et al., J. Chem. Thermodynamics 651-655, 49 (2011)
[3] J van Miltenburg et al., J. Chem. Thermodynamics 1129-1137, 19 (1987)
[4] K Bakker et al., Journal of Nuclear Materials 1-12, 250 (1997)

The study of thermal cycling effect on the stability of a δ-stabilised Pu-Ga alloy

M Ling

Atomic Weapons Establishment, Aldermaston, Reading, Berkshire, RG7 4PR, United Kingdom
email: michael.ling@awe.co.uk

A δ-stabilised Pu-Ga alloy at room temperature is currently accepted to be thermodynamically meta-stable. It is well-known that for a meta-stable alloy there always exists a thermodynamic driving force that tries to push it to transform into thermodynamically stable phase(s). Whether such transformations occur or not depends on if suitable kinetic conditions for the transformation can be met. Any method that is able to enhance the kinetics of the transformation will drive and accelerate the system toward its "equilibrium" state. Thermal cycling could be one of such methods that may dramatically change the kinetics of the material system.

In this study, the effect of thermal cycling on the stability of a δ-stabilised Pu-Ga alloy in the temperature range of 25 °C to 180 °C has been investigated for the first time using both differential scanning calorimetry (DSC) and x-ray diffraction (XRD). The 10-year old aged Pu-Ga alloy sample with a nominal Ga concentration of 2 at% was thermally cycled within the DSC furnace enabling coincident collection of phase transformation information. The cycling was carried out with various isothermal hold periods at 25 °C between each DSC run.

The α-phase was detected in "as-received" sample of the original well-homogenised alloy and the amount of α phase was found to increase as a function of both the number of thermal cycles and hold time. Nearly 8% alpha phase was detected after 210 cycles, with no sign that α phase in-growth had ceased or slowed.

Possible mechanisms, by which thermal cycling facilitates the nucleation and in-growth of the increasing α phase content are discussed. The continual increase of α-phase content as a function of the number of thermal cycles was attributed to the δ-phase to α-phase transformation which is proposed to proceed via an intermediate β-phase at elevated temperature during the thermal cycling procedure. The effect of thermal cycling on the acceleration of δ→α transformation is currently thought likely to be due to thermally induced dislocations and the heterogeneous distribution of thermal stress.

Through this investigation, it was shown that thermal cycling treatment had a significant effect on the stability of the δ-stabilised Pu alloy. It could effectively enhance the kinetics of the eutectoid reaction and drive and accelerate the material system toward its "equilibrium" state. It therefore may be used as an alternative experimental method to the one adopted and reported by Russian researchers that has been described in [1] to experimentally derive the equilibrium Pu-Ga phase diagram.

Reference

[1] S Hecker, L Timofeeva, (2000) Los Alamos Sci. 26, 244-251

Forensics
New aspects in nuclear forensics **I Halevy, A Hen, A Sharon**
Nuclear forensics analytical approaches and simulations **I Halevy, A Hen, A Sharon**
Mikro-kopter, chopper and mini UAV system for monitoring a radioactive dispersion scene in RDD scenario **A Hen, I Halevy, A Sharon, E Boublil, M Ghelman, T Ridnik, I Yaar**
Nuclear terrorism: A brief review of threats and responses **I Halevy, A Hen, A Sharon**

New aspects in nuclear forensics

I Halevy[1,2], A Hen[2,3], A Sharon[1]

[1]Physics Department, Nuclear Research Center - Negev, P.O. Box 9001, IL84190 Beer-Sheva, Israel
e-mail: ihalevyi@caltech.edu
[2]Nuclear Engineering Department, Ben-Gurion University, IL84105 Beer-Sheva, Israel
[3]European Commission, Joint Research Centre, Institute for Transuranium Elements, Postfach 2340, DE-76125 Karlsruhe, Germany

Nuclear forensic science aims at providing clues on nuclear or other radioactive material involved in illicit incidents.

Those incidents can lead to RDD scenarios and uncontrolled amount of on nuclear or other radioactive material. A large number of cases of illicit trafficking have been reported to the IAEA Illicit Trafficking Database. For sure, this number is only the tip of large iceberg.

Today we understand the needs for analytical and interpretation capabilities as well as for close international collaboration.

Credibility in nuclear forensics can be achieved only if all evidence and case history are preserved and made available for data interpretation and source attribution.

Hence, nuclear forensics investigations have to start at the 'crime scene'. As a consequence, a comprehensive response plan is required, clearly describing the responsibilities of the authorities involved and the role of the individual actors. Full nuclear forensics capabilities are only available in a few specialised laboratories.

The Institute for Transuranium Elements (ITU) has established collaboration schemes with European Union member states and also provides nuclear forensics support to other countries that request it. The lecture is based on the presentation of K Mayer in the big conference "Illicit Nuclear Trafficking: Collective Experience and the Way Forward, Edinburgh, 19-22 November 2007, International Atomic Energy Agency, Vienna, 2008 Proceedings Series" [1].

This nuclear forensics support was tested by a number of the new European Union member states, when seized material was subject to joint analyses using the analytical infra-structure at ITU. Nuclear forensics remains a discipline challenging the capabilities of the analysts involved in the case investigations. Information on the origin of the nuclear material is inherent to the samples. Reading and understanding this information has, to a large extent, been established and appropriate laboratory protocols have been developed, validated and tested.

Further research activities focus on the application of classical forensic methods to contaminated evidence. Emphasis was given to the two most prominent forensic techniques: taking of fingerprints and DNA analysis. In addition to the conceptual and operational developments, appropriate training has been provided to the authorities involved. The experience gained in joint nuclear forensic analysis of material seized in European Union member states is discussed, as well as recent advances in adapting classical forensic techniques for radioactively contaminated pieces of evidence.

The lecture will focus in few aspects:

- Nuclear forensics methodology - shaping a systematic approach
- Reference information for interpretation and attribution
- Applying classical forensics to contaminated evidence
- Joint analysis - testing the mechanisms for nuclear forensics support

- Training - from awareness building to specific knowledge
- International cooperation

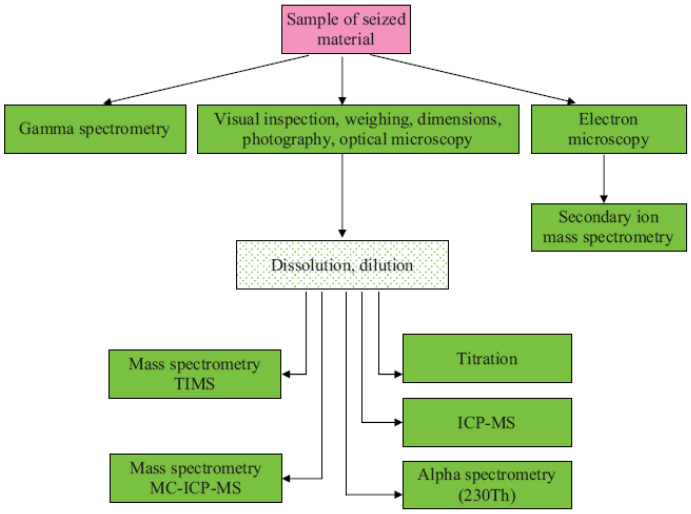

FIG. 1. Generic analysis scheme for nuclear forensic investigations.

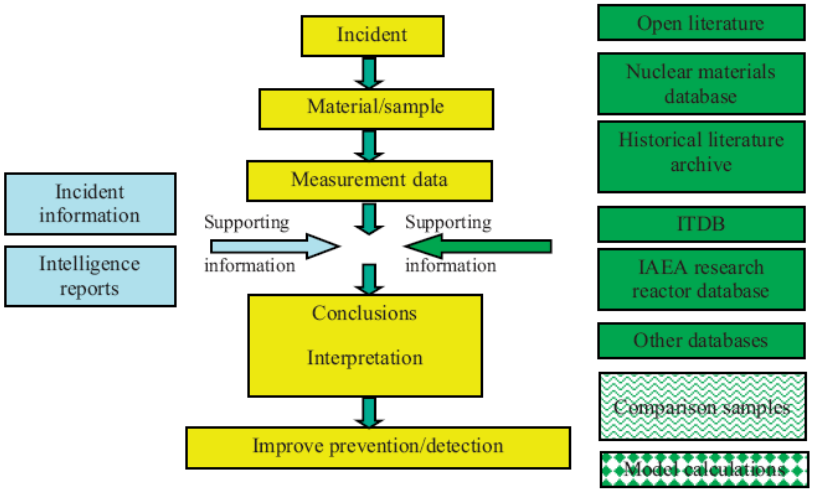

FIG. 2. Flow chart illustrating the importance of reference information for the interpretation of measurement data in nuclear forensic investigations.

[1] K Mayer, E Dahms, J Horta, K. Lützenkirchen, S Millet, A Nicholl, J Schönfeld, A Schubert, H Thiele, M Wallenius, T Wiss, Nuclear forensics from specialized analytical measurements to a fully developed discipline in science, Illicit Nuclear Trafficking: Collective Experience and the Way Forward, Edinburgh, 19-22 November 2007, International Atomic Energy Agency, Vienna, 2008 Proceedings Series.

Nuclear forensics analytical approaches and simulations

I Halevy[1,2], A Hen[2,3], A Sharon[1]

[1]Physics Department, Nuclear Research Center Negev, P.O. Box 9001, IL84190 Beer-Sheva, Israel
e-mail: ihalevyi@caltech.edu
[2]Nuclear Engineering Department, Ben-Gurion University, IL84105 Beer-Sheva, Israel
[3]European Commission, Joint Research Centre, Institute for Transuranium Elements, Postfach 2340, DE-76125 Karlsruhe, Germany

- Big picture questions
- Nuclear forensics focus
- Materials of interest
  - Special nuclear material - ^{252}Cf, ^{239}Pu, ^{235}U, ^{233}U
  - Other nuclear material - ^{237}Np, ^{241}Am, ^{252}Cf, ^{6}Li, ^{3}H
  - HEU (>90% ^{235}U)
  - UF_6
  - U metal
- Nuclear forensics capabilities based on active programmes
- Sampling science and collection
- Nuclear forensics analytical approaches
- Radiochemical analysis (laboratories/techniques)
- Development of trace forensics
- Application of reactor analysis to nuclear forensics
- Modelling and simulation:
  - Advancing radiation transport methods and codes

Mikro-kopter, chopper and mini UAV system for monitoring a radioactive dispersion scene in RDD scenario

A Hen, I Halevy, A Sharon, E Boublil, M Ghelman, T Ridnik, I Yaar

Nuclear Research Center - Negev, P.O. Box 9001, IL84190 Beer-Sheva, Israel

An comparative experimental study of dispersion of radioactive material and hidden sources were conducted by chopper (AIR_RAM2000), mini UAV system (Casper 250) and the Mikro-kopter.

The Mikro-kopter is the ultimate tool for aerial photography or security missions for short distances, time and low payload.

The Mikro-kopter used enables 20-90 min flights. The large arms angle allows wide angle photography and 300-1500 g of payload.

The Mikro-kopter has a stabilising system; together with a GPS it can keep the location and height in the air, and automatically return to the take-off point. Using a computer interface it can communicate with the ground system at real time, sending it to predetermined landmarks (or enter them in real time). After the flight, it returns automatically to the take-off point.

The Mikro-kopter's six powerful electric engines give the ability to simultaneously lift weight and keep high maneuverability.

The ground station includes all the functions needed to fly the Mikro-kopter and controlling the payload on it. No eye contact is need, but it will help for durable in hard missions.

Figure 1. The Mikro-kopter with its batteries and six electric propellers. A small camera is located as is payload.

A PDS detector, NaI(Tl), was attached to the Mikro-kopter for aerial radiation field detection. Two flights of 10 minutes each were performed in the scene.

The Mikro-kopter measuring the radioactive field of hidden source is presented in Figure 2.

Figure 2. The Mikro-kopter measuring the radioactive field of hidden source.

The results of the aerial radiation field detection are shown in Figure 3.

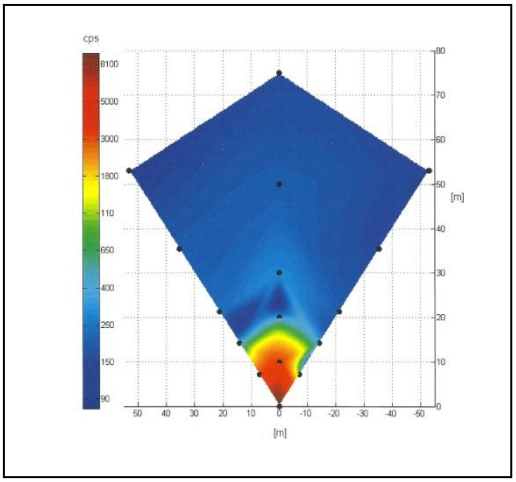

Figure 3. The results of the aerial radiation field detection in the scene.

Advantages and disadvantages in the Mikro-kopter:

Advantages	Disadvantages
• High mobility all-terrain vehicle • Monitoring large area in sort time • Low exposure to personal • Automated monitoring	• High sensitivity to weather condition • Short operation time • Short operation distances • Low weight payload

Nuclear terrorism: A brief review of threats and responses

I Halevy[1,2], A Hen[2,3], A Sharon[1]

[1]Physics Department, Nuclear Research Center Negev, P.O. Box 9001, IL84190 Beer-Sheva, Israel
e-mail: ihalevyi@caltech.edu
[2]Nuclear Engineering Department, Ben-Gurion University, IL84105 Beer-Sheva, Israel
[3]European Commission, Joint Research Centre, Institute for Transuranium Elements, Postfach 2340, DE-76125 Karlsruhe, Germany

- Isotopic signatures and nuclear forensics
- Pre- vs post-explosion forensics
- Beyond detection: Tracing the origin of radioactive and nuclear material
- Nuclear forensic field exercises
- Nuclear forensic simulation with HOTSPOT
- Nuclear forensic methods in safeguards
- Nuclear forensics and the nuclear attribution process
- Roles of forensics and attribution in preventing nuclear terrorism
- International cooperation
- Making best use of exercises
- Applied techniques for nuclear forensics and environmental analysis
- Analysis of single particles by LA-ICP-MS and FTA techniques
- Building a knowledge base, developing signatures
- Using unmanned chopper for radiation and contamination monitoring

Physics 5
Suppression of magnetic order in $U_2(Ni_{1-x}Fe_x)_2Sn$ **S Mašková, L Havela, A Kolomiets, J Peterson, H Nakotte, K Miliyanchuk, A Andreev**
Focused ion beams in actinides research **P Heard**
XMCD in magnetic properties research **A Hen, I Halevy**
Mössbauer and SQUID under high pressure in actinides research **I Halevy, A Hen, M Pasternak**
Atom probe in materials science research **O Beeri**

Suppression of magnetic order in $U_2(Ni_{1-x}Fe_x)_2Sn$

S Mašková[1], L Havela[1], A Kolomiets[1,2], J Peterson[3], H Nakotte[3], K Miliyanchuk[4], A Andreev[5]

[1]*Department of Condensed Matter Physics, Charles University, Ke Karlovu 5, 12116 Prague 2, Czech Republic*
e-mail: maskova@mag.mff.cuni.cz
[2]*Department of Physics, Lviv Polytechnic National University, 12 Bandera Str., 79013 Lviv, Ukraine*
[3]*Department of Physics, New Mexico State University, 88003-8001 Las Cruses, USA-NM*
[4]*Faculty of Chemistry, Ivan Franko National University of Lviv, Kyryla i Mefodiya Str. 6, 79005 Lviv, Ukraine*
[5]*Institute of Physics, AVCR, Na Slovance 2, 18221 Prague 8, Czech Republic*

U_2Ni_2Sn is an antiferromagnet with T_N = 26 K, while U_2Fe_2Sn does not show any long-range magnetic order. It is therefore interesting to study the gradual suppression of magnetic order with increasing Fe concentration. Nearly magnetic U_2Co_2Sn exhibits a non-Fermi liquid behaviour [1]. We were particularly interested whether there is the possibility to simulate this behaviour in a certain Fe concentration range, as Co lies in the periodic table between Fe and Ni. Several compounds $U_2(Ni_{1-x}Fe_x)_2Sn$ with various concentrations of Fe (x = 0.05, 0.1, 0.15, 0.2, 0.4, 0.6, 0.8) were prepared. Their magnetic properties were studied by means of magnetic susceptibility and specific heat measurement. These compounds also bring great opportunity to study their properties by Mössbauer spectroscopy as they contain two Mössbauer isotopes ^{57}Fe and ^{119}Sn.

Hydrogenation of U compounds often leads to dramatic variations both in the size and stability of magnetic moments and their interactions. Doping by hydrogen, which occupies interstitial positions, leads to the unit cell expansion which affects the U-U spacing considered as the most critical parameter tuning magnetic properties. Therefore the expansion leads typically to stronger magnetism. The study of hydrogenation $U_2(Ni_{1-x}Fe_x)_2Sn$ was undertaken to see the interplay between these two effects (strengthening of magnetic properties due to hydrogenation and suppression of magnetic order due to Fe substitution).

Starting from U_2Ni_2Sn, the hydrogenation leads to stronger magnetic interactions in $U_2Ni_2SnH_{1.8}$. The Néel temperature increases to 87 K. As for the concentration dependence of magnetic properties, we can clearly see from the specific heat data that the antiferromagnetic order is suppressed with increasing Fe concentration reaching the NFL behaviour for $U_2(Ni_{0.8}Fe_{0.2})_2Sn$ (Figure 1). Also the temperature dependence of magnetic susceptibility of the sample with 20 % Fe reveals a great similarity to previously studied heavy fermion U_2Co_2Sn with NFL behaviour (Figure 2) although at low temperatures it does not increase so much. The upturn in specific heat, which is very resistant to magnetic fields, is suppressed with further increasing Fe concentration.

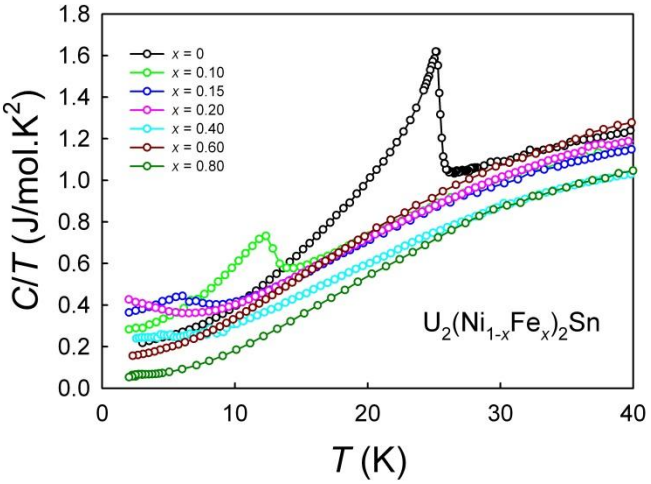

Figure 1. Temperature dependence of the specific heat (in the C/T vs. T representation) for $U_2(Ni_{1-x}Fe_x)_2Sn$.

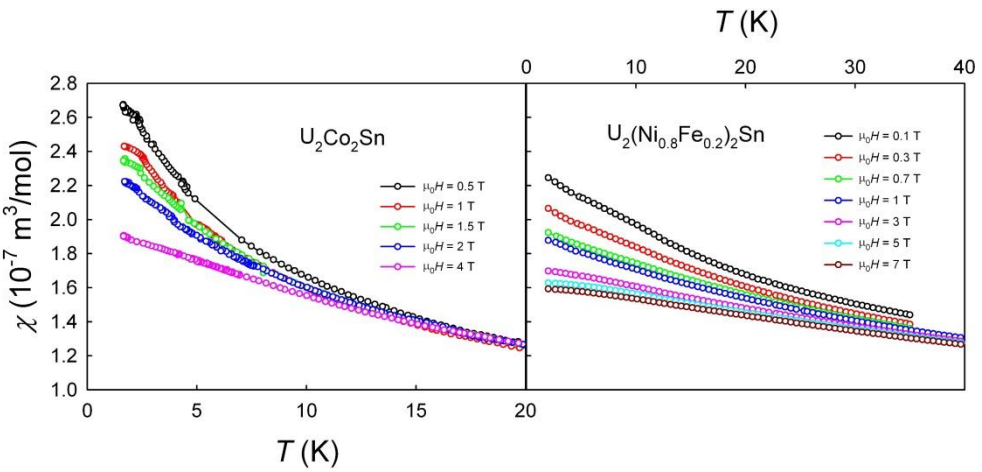

Figure 2. Temperature dependence of magnetic susceptibility of $U_2(Ni_{0.8}Fe_{0.2})_2Sn$ compared with the magnetic susceptibility of U_2Co_2Sn.

Hydrogen absorption of approx. 2 H/f.u. could be achieved for high H pressures (100 bar). The hydrogenation does not change the crystal structure (Mo_2FeB_2 structure type, space group *P4/mbm)*. In all cases it leads to a unit-cell expansion by 7 to 10 %. Comparing magnetic properties of hydrides of studied compounds we can see that increasing of Fe concentration leads to the crossover of magnetic order. Hydride of starting compound U_2Ni_2Sn orders antiferromagnetically, magnetic order is clearly suppressed in the hydride with 20 % Fe, further increment of Fe concentration leads to a ferromagnetic order in the hydrides.

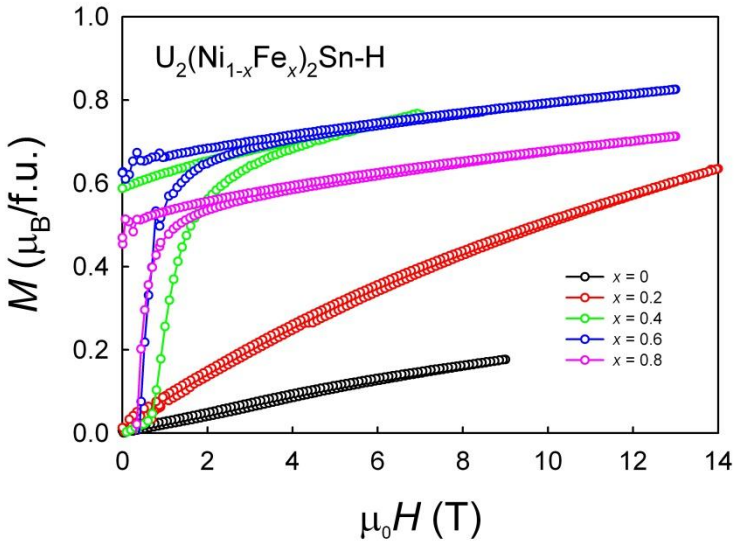

Figure 3. Comparison of the field dependence of magnetisation of $U_2(Ni_{1-x}Fe_x)_2Sn$ hydrides.

Acknowledgements
This work was supported by the Grant Agency of the Czech Republic under the grants No. 204/12/0285 and 204/10/0330. The support of the Charles University Grant Agency (project No. 436111) is recognised, as well.

References
[1] J Kim et al., Phys. Rev. B 62, 6986 (2000).

Focused ion beams in actinides research

P Heard, C Jones, T Scott

Interface Analysis Centre, University of Bristol, Oldbury House, 121 St. Michaels Hill, Bristol, BS2 8BS, United Kingdom
e-mail: peter.heard@bristol.ac.uk

During the last 25 years, focused ion beam (FIB) instrumentation has become an important technology for a wide array of materials science applications, from circuit editing and transmission electron microscopy (TEM) sample preparation to microstructural analysis and prototype nanomachining. It has only been in the past few years that research using FIB technologies has been applied to the study of actinide and nuclear materials in general.

The FIB instrument is similar to a scanning electron microscope (SEM), except that the beam that is rastered over the sample is an ion beam rather than an electron beam. Secondary electrons are generated by the interaction of the ion beam with the sample surface and can be used to obtain high-spatial-resolution images. In most commercially available systems, Ga ions are used, and their sputtering action enables precise machining of samples. In conjunction with the gas-injection capabilities on these systems, which enable ion-beam-activated deposition and enhanced etching, a range of sample fabrication schemes are possible. Most modern FIB instruments supplement the FIB column with an additional SEM column so that the instrument becomes a versatile “dual-beam” platform (FIB-SEM) for imaging, material removal and deposition at length scales of a few nanometers to hundreds of microns. Furthermore, the FIB instrument becomes a powerful tool for nano-manipulation and fabrication when augmented with micromanipulators and gas injectors for local chemical vapour deposition (CVD).

The current talk provides an introductory overview of the FIB technique applied to research on actinide materials, outlining capabilities and limitations for the investigation of sample materials of different types. The talk also covers the basic FIB instrument and the fundamentals of ion–solid interactions that lead to the many unique FIB capabilities as well as some of the unwanted artifacts associated with FIB instruments.

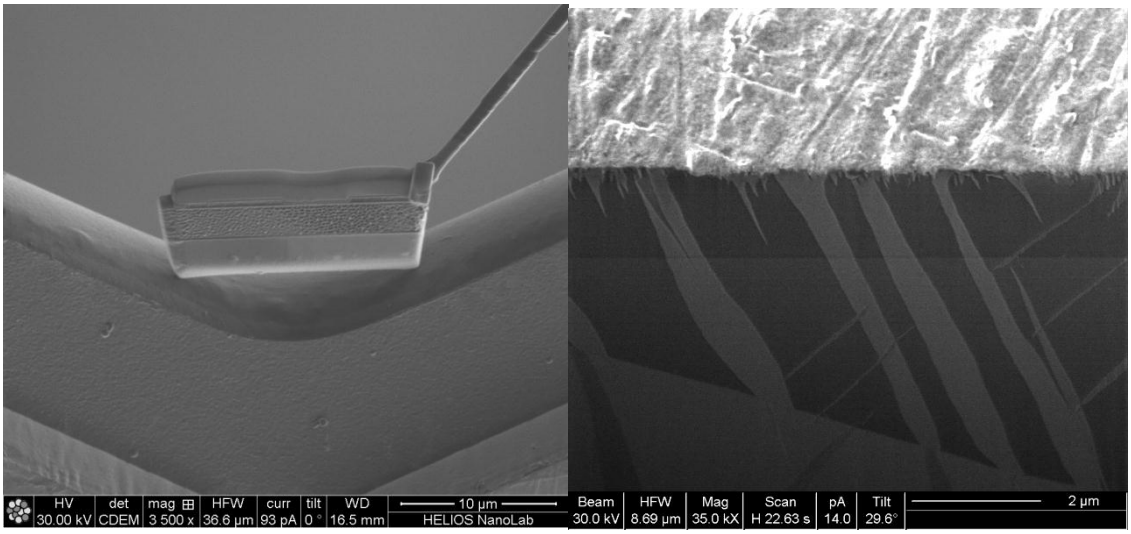

Figure 1. FIB images showing (left) TEM lamellae preparation and (right) in situ ion beam sectioning.

XMCD in magnetic properties research

A Hen, I Halevy

Nuclear Research Center - Negev, P.O. Box 9001, IL84190 Beer-Sheva, Israel

Mössbauer and SQUID under high pressure in actinides research

I Halevy[1,2], A Hen[2,3], M Pasternak[4]

[1]*Physics Department, Nuclear Research Center Negev, P.O. Box 9001, IL84190 Beer-Sheva, Israel*
e-mail: ihalevyi@caltech.edu
[2]*Nuclear Engineering Department, Ben-Gurion University, IL84105 Beer-Sheva, Israel*
[3]*European Commission, Joint Research Centre, Institute for Transuranium Elements, Postfach 2340, DE-76125 Karlsruhe, Germany*
[4]*Physics Department* Tel Aviv University, Ramat Aviv 69978, Israel

High-pressure- SQUID

High-pressure synthesis is increasingly being used in the search for new materials. This is particularly the case for superconductors [1], but the synthesis products are difficult to analyse because they are small in size (~50 mg) and often consist of a mixture of unknown phases exhibiting a low superconducting volume fraction.

X-ray or electron diffraction cannot identify a superconductor unambiguously if it is a minority constituent. The methodology is to combine the use of a SQUID and other magnetic techniques.

New SQUID diamond anvil cells (DACs) are available with a low magnetic contribution. Those cells are very small because of cryogenic and space consideration.

An example is the Edinburgh DAC (Figure 1).

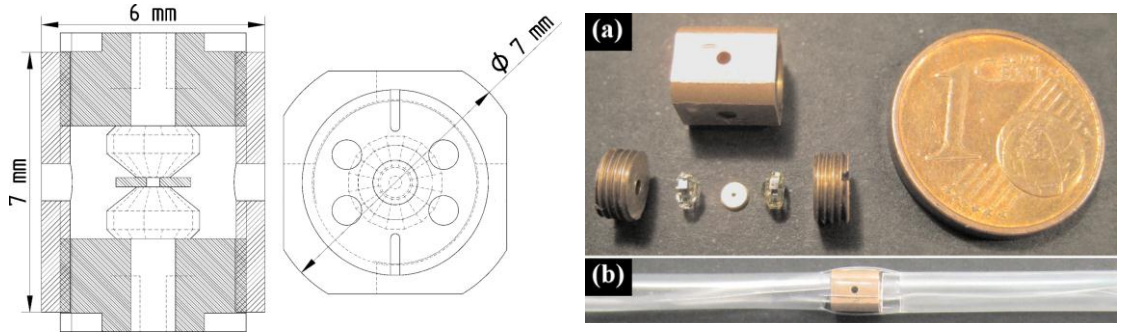

Figure 1: Drawings of the TM-DAC with key dimensions. (a) Parts and the assembled TMDAC. (b) The standard plastic straw holder of MPMS.

High-pressure- Mössbauer [1]

The new perforated diamonds design specially for high-pressure Mössbauer measurements.

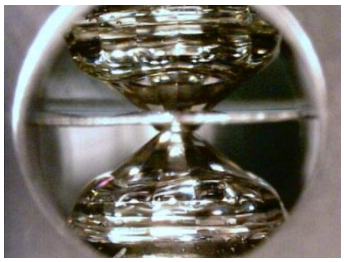

The low-weight *mini-Mighty* diamond anvil cells (10-14 grams) are integrated into the cryogenic system allowing for fast cooling- and warming-periods

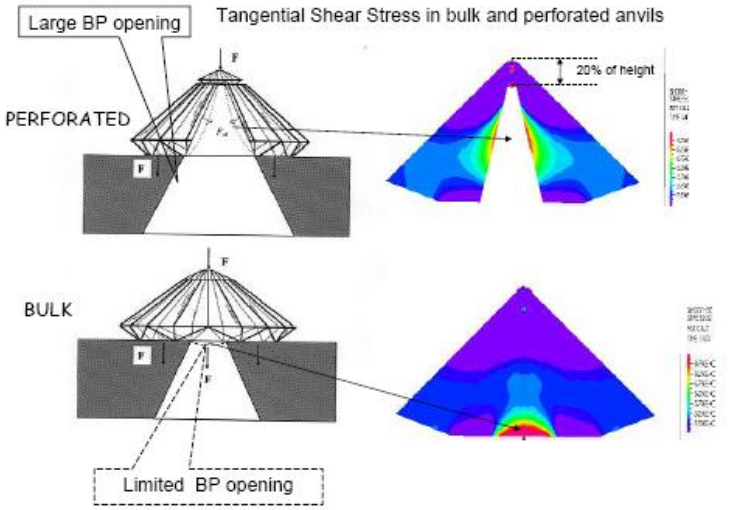

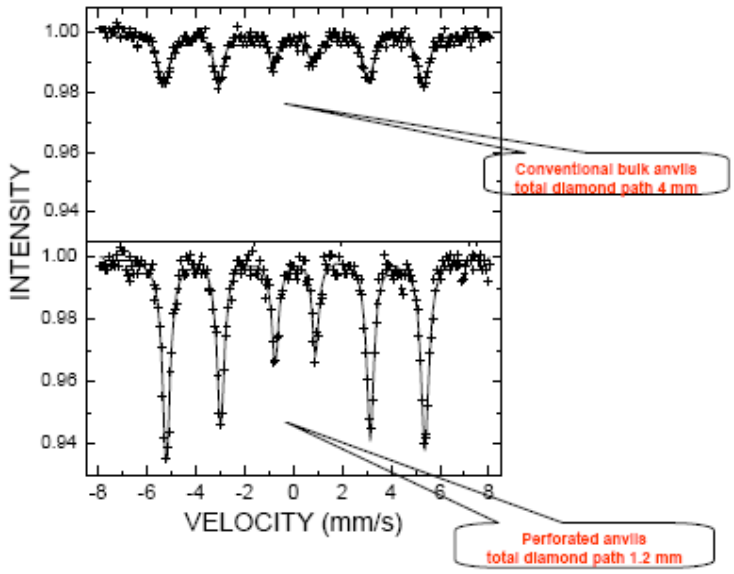

References

[1] M Pasternak, P.O. Box 1200, Hod-Hasharon 45111, Israel
Fax: +972-9-7669133, e-mail: anvils AT danvils.com
http://danvils.com/pressure-temperature-systems/low-temperature.html

Atom probe in materials science research

O Beeri

Physics Department, Nuclear Research Center - Negev, P.O. Box 9001, Beer-Sheva, Israel
e-mail: ofer.beeri@gmail.com

Atom probe tomography (APT) is an evolution of Field Ion Microscopy (FIM). The FIM was invented by Müller and Panitz in the late sixties and was the first experimental method that allowed the visualisation of single atoms, ahead of high resolution TEMs. This method is based on physical adsorption of inert gas atoms on the surface of a needle-like sample placed under DC voltage. Individual gas atoms adsorb on the top of a sample atom. Applying pulses of extra voltage causes field evaporation of the gas atoms (ions) from the sample tip. The evaporated inert gas ions, moving along the trajectories of the electrical field, are accelerated towards a position sensitive detector. In the past, this position sensitive detector was made from a fluorescent material, allowing on-line visualisation of the sample's tip atom arrangement (a magnified replica).

Samples for APT are also needle-like but are placed in a high vacuum and, instead of accelerating inert gas ions, atoms in the tip of the sample are field evaporated and collected by the position sensitive detector, which is a multi-channel plate (MCP). Knowing the exact time of applying the pulses of extra voltage, the time the evaporated ions hit the MCP and the distance and voltage gradient between the sample tip and the MCP, it is possible to calculate the mass to charge ratio (m/c) of the evaporated ion. This makes this instrument a position sensitive time of flight mass spectrometer.

Each hit of an ion at the MCP is called an event. The collection of all the events in a computer allows the application of different treatments and analyses, and especially the formation of 3D reconstructions of the sample at atomic resolution.

Today this method is further developed by the introduction of commercial companies to the field and the production of user friendly instruments, enabling fast and simple operation, high speed data collection and the treatment of large data sets. Also, the use of laser pulses to heat the sample tip, instead of electrical voltage, brings some more advantages to this field, including the ability to investigate semiconductors.

In my talk, I will explain the principle of APT and give some examples of cases that cannot be solved using any other experimental method.

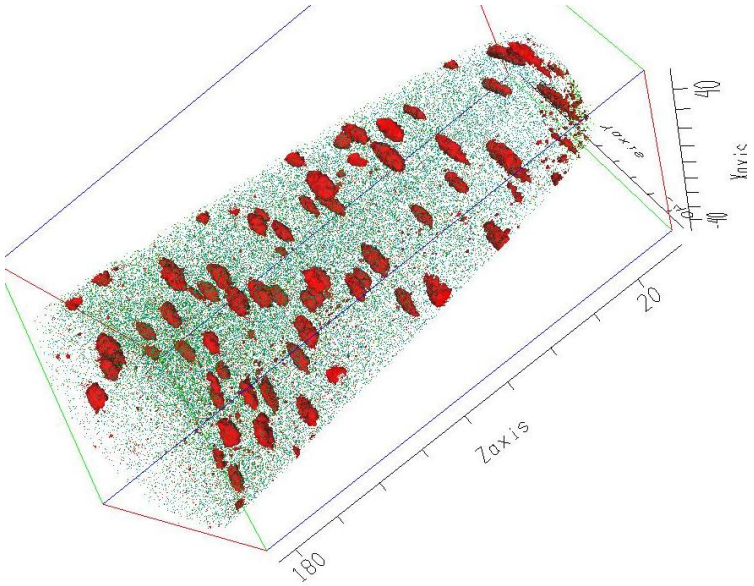

Figure 1. APT 3D reconstruction of an aluminium sample containing nanometer Al_3Sc precipitates (red). This data set contains 28 million atoms and 73 precipitates. Units on axes are in nanometers.

Posters
Isothermal and isochronal ageing behaviour of dilute Al-Sc-AC (AC=Th,U) alloys **O Beeri, A Bram, M Shandalov, D Dunand, D Seidman**
The influence of transitional metal in Al-T-Th system on stability of ternary intermetallic phases formed **A Bram, A Venkert, L Meshi**
The corrosion of uranium niobium alloys **C Coe, P Morrall, J Glascott, T Scott**
A comparison between the two novel polar intermetallics $Yb_3Pd_2Sn_2$ and $Eu_3Pd_2Sn_2$ **M Giovannini, P Solokha, A Saccone, M Reiffers, I Čurlik, P Lemoine, J Cadogan, N Hone, D Ryan**
Uranium carbide material investigations at CERN-ISOLDE and at the Swiss Light Source **A Gottberg, T Stora, R Catherall, C Degueldre, D Grolimund, I Günther-Leopold, H Frånberg-Delahaye, A Andrighetto, P Bricault, C Lau**
On the structural distortion of UFeGe **M Henriques, L Havela, S Mašková, T Klimczuk, A Rudajevová, O Tougait, R Vilar, A Gonçalves**
Electrochemical properties of uranium in LiCl-KCl-CsCl eutectic melt **D Maltsev, V Volkovich, D Aleksandrov, E Vladykin, P Likhachyov, I Polovov, B Vasin**
Solubility of uranium in gallium-indium eutectic alloy **D Maltsev, V Volkovich, L Yamschikov, A Osipenko, S Raspopin, M Kormilitsyn**
Mine waters radioactive decontamination using p-hexasulfonated calix[6] arene acid as delivery vehicle in a liquid membrane **I-C Popescu, D Humelnicu, I Humelnicu, M Mateescu**
The bulk hydriding kinetics of cerium **G Rule, J Knowles**
Characterisation and recrystallisation of the surface over-layer of gadolinium following beam welding **C Stitt, T Scott**
Preparation of ^{235}U targets by molecular plating **D Vanleeuw, A Moens, R Eykens, G Sibbens**
Crystal structure and physical properties of the new $UCu_{7-x}Al_{4+x}$ (x = 0.32) phase **Yu Verbovytskyy, E Bauer, H Michor, A Gonçalves**
Investigating the structure of splat-cooled uranium and uranium-molybdenum alloys **A Warren, T Scott**

Isothermal and isochronal ageing behaviour of dilute Al-Sc-AC (AC=Th,U) alloys

O Beeri[1], A Bram[2,3], M Shandalov[1], D Dunand[4], D Seidman[4,5]

[1]*Physics Department, Nuclear Research Center - Negev, P.O. Box 9001, Beer-Sheva, Israel*
e-mail: ofer.beeri@gmail.com
[2]*Department of Material Engineering, Ben-Gurion University of the Negev, P.O. Box 653, Beer-Sheva, Israel*
[3]*Ilse Katz institute for nanotechnology, Ben-Gurion University of the Negev, Beer-Sheva 84105, Israel*
[4]*Department of Materials Science and Engineering, Northwestern University, Evanston IL 60208, USA*
[5]*Northwestern University Center for Atom-Probe Tomography (NUCAPT), Evanston IL 60208, USA*

The Al(Sc)-based alloys have excellent creep properties, and are promising candidates for use in the aerospace and ground vehicle industries. Their strain is raised from the formation of nanosize Al_3Sc precipitates, which are formed homogeneously during aging from a single-phase supersaturated solid-solution.

Modification of the binary Al-Sc alloy properties is feasible by adding another alloying element (M), usually one that can also form precipitates of the form Al_3M. In many cases this element react with the Al_3Sc precipitates to form precipitates of the form $Al_3(Sc,M)$. The properties of the $Al_3(Sc,M)$ precipitates are differ from the properties of the Al_3Sc, and hence the properties of the alloy as well.

Many ternary alloys of the family Al-Sc-M have been investigated, however, as much as we know, none investigated the systems Al-Sc-AC (AC=Th,U), although both elements, uranium and thorium, can form precipitates of the form Al_3AC.

In this research we investigated the ageing behaviour of dilute Al-Sc-AC alloys, with Sc, U and Th concentrations of ~900 at.ppm, ~60 at.ppm and ~75 at.ppm, respectively. A reference binary alloy (Al-Sc) was investigated as well. The alloys where homogenised at 640°C for few days and then water quenched. Then two different ageing treatments where employed, isochronal of 8 steps, 3 hours each, up to 400°C and isothermal at 300°C up to two months.

The samples where characterised by variant techniques, including Vickers micro-hardness, conductivity measurements, SEM+EDS and TEM.

For both ageing treatments, the alloy containing Th has the same ageing behaviour as the binary one, while the alloy containing U shows much faster precipitation kinetics at the early stages, but after reaching its peak ageing its behaviour is also flowing the one of the binary alloy, having about the same maximal micro-hardness values and over-ageing time. This behaviour of the alloy containing U seems to be the result of early precipitation of nanometer scale U reach precipitates, while at later ageing stages the Sc reach precipitates are dominant.

The influence of transitional metal in Al-T-Th system on stability of ternary intermetallic phases formed

A Bram[1,2], A Venkert[3], L Meshi[1,2]

[1]*Department of Materials Engineering, Ben-Gurion University of the Negev, Beer-Sheva 84105, Israel*
[2]*Ilse Katz Institute for Nanotechnology, Ben-Gurion University of the Negev, Beer Sheva 84105, Israel*
[3]*Nuclear Research Center - Negev, POB 9001, Beer-Sheva, Israel*

The investigations of ternary systems of the lanthanoids (Ln) and actinoids (Ac) with transition elements and aluminium have resulted in the characterisation of numerous aluminides: tetragonal AT_4Al_8 (A=Ln,Ac; T=Cr,Mn,Fe,Cu) [1-3], hexagonal $A_6T_4Al_{43}$ (A=Y,Nd,Sm,Gd-Lu,Th,U; T=Cr,Mo,W) [4] and cubic AT_2Al_{20} (A=rare earth elements and U; T=Ti,Nb,Ta,Mo,V,W) [5, 6], to name just a few series with many representatives. It can be noticed that not in all possible A-T-Al (where A=Ac,Ln, T=transitional metal) systems - all series, proposed by different researchers, are present. The reason for that is the stability of these phases. One of the approaches to ascertain the main physical factors responsible for the stability and the symmetry of the structures formed in complex systems is based on the ideas of the theory of coordination compounds [7]. In this theory, the phase stability was related to the degree of distortion of the coordination polyhedra around heavy atoms; their symmetry and stability were determined by the degree of splitting of degenerated energy levels of the *d*-electrons in atoms of transition metals [8].

Present research was undertaken with the purpose to characterise aluminides found in the A-T-Al systems. As an example, Th-T-Al (where T=V,Fe,Cu) system was chosen. The alloys were prepared with the same 87at%Al-8at%T-4at%Th composition and homogenised. The structure of the aluminides found in these alloys (before and after the heat treatment) was studied using electron microscopy and x-ray powder diffraction methods. Mentioned theory was successfully applied in order to explain the results.

References

[1] K Buschow et al., J. Less-Common Met.50 (1976) 145
[2] I Felner, I Nowik, J. Phys. Chem. Solids 39 (1978) 951
[3] I Felner, I Nowik, J. Phys. Chem. Solids 40 (1979) 1035
[4] S Niemann, W Jeitschko, Z. Metallkd. 85 (1994) 345
[5] S Niemann, W Jeitschko, J. Solid State Chem.114 (1995) 337
[6] I Halevy et al., J. Alloys and Comp.319 (2001) 19
[7] L Pauling, Phys. Rev. 54 (1938)899
[8] A Kiv, V Ezersky, M Talianker, Mat, Science and Eng. A352 (2003) 100

The corrosion of uranium niobium alloys

C Coe[1], P Morrall[1], J Glascott[1], T Scott[2]

[1]Atomic Weapons Establishment, Aldermaston, Reading, Berkshire, RG7 4PR, United Kingdom
e-mail: camille.coe@awe.co.uk
[2]Interface Analysis Centre, University of Bristol, Oldbury House, 121 St. Michaels Hill, Bristol, BS2 8BS, United Kingdom

Safe consignment of uranium metal for long periods requires a thorough understanding of its corrosion reactions in a variety of environments. The addition of niobium to uranium metal enhances its corrosion resistance. Previous work on niobium metal has shown the reaction rate with oxygen and water to be parabolic for the temperatures studied here (below 250 °C), and that the addition of oxygen to the water vapour reaction accelerates the rate [1]. For uranium and the UNb alloys the rate of reaction has been shown to be faster in water vapour than oxygen and the addition of oxygen to the water reaction reduces the rate until the oxygen is consumed [2].

In this study, isotopically labeled oxygen and water (^{18}O, D_2O and $H_2{}^{18}O$) are used to allow depth profile analysis using secondary ion mass spectrometry. The appearance of the different isotopes should enable the diffusing species and mechanism of each reaction (oxygen, water and a mixture of the two) to be determined. With regards to kinetics, both temperature and pressure are explored. For the UNb alloys the effect of increasing niobium content on the kinetics and mechanism is investigated.

Experiments using oxygen involve a gas rig and a differential pressure transducer. The transducer measures any change in pressure between two cells of equal volume. Both cells are placed in a furnace; therefore any change in pressure is due to oxidation and not temperature fluctuations.

Experiments using water vapour use saturated salt solutions to create constant pressures at different temperatures. The solution and material are placed in one pot and left to react with a pressure transducer attached. Due to the enhanced corrosion resistance the reaction for the UNb alloys is very slow in the order of several months to years.

Initial data from the water experiments indicates that as temperature increases the reaction rate also increases. Similarly, for niobium metal, early data shows that at 70 °C as the pressure is increased the rate increases. The increase in niobium content in the alloys has shown to reduce the rate. It has also been shown that uranium reacts much faster than the alloys and niobium oxidises at a similar rate to the highest content alloy used of 6 wt% niobium. SIMS analysis will be conducted on the corroded samples in order to determine the oxide structure and the mechanism of the reaction.

References

[1] P.E Blackburn, J. Electrochemical Soc. 109, 1142 (1962)
[2] J C McGurk, Nexia Solutions (2007), Private communication

A comparison between the two novel polar intermetallics $Yb_3Pd_2Sn_2$ and $Eu_3Pd_2Sn_2$

M Giovannini[1], P Solokha[1], A Saccone[1], M Reiffers[2,3], I Čurlik[2], P Lemoine[4], J Cadogan[4], N Hone[5], D Ryan[5]

[1]Dipartimento di Chimica e Chimica Industriale, Università di Genova,Via Dodecaneso 31, 16146 Genova, Italy
e-mail: giovam@chimica.unige.it
[2]Institute of Experimental Physics, Watsonova 47, 043 53 Košice, Slovakia
[3]Faculty of Sciences, University of Prešov, 17.novembra, SK-080 78 Prešov, Slovakia
[4]Department of Physics and Astronomy, University of Manitoba, Winnipeg, Manitoba, R3T 2N2 Canada
[5]Centre for the Physics of Materials and Physics Department, McGill University, 3600 University St., Montreal, Quebec, H3A 2T8 Canada

Ytterbium and europium compounds show a great variety of anomalous physical properties due to the fact that these lanthanides can exist in the trivalent or in the divalent state. The divalent and trivalent oxidation states may coexist in some compounds called heterogeneous mixed valence systems, with inequivalent crystallographic R-sites (R = rare-earth). A different situation is that of an intermediate valence system, where each lanthanide has the same, non-integer valence due to hybridisation between f- and conduction electrons.

Here we present a comparison between the structure and the physical properties of two novel compounds with inequivalent crystallographic R-sites, namely $Yb_3Pd_2Sn_2$ and $Eu_3Pd_2Sn_2$. In fact, during our investigation on the Yb-Pd-Sn system [1], a compound with the formula $Yb_3Pd_2Sn_2$ and an orthorhombic cell was found. The crystal structure of this compound has been determined *ab initio* from powder x-ray diffraction data and it is representative of a new structure type with Yb-atoms occupying four inequivalent crystallographic positions [2]. Searching for other $R_3Pd_2Sn_2$ compounds, the existence of $Eu_3Pd_2Sn_2$ crystallising in the $La_3Ni_2Ga_2$ structure-type (with Eu-atoms occupying two inequivalent sites) has been found. The structure of $Yb_3Pd_2Sn_2$ is closely related to the $La_3Ni_2Ga_2$ structure-type, and therefore to the structure of $Eu_3Pd_2Sn_2$. In both cases, polyanionic networks $[Pd_2Sn_2]_\infty$ have pronounced 2D characters and, making an analogy with structural organic chemistry, could be defined as *cis*-$[Pd_2Sn_2]_\infty$ and *trans*-$[Pd_2Sn_2]_\infty$ conformations for $Eu_3Pd_2Sn_2$ and $Yb_3Pd_2Sn_2$, respectively (see Figure 1).

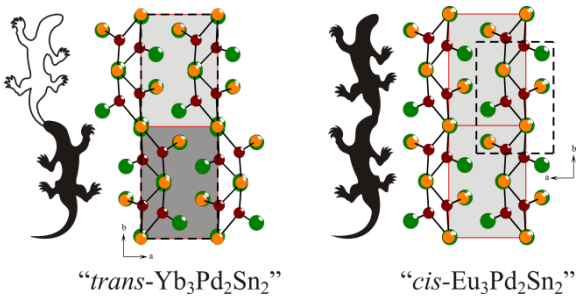

Figure 1. Structural relation between $Eu_3Pd_2Sn_2$ and $Yb_3Pd_2Sn_2$.

$Yb_3Pd_2Sn_2$ shows no phase transition down to 0.3 K and it behaves as an ordinary metal. The magnetic susceptibility shows a very weak temperature dependence in the whole temperature range with a small upturn at low temperatures likely due to paramagnetic impurities (Figure 2).

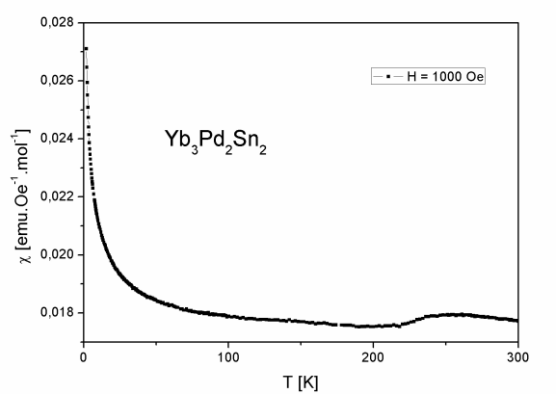

Figure 2. Temperature dependence of DC magnetic susceptibility of $Yb_3Pd_2Sn_2$ at H = 1000 Oe.

The nearly constant susceptibility indicates a close to divalent Yb-behaviour, although a tiny broad bump above 200 K may indicate some degree of hybridisation between 4f and conduction electrons. Also the γ Sommerfeld coefficient determined from heat capacity, showing a slightly enhanced value of 67 mJ mol^{-1} K^{-2}, suggests a certain degree of c-f hybridisation. Nevertheless, a possible scenario where $Yb_3Pd_2Sn_2$ is a heterogeneous mixed valent compound is ruled out by the results of ^{170}Yb-Mössbauer spectroscopy [2].

For $Eu_3Pd_2Sn_2$ the plot of inverse susceptibility in the paramagnetic regime follows the Curie-Weiss law, with an effective moment of 7.94 μ_B, in agreement with the value for the free ion Eu^{2+}. The paramagnetic Curie temperature θp = -5 K is negative indicating the presence of antiferromagnetic exchange. In fact, magnetic susceptibility at lower temperatures shows a main magnetic transition at 22 K with two other effects likely due to spurious phases. Eu-Mössbauer measurements confirm the existence of an intrinsic magnetic transition at 22 K.

Neutron powder diffraction patterns recorded at 40 K and 3.6 K (Figure 3) using a large-area flat-plate geometry sample holder [3] confirm the $La_3Ni_2Ga_2$ type-structure and the divalent state of the Eu atoms in $Eu_3Pd_2Sn_2$. The appearance of additional magnetic peaks at low temperature indicates antiferromagnetic order of the Eu sublattice.

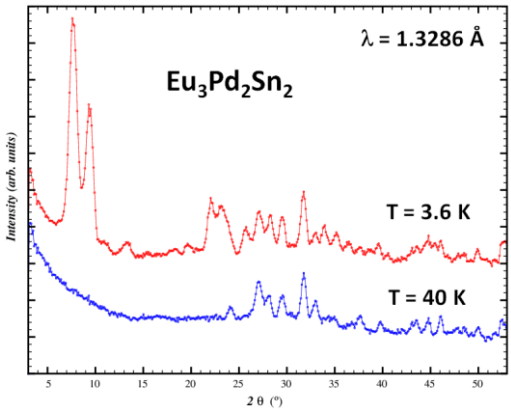

Figure 3. Neutron powder diffraction patterns of $Eu_3Pd_2Sn_2$ recorded at 40 K and 3.6 K with = 1.3286 Å.

Acknowledgements
This work has been supported by the Slovak Research and Development Agency under the contract No. APVV - SK-IT-0023-08; the Slovak grant agency VEGA 2/0070/12.

References
[1] M Giovannini et al. Intermetallics 18, 429 (2010)
[2] P Solokha et al., Journal Solid State Chemistry 184, 2498 (2011)
[3] D Ryan and L Cranswick, J. Appl. Cryst., 41, 198 (2008)

Uranium carbide material investigations at CERN-ISOLDE and at the Swiss Light Source

A Gottberg[1], T Stora[1], R Catherall[1], C Degueldre[2], D Grolimund[2], I Günther-Leopold[2], H Frånberg-Delahaye[3], A Andrighetto[4], P Bricault[5], C Lau[6]

[1]CERN - European Organization for Nuclear Research, CH-1211 Genève 23, Switzerland
e-mail: alexander.gottberg@cern.ch
[2]Paul Scherrer Institut, 5232 Villigen, Switzerland
[3]GANIL, Bd Henri Becquerel, 14076 CAEN Cedex 05, France
[4]INFN-LNL, Viale dell'Università 2, 35020 Legnaro , Italy
[5]TRIUMF, 4004 Wesbrook Mall, Vancouver, BC, Canada
[6]IPN-Orsay, 15 rue Georges Clémenceau, 91406 Orsay Cedex, France

Targets based on uranium and thorium refractory compounds have been at the heart of the isotope mass-separation online (ISOL) technique since its first pioneer experiment in 1951. Such targets brought to high temperatures (>2000°C) produce a wide range of radioisotopes through fragmentation, fission and spallation reaction channels when brought to interaction with a high energy particle beam. At ISOLDE a pulsed proton beam of 1.4 GeV provided by CERN's proton synchrotron booster is acting as a driver for these nuclear reactions [1]. Europe's next-generation facilities currently under construction such as HIE-ISOLDE at CERN, SPIRAL 2 at GANIL in France or SPES in Italy will be operated using this principle.

Different developments took place along the years in the various institutes, and today porous uranium carbides with excess graphite phase are used throughout the different operating facilities. Even though uranium carbide is also commonly used in pin-type nuclear fuel elements and the isotope release properties are expected to be closely related to the material's microstructure [2] only very little is known about the influence of crystallography, morphology and chemistry. Characterisations of the target material before irradiation done or commissioned by CERN reveal coexisting phases of UC_2, UC and C and a large distribution of grain sizes from 3 to 50 µm. Its reduced density of only 3.5 g/cm^3 (13.6 g/cm^3 for bulk UC_2) is a well-established parameter for the release of isotopes [3]. It is also well known that small concentrations of elements that e.g. segregate at interfaces, as they are produced during irradiation or added during the synthesis influence diffusion properties of these matrices considerably [4].

Recent investigations at ISOLDE have proven that submicron and nanostructured porous materials, such as SiC and Y_2O_3, could significantly improve the release and yields of exotic isotopes such as ^{21}Mg or ^{72}Kr [5]. In this way systematic investigations of phase and chemical evolution of uranium carbide materials in the length scale of its crystallographic grains, both before and in particular after pulsed high energy proton irradiation, in combination with methodical variation of surfactants and micro structure, are expected to provide important missing insights for the synthesis of future target materials required for next generation isotope mass separation online facilities. Therefore a campaign for a thorough analysis of uranium carbide based materials has been launched within a large international collaboration in the framework of ActiLab in FP7-ENSAR: Integrating R&D on ISOL UC targets. Towards the approach of more defined materials and within this collaboration, a uranium monocarbide target was tested at ISOLDE in October 2010. This material is made of monophasic UC grains from 3 to 9 µm in diameter and has a density of 12.3 g/cm^3. During these tests the material was found to release alkali and silver isotopes in quantities that did not match the density scaling of x4 between this material and the reference ISOLDE UC_x target, while there were evidences for shorter release times compared to the ones of conventional UC_x material used at ISOLDE [6].

In addition to these online tests at CERN various investigations, such as EXAFS, XFS, and micro XRD using micro-focused synchrotron radiation have already been achieved or are planned on this materials in their pristine and irradiated state.

This contribution will present a number of material studies performed on uranium carbides and reveal the strong impact of their results on exotic radioactive ion beam production in the near future. Furthermore the first x-ray absorption spectroscopy ever performed from this exotic material will be presented.

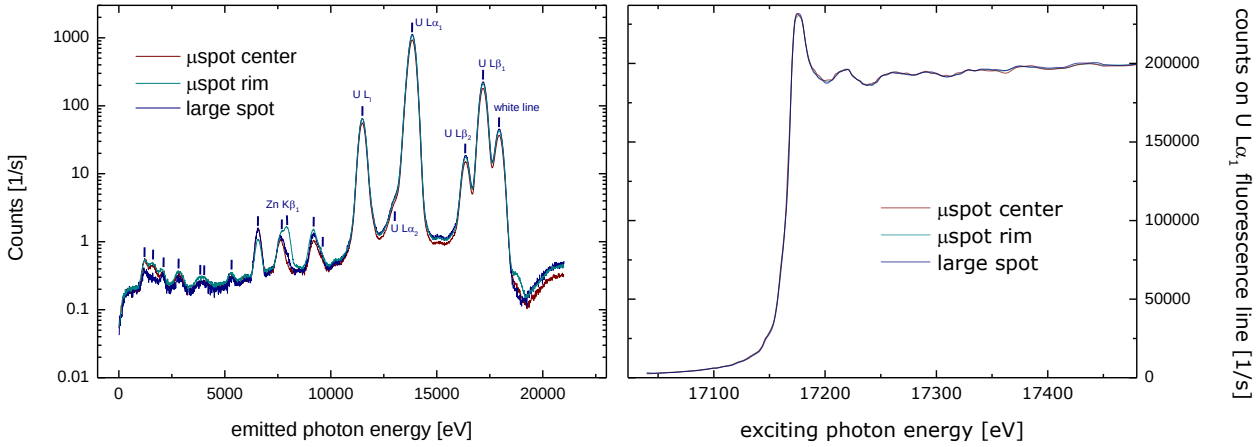

Figure 1: X-ray fluorescence spectra (left) and EXAFS spectra (right) of uranium monocarbide using different focal settings of the synchrotron beam

References

[1] E Kugler, Hyperfine Interactions 129, 23 (2000)
[2] A Krauth et al.; Journal of Nuclear Materials, 45, 163-170 (1972)
[3] L Biasetto et al.; Journal of Nuclear Materials, 404, 68-76 (2010)
[4] J Bennett, in: K Shepard (Ed.), Proceedings of the Eight International Conference on Heavy, Ion Accelerator Technology, Argonne National Laboratory, Chicago, 5 to 9 October 1998, AIP Conference Proceedings, 473, AIP, New York, p. 490 (1999)
[5] S Fernandes, PhD Thesis EPFL (2011) http://cdsweb.cern.ch/record/1312950/
[6] A Gottberg, Online Tests of a High Density UC target at CERN-ISOLDE, ARIS (2011) https://iks32.fys.kuleuven.be/indico/contributionDisplay.py?contribId=204&sessionId=4&confId=0

On the structural distortion of UFeGe

M Henriques[1], L Havela[2], S Mašková[2], T Klimczuk[3], A Rudajevová[2], O Tougait[4], R Vilar[5], A Gonçalves[1]

[1]IST-ITN/CFMC-UL, Estrada Nacional 10, 2863-953 Sacavém, Portugal
e-mail: mish@itn.pt
[2]Dept. Condensed Matter Physics, Charles University, Ke Karlovu 5, 12116 Prague, Czech Republic
[3]European Commission, JRC, ITU, 76125 Karlsruhe, Germany
[4]LCSIM, UMR CNRS 6511, Univ. Rennes 1, France
[5]DEQB, ICEMS, Instituto Superior Técnico, Av. Rovisco Pais, 1049-001 Lisboa, Portugal

The coexistence of ferromagnetism and exotic superconductivity was found in UGe_2, UIr, URhGe and UCoGe. Interestingly, both URhGe and UCoGe crystallise in the orthorhombic TiNiSi-type structure [1, 2], which consists of channelled zig-zag chains of nearest U atoms. UFeGe is a compound belonging to the same family and crystallising in the same structure type, but it undergoes a monoclinic distortion below ≈500 K [3], being a weak paramagnet with no superconducting behaviour. Nevertheless, no studies of the orthorhombic UFeGe have been reported so far. In this work we have investigated the preparation and basic properties of this phase.

The stabilisation of the orthorhombic phase was attempted via substitution into the U sublattice. Samples with general formula $U_{1-x}T_xFeGe$, where *T* stands for Ti, Nb, Mo, Ta, and Zr, were prepared for $x = 0.05$. In the case of zirconium substituted samples, $U_{1-x}Zr_xFeGe$, we tested *x* up to 0.15. It was found for all samples with 5% of any alloying element that the monoclinic phase remains the main phase. The minor phase, when present, was indexed as the new $U_3Fe_4Ge_4$ compound [4] in all the alloys prepared. If Zr content increases to 8%, x-rays patterns taken from the annealed sample showed that the monoclinic and the orthorhombic phases are almost equally present. For a higher Zr content, the orthorhombic TiNiSi structure represents >95 vol% of the sample, with the remaining phase being $U_3Fe_4Ge_4$. First studies on polycrystalline samples of $U_3Fe_4Ge_4$ have showed that it has a ferromagnetic transition around 20 K [4].

Magnetisation measurements showed that magnetic susceptibility of all Zr samples slightly increases with decreasing temperature, reaching 3×10^{-8} m^3/mol for 5% doping, and it decreases with the Zr content (Figure 1). This value and tendency are similar to those reported for pure monoclinic UFeGe, where χ maximum reaches 4×10^{-8} m^3/mol [5]. For samples $U_{0.95}T_{0.05}FeGe$ with *T* = Ti, Nb, Mo and Ta, χ was found to be higher than that for *T* = Zr in all the temperature range.

Specific heat studies revealed that the orthorhombic material UFeGe has the γ-coefficient ≈30 mJ/mol K^2, i.e. about 3 times higher than the monoclinic phase (γ≈12 mJ/mol K^2). From these results, we can suppose that the distortion from the orthorhombic phase to the monoclinic phase might happen due to the tendency to decrease the density of states at the Fermi level. We see a similar effect in many cases in actinides, that the susceptibility does not reflect variations of γ (as in Pu phases). One of the reasons may be that χ is predominantly affected by orbital polarisation effects.

An interesting comparison is provided by the DSC study of samples containing 0 and 5% of Zr. The doping reduces the structural transition temperature to approximately 380 K and the related enthalpy is 25% lower than that of the parent compound (Figure 2).

We can speculate that the tendency to remove high density of states from the Fermi level (so as to reduce the total energy when the magnetic order is not favourable) is the reason for the structure distortion.

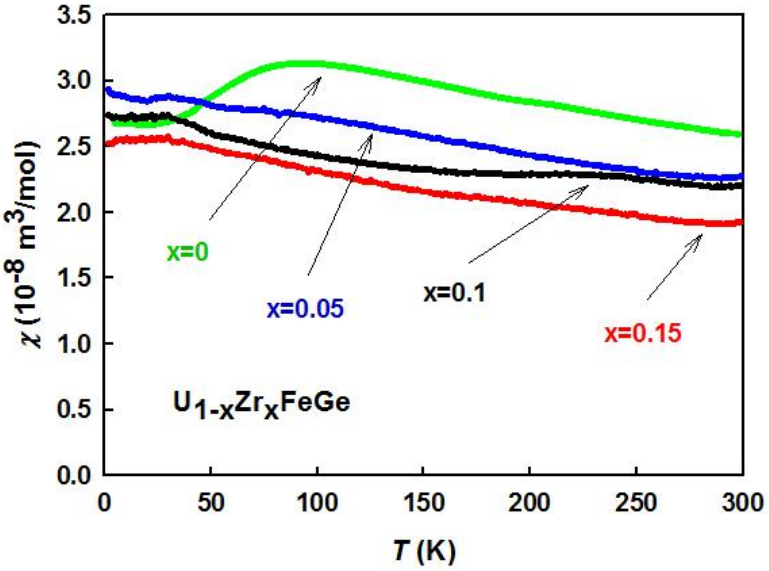

Figure 1. Magnetic susceptibility for various concentrations of zirconium corrected for the ferromagnetic $U_3Fe_4Ge_4$ impurity.

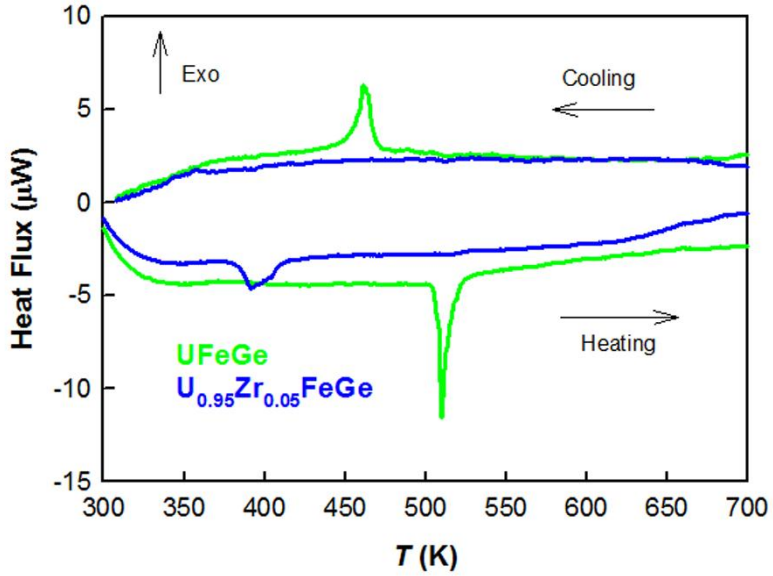

Figure 2. DSC scans for UFeGe pure and doped with 5% of Zr showing the structural transition.

References

[1] D Aoki et al., Nature 413, 613 (2001)
[2] N Huy et al., Phys. Rev. Lett. 99, 067006 (2007)
[3] F Canepa et al., J. Alloys Compd. 234, 225 (1996)
[4] D Bertherbaud et al., manuscript in preparation
[5] L Havela et al., J. Magn. Magn. Mat. 177-181, 47 (1998)

Electrochemical properties of uranium in LiCl-KCl-CsCl eutectic melt

D Maltsev, V Volkovich, D Aleksandrov, E Vladykin, P Likhachyov, I Polovov, B Vasin

Department of Rare Metals and Nanomaterials, Ural Federal University, 19 Mira St., Ekaterinburg, 620002, Russian Federation
e-mail: d.s.maltsev@gmail.com

Understanding chemical and electrochemical behaviour of uranium and fission products in ionic melts is a key factor of developing a feasible technology for non-aqueous pyrochemical reprocessing of spent nuclear fuels. Lowering working temperatures reduces energy consumption and increases the choice of construction materials. Salt mixtures of eutectic compositions can significantly reduce melting points and amongst alkali chlorides the ternary LiCl-KCl-CsCl eutectic offers one of the lowest melting points, around 540 K.

In the present work a variety of stationary and non-stationary electrochemical techniques (potentiometry, chronopotentiometry, cyclic and square wave voltammetry, impedance spectroscopy) were employed to study uranium behaviour in the LiCl-KCl-CsCl eutectic based melts.

Anodic dissolution of uranium metal in chloride melts results in uranium (III) chloro-species formation. These melts were used for determining uranium electrode potentials (with chlorine electrode acting as a reference). After completing anodic dissolution it takes around 15-30 minutes for the potential to reach a stationary value and then the potential remains essentially unchanged for at least two hours. After completing the measurements uranium concentration in the melt was determined from the results of chemical analysis of melt samples rapidly quenched under argon. The formal electrode potential of uranium was measured between 775-979 K, Figure 1, and its temperature dependence is satisfactorily described by the following equation:

$$E^*_{U(III)/U(0)} = -2.892 + 6.54 \cdot 10^{-4} T \text{ (V)} \quad (1)$$

The Gibbs free energy change of the formation of UCl_3 species in the LiCl-KCl-CsCl eutectic was calculated based on the results of the performed experiments. Its temperature dependence is described by the following equation:

$$\Delta G^*_{UCl3} = -837{,}15 + 0{,}189\ T \text{ (kJ/mol)} \quad (2)$$

The Gibbs free energy change of mixing of UCl_3 with the ternary eutectic was found to be -6.6, -7.7 and -11,1 kJ/mol at 979, 875 and 775 K, respectively.

A series of experiments was performed to study the electrochemical behaviour of uranium in LiCl-KCl-CsCl melts using cyclic voltammetry and glassy carbon or tungsten electrodes. An example of measured voltammograms in the region of U(IV)/U(III) recharge is shown in Figure 2. There is only one cathodic and one corresponding anodic peaks. Potentiostatic electrolysis at the cathodic peak potential did not result in the formation of any solid deposit on the electrode surface. Taking into account the shape of the peaks we can conclude that this electrochemical process results in the formation of a soluble product and corresponds to the reversible recharge of U(III) to U(IV) chloro-ions. These peaks are present in the voltammograms measured at the scan rates up to 2 V/sec. At the scan rates below 100 mV/sec the potential of the cathodic peak is around -(1.6-1.7) V and that of the anodic peak is around -(1.35-1.55) V. At low scan rates the cathodic peak current changes linearly with the square root of the polarisation rate showing that the reaction is diffusion controlled. The diffusion coefficients of U(IV) determined at various temperatures from the analysis of cyclic voltammograms are presented in Figure 3.

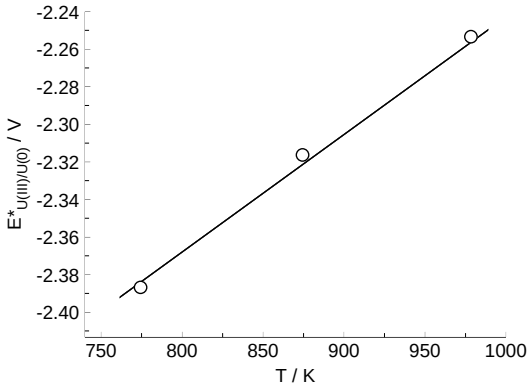

Figure 1. The temperature dependence of uranium formal standard potential $E^*_{U(III)/U(0)}$ in the LiCl-KCl-CsCl eutectic.

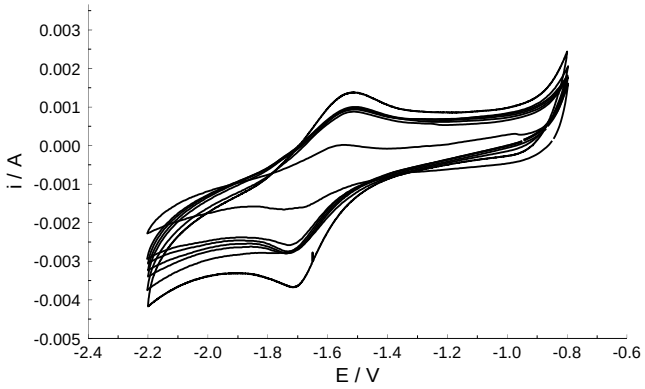

Figure 2. Cyclic voltammograms of uranium(III)/(IV) couple in LiCl-KCl-CsCl melt, 673 K. WE - glassy carbon, RE - Cl^-/Cl_2. [U] = 0.403 wt.%. Scan rate, mV/s: 10, 40, 50, 70, 80, 90 and 100.

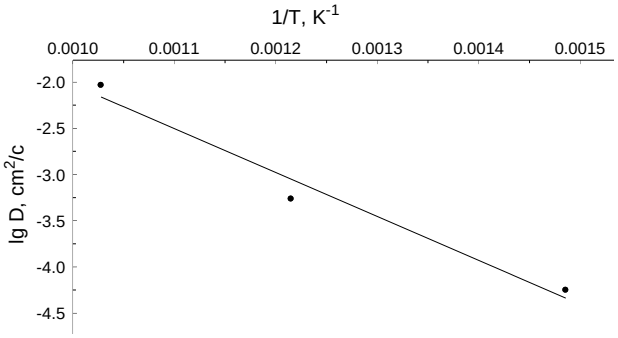

Figure 3. U(IV) chloro ions diffusion coefficients in LiCl-KCl-CsCl eutectic based melts.

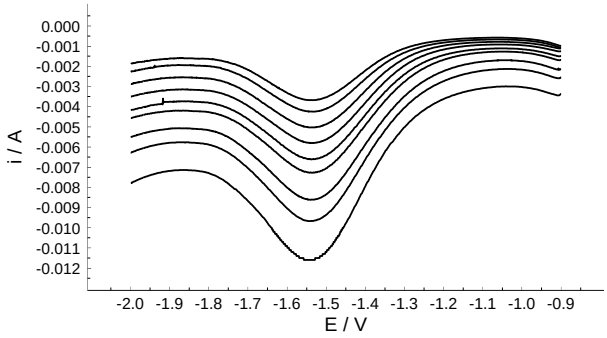

Figure 4. Square wave voltammograms, measured at 823 K in uranium containing LiCl-KCl-CsCl melt. Frequency (top to bottom), Hz: 8, 12, 20, 30, 45, 60, 99, 140, 240. WE - glassy carbon, RE- Cl^-/Cl_2. [U] = 0.403 wt.%.

A special series of experiments was performed using square wave voltammetry, Figure 4. The step of change potential is 20 mV, the frequency of potential sweep variety from 8 to 240 Hz. The voltammograms contain a single peak around -(1.53-1.55) V, associated with U(IV)/U(III) recharge.

Impedance spectroscopy measurements were performed at 673 and 823 K with the spectra recorded between 100 mHz and 10 kHz. The dependencies between the real and imaginary components of complex resistance and conductivity, as well as dependence of module of complex resistance and faze *vs*. frequency of alternative current were obtained.

Solubility of uranium in gallium-indium eutectic alloy

D Maltsev[1], V Volkovich[1], L Yamschikov[1], A Osipenko[2], S Raspopin[1], M Kormilitsyn[2]

[1]Department of Rare Metals and Nanomaterials, Ural Federal University, 19 Mira St., Ekaterinburg, 620002, Russian Federation
e-mail: d.s.maltsev@gmail.com
[2]JSC "State Scientific Center Research Institute of Atomic Reactors", Dimitrovgrad, 433510, Russian Federation

Molten salts and metals exhibit high thermal and radiation stability and are considered as prospective working media for pyrochemical reprocessing of spent nuclear fuels (SNF) as well as realisation of closed nuclear fuel cycle. Having both the salt and the metal in liquid state, especially at relatively low temperatures, allows solving important problem of phase separation in radiochemical technology. Understanding processes occurring in molten salts and liquid metals as well as behaviour of uranium and SNF components is important for designing a feasible process. Low-melting metals can be effectively employed for separating SNF components in a "liquid metal - molten salt" system.

Multicomponent alloys of eutectic compositions can be used to further reduce the operation temperature. However information about the behaviour and thermodynamic properties of SNF components (particular uranium) in three-component liquid metal alloys is virtually absent. In the present work uranium solubility, activity coefficients and activity were determined between 573 and 1073 K in one of the lowest melting point alloys - Ga-In eutectic (m.p. 289 K).

The activity and solubility of uranium in the liquid metal phase were determined using the e.m.f. method by studying the following galvanic cell:

(-) U | chloride melt - UCl_3 | U + Ga-In (+),

where ternary LiCl-KCl-CsCl eutectic (m.p. 536 K) was used as the "chloride melt".

When determining uranium activity and activity coefficients were determined γ-uranium and super cooled liquid uranium were taken for the standard state and the following correction was applied to the experimentally measured electrode potentials:

$$\Delta E = -\left(\frac{R \cdot T}{n \cdot F}\right) \cdot \ln a_0 , \qquad (1)$$

where a_0 is the activity of uranium at the working temperature relative to γ-uranium or super cooled liquid uranium. The value of $\ln a_0$ was calculated from known thermodynamic parameters of uranium phase transformations.

The activity of uranium was determined by measuring e.m.f. of liquid alloys saturated with uranium. The activity coefficients were calculated from e.m.f. measurements of diluted (homogeneous) alloys with known uranium concentration. The solubility of uranium in liquid metal alloys was estimated from the difference between the temperature dependences of the activity and the activity coefficients.

The temperature dependence of e.m.f. of two-phase U-Ga-In alloys is shown in Figure 1. This dependence is nonlinear in the studied temperature range and it has an inflection around 900 K. Similar inflection observed in the temperature dependence of emf in U-Ga system near 920 K was explained by the existence of two modifications of UGa_3 intermetallic compound. The temperature dependence of e.m.f. of U-Ga-In binary-phase alloys between 569-1080K is satisfactorily described by following equations (with γ-U or liquid uranium taken as the standard state):

$$E_{\gamma\text{-}U(Ga\text{-}In)} = -2.87\cdot10^{-10}\cdot T^3 + 5.38\cdot10^{-7}\cdot T^2 - 5.45\cdot10^{-4}\cdot T + 0.653\ (\pm 0.012\ V) \qquad (2)$$

$$E_{l\text{-}U(Ga\text{-}In)} = -3.34\cdot10^{-10}\cdot T^3 + 6.50\cdot10^{-7}\cdot T^2 - 6.54\cdot10^{-4}\cdot T + 0.706\ (\pm 0.012\ V) \qquad (3)$$

The activity of γ-U and super cooled liquid uranium was calculated from measured e.m.f. values, Figure 2. The temperature dependence of the activity of uranium is described by the following equations:

$$\lg a_{\gamma\text{-}U(Ga\text{-}In)} = 1.04\cdot10^{6}\cdot T^{-2} - 1.19\cdot10^{4}\cdot T^{-1} + 5.49\ (\pm0.24) \quad (6)$$

$$\lg a_{l\text{-}U(Ga\text{-}In)} = 1.04\cdot10^{6}\cdot T^{-2} - 1.24\cdot10^{4}\cdot T^{-1} + 5.81\ (\pm0.24) \quad (7)$$

Comparison of uranium activity in Ga-In based alloys obtained in the present work with the literature data on the activity of uranium in binary Ga-U and In-U alloys showed that activity of uranium in Ga-In eutectic based alloys is close to that in alloys with Ga and significantly lower than activity of uranium in alloys with In. Since the literature contains information about uranium activity in liquid Ga and In alloys only at relatively high temperatures it was of interest to measure the activity of uranium in these systems at lower temperatures. The results obtained at 573-1073 K can be described by following equations:

$$\lg a_{\gamma\text{-}U(Ga)} = 1.62\cdot10^{6}\cdot T^{-2} - 1.31\cdot10^{4}\cdot T^{-1} + 5.88\ (\pm0.08) \quad (8)$$

$$\lg a_{\gamma\text{-}U(In)} = 1.03\cdot10^{6}\cdot T^{-2} - 9.64\cdot10^{3}\cdot T^{-1} + 5.78\ (\pm0.23) \quad (9)$$

The closeness of uranium activity in liquid Ga-In-U and Ga-U alloys indicates that the same compound is present in the equilibrium with the liquid phase in binary-phase alloys based on Ga-In eutectic saturated with uranium as in Ga-U system, *i.e.* UGa_3.

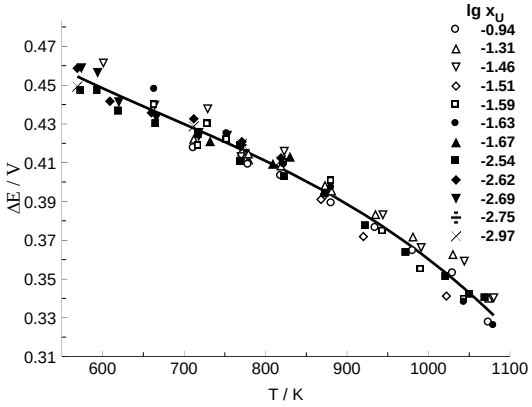

Figure 1. Effect of temperature on e.m.f. of U │ MCl-UCl_3 │ U + Ga-In cell. Uranium concentration (x_U in m.f.) is given for each set of data.

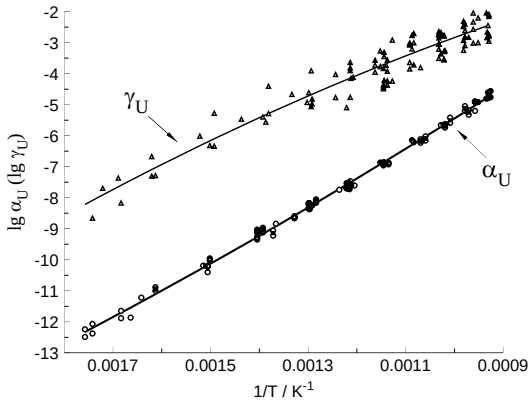

Figure 2. Activity (α_U) and activity coefficients (γ_U) of uranium in Ga-In eutectic alloy. Symbols - experimental points, lines - average values.

The activity coefficients of γ-U and super cooled liquid uranium were determined in Ga-In eutectic based alloys from the results of measurements of e.m.f. of dilute (homogeneous) Ga-In-U alloys. The temperature dependence of the activity coefficients of uranium in Ga-In-U alloys, Figure 2, is nonlinear and between 574-1076 K can be described by the following equations:

$$\lg\gamma_{\gamma\text{-}U(Ga\text{-}In)} = -1.91\cdot10^{6}\cdot T^{-2} - 2.15\cdot10^{3}\cdot T^{-1} + 1.42\ (\pm0.67) \quad (10)$$

$$\lg\gamma_{l\text{-}U(Ga\text{-}In)} = -1.84\cdot10^{6}\cdot T^{-2} - 2.80\cdot10^{3}\cdot T^{-1} + 1.89\ (\pm0.67) \quad (11)$$

Solubility of uranium in Ga-In eutectic was calculated using the obtained temperature dependences of activity and activity coefficients. The dependence of the solubility on temperature is described by the following equation:

$$\lg x_{U(Ga\text{-}In)} = 2.94\cdot10^{6}\cdot T^{-2} - 9.79\cdot10^{3}\cdot T^{-1} + 4.07 \quad (12)$$

Thus, in this work the activity, activity coefficients and solubility of uranium in Ga-In eutectic alloy in temperature range 573-1073K were determined for the first time. It was shown that in binary phase systems saturated with uranium UGa_3 is present in the equilibrium with the liquid phase. Activity of uranium in alloys with gallium or indium was also determined from 573 K.

Mine waters radioactive decontamination using p-hexasulfonated calix[6] arene acid as delivery vehicle in a liquid membrane

I-C Popescu[1], D Humelnicu[2], I Humelnicu[2], M Mateescu[3]

[1]*Laboratory of Environment Protection Techniques and Technologies, R&D National Institute for Metals and Radioactive Resources, B-dul Carol I no.70, sector 2, Bucharest 020917, Romania*
e-mail: ioana.popescu@icpmrr.ro; janepopescu@gmail.com
[2]*"Al.I. Cuza" University of Iasi, The Faculty of Chemistry, Inorganic and Analytical Chemistry Department, Bd. Carol-I No. 11, Iasi 700506, Romania*
[3]*National R& D Institute for Chemistry and Petrochemistry, Splaiul Independenţei nr. 202, Bucharest 060021, Romania*

Radioactive pollution represents a threat for the people's health. Therefore highly effective radioactive decontamination methods are required. Ion exchange, biotechnologies and phytoremediation in constructed wetlands have been used as radioactive decontamination technologies for uranium contaminated soil and water remediation [1, 2, 7]. Recently, beside those classical methods the calix[n]arenic derivatives' utilisation as radioactive decontaminators has jogged attention[3-6].

The present work aims to present the preliminary research results at the uranyl ion transportation using a liquid membrane based on hexasulfonated calix[6] arene acid from a synthetic solution and mine water samples.

The hexasulfonated calix[6] arene acid has been synthesised and provided by the research team from National R&D Institute for Petrol and Chemistry Bucharest Romania.

The liquid membrane was prepared using 0.1404 g of hexasulfonated calix[6]arene acid added to about 0.5 ml of methyl-tri-n-octyl ammonium chloride (MERCK) in up to 500 ml chloroform (MERCK); 0.4 g of sodium hydroxide (MERCK) was added in order to stabilise the liquid membrane.

The synthetic solution was prepared using as uranium source uranyl acetate, sodium carbonate and sodium bicarbonate mixture, hydrochloric acid and sodium chloride. It contains 10 ppm uranium, 1000 ppm carbonates, 35 ppm chloride and the pH is 8.7. That chemical composition corresponds to a mine water sample. The uranium content was determined using a CECIL CE 1101 photocolourimeter and the wavelength of 670 nm.

A lab set up was built and 2N sulphuric acid solution was used as receiving phase.

Figure 1 illustrates the phases in contact.

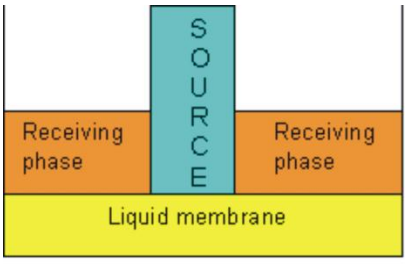

Figure 1. Diagram of phases in contact.

Uranyl ion's separation efficiency using the liquid membrane was of 90% in the synthetic solution case. The uranyl ion transport via the liquid membrane has also been investigated in the case of two different mine water samples C(without organics) and L(with organics) respectively.

In the case of C uranyl transport yield was of 50 %.

As L sample concerns the transport yield has been of 60%.

The increase of transport yield could be explained due to the presence of natural occurring organic matter that contributes to its improvement. A relatively stable complex is formed between hexasulfonated calix[6] arene acid and uranyl.

The preliminary test results pointed out that the uranyl transport yield is highly influenced by the source phase chemical composition.

References

[1] Gh Crutu et.al, 2nd Int. Workshop in Geoenvironmental and Geotechnics (GEOENV 2008) , Milos Island, Greece, Heliotopus Publication ISBN 978-960-6745-01-7, 117-120 (2008)
[2] Al Cecal et al. (1997), Waste Management, 17, (1), 97-99
[3] C Gutsche, “Calixarenes”,The Royal Society of Chemistry. (1989)
[4] H-J Buschmann, et al., Acta Chim. Slov., 47, 55 . (2000)
[5] C Bouvier-Capely et al. J Radioanal. Nucl. Chem., 282, 611-615(2009)
[6] J Vicens, V Böhmer, Calixarenes - A Versatile Class of Macrocyclic Compounds, Topics in Inclusion Science, Kluwer Academic Publishers, Dordrecht, Holland (1991)
[7] C Manea et al. (2008), 2nd Int. Workshop in Geoenvironmental and Geotechnics (GEOENV 2008), Milos Island, Greece, Heliotopus Publication , ISBN 978-960-6745-01-7, 121-124(2008)

The bulk hydriding kinetics of cerium

G Rule[1,2], J Knowles[1]

[1]Atomic Weapons Establishment, Aldermaston, Reading, Berkshire, RG7 4PR, United Kingdom
e-mail: georgia.rule@awe.co.uk
[2]University of Nottingham, Nottinghamshire, NG7 2RD, United Kingdom

The bulk hydriding kinetics of cerium (99.99 %) have been studied within the temperature range 45 °C - 120 °C using ultrahigh purity hydrogen (99.9998 %) at pressures up to and including 1 bar. X-ray diffraction revealed the as polished samples (γ phase) to be coated with a thin oxide over-layer and metallography found the average grain size to be 16 μm (Figure 1) with a Vickers hardness of 24.6 kg/mm^2.

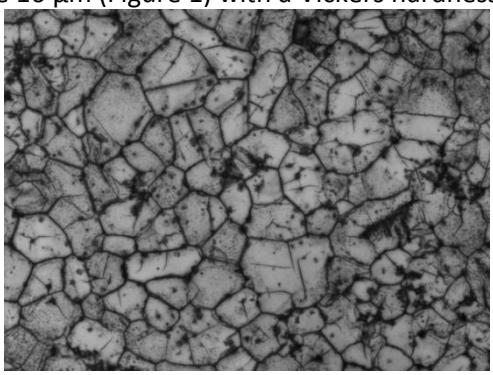

Figure 1. Cerium microstructure (x 50 magnification).

Bulk hydriding rates were calculated from pressure, volume and temperature measurements. To enhance the measurement of bulk hydridng rates, samples underwent a vacuum thermal pre-treatment at 300 °C to activate the samples so that induction periods were not observed.

Arrhenius analysis indicates the apparent activation energy to be 27.3 kJ/mol^{-1} which is in good agreement with the relevant literature. The molar ratios of Ce:H reacted show a clear relationship with the reaction temperature as expected from the thermal stability of the hydride. A square root pressure dependence between 0-1 bar has been established which does not appear to vary with temperature.

Characterisation and recrystallisation of the surface over-layer of gadolinium following beam welding

C Stitt, T Scott

Interface Analysis Centre, University of Bristol, Oldbury House, 121 St. Michaels Hill, Bristol, BS2 8BS, United Kingdom
e-mail: camilla.stitt@bristol.ac.uk

The safe long term containment of radioactive waste is an essential goal for the UK nuclear community. Within the UK radioactive waste inventory, metallic uranium fuel is a key 'reactive' material requiring long term containment. To better understand the long-term behaviour of uranium in both storage and disposal environments, we have been studying gadolinium, an f block element, but a close chemical surrogate to uranium.

The corrosion of gadolinium is a relatively undeveloped area of research, but one that is becoming increasingly important as its availability and applications prosper; particularly in the nuclear industry. Gadolinium has the highest thermal neutron capture cross section that is known (49 000 barns), therefore making it a suitable candidate for neutron shielding material in nuclear power stations, nuclear waste storage, transportation vessels and even protective clothing [1] [2]. For example copper and aluminum gadolinium alloys have been proven to have a high neutron capture cross section, whilst also being stable at high temperatures, resistant to low temperature embrittlement and possessing good working and mechanical properties at a moderately low cost [3]. Many of these processes require the welding of gadolinium as a pure metal or alloy, but the corrosion behaviour is not well understood.

We have developed the first quantitative microstructure study of gadolinium, using electron back scatter diffraction (EBSD), on a series of laser beam welds (see Figure 1.). The aim of the laser beam welding was to apply a localised stress on the metal, to show that areas of high stress encourage preferential corrosion. In a repository environment, this is important because 'stressed' uranium and gadolinium may be a significant source of corrosion and therefore hydrogen production, leading to hydriding of these metals in the repository environment. Characterising corrosion characteristics allows us to contribute towards the comprehension of the mechanisms involved in these processes.

During laser beam welding, the metal is rapidly exposed to high temperatures exceeding 3000°C, causing flash melting. Gadolinium has one polymorphic phase transition; at room temperature, it exists as a hexagonal closed packed α-Gd and above 1235°C it transforms into β-Gd, which has a body centred cubic structure [1]. Using EBSD, we have shown that during laser beam welding, the molten gadolinium is rapidly cooled, sufficient to entrap small volumes of the metal in the β-Gd phase, with the remainder reverting to the lower temperature α-Gd.

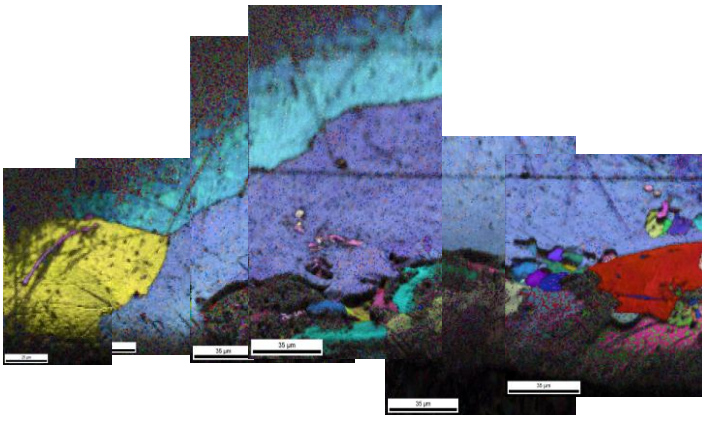

Figure 1. EBSD inverse pole figure map of an electron beam weld in gadolinium.

The corrosion analysis of gadolinium is important for the nuclear industry throughout the fuel cycle. Additionally, using gadolinium provides a means of predicting uranium reactions and demonstrating the feasibility of uranium experiments in a safer environment.

References

[1] CRC. CRC Handbook of Chemistry and Physics, 92nd edition. s.l.: Taylor and Francis Group, (2011-2012)
[2] M Byeong et al., KR857230-B1 (2008)
[3] C Planchamp, EP258177-A (1988)

Preparation of ^{235}U targets by molecular plating

D Vanleeuw, A Moens, R Eykens, G Sibbens

European Commission, Joint Research Centre, Institute for Reference Materials and Measurements (IRMM), Retieseweg 111, B-2440 Geel, Belgium
e-mail: david.vanleeuw@ec.europa.eu

The Institute for Reference Materials and Measurements (IRMM) has a long experience in providing and characterising targets for measurements in nuclear physics. Molecular plating is a high-yielding method for the preparation of thin homogeneous layers. The technique is applied at IRMM for the production of actinide targets for nuclear data experiments [1].

The equipment consists of a custom-made electroplating cell with a platinum anode and a metallic substrate acting as cathode (Figure 1). A stainless steel substrate holder provides the electrical connection between the substrate and the cathode. The applied current produces a migration of the dissolved actinide compounds towards the cathode where the actinide material deposits on the substrate. Besides the current, special attention goes to the shape and rotation of the anode as well as to the type and concentration of the electrolyte.

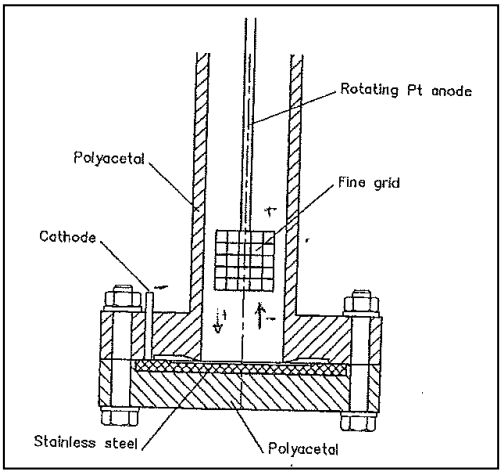

Figure 1 Schematic view of the molecular plating cell

The poster gives an overview of the different steps in the molecular plating process including preparation of the substrates, preparation and testing of the molecular plating cell, dissolution of uranium oxide and preparation of the mother solution, preparation of the organic electrolyte, molecular plating and characterisation of the targets.

As example the preparation of highly enriched ^{235}U layers on thin Al foils is discussed. These targets will be used for measurements of the neutron capture cross section of ^{235}U at CERN in the frame of the n_TOF collaboration. ^{235}U layers with an areal density of 300 µg·cm^{-2} are prepared on fragile Al substrates (Figure 2). These substrates are 30 µm thin Al foils stretched on an Al ring with an outer diameter of 55 mm.

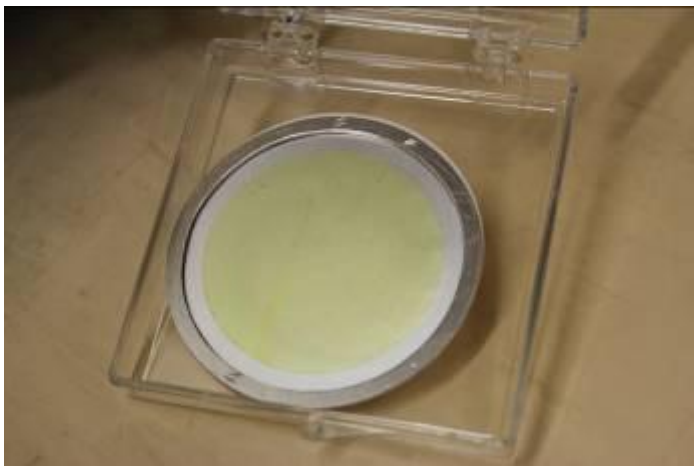

Figure 2. Thin ^{235}U layer prepared by molecular plating on a thin Al foil.

The molecular plating cell is designed and manufactured at IRMM according to the mechanical dimensions of the substrates (Figure 3). Several tests are performed in order to verify the leak tightness of the cell and to establish the different parameters important for the molecular plating, such as the preparation of the organic electrolyte and the applied current density. The process is performed in a glove box dedicated to ^{235}U to avoid cross contamination.

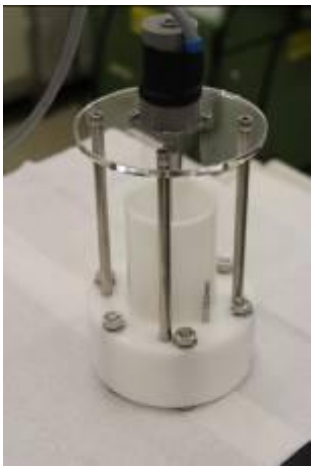

Figure 3. Picture of the molecular plating cell used to prepare thin ^{235}U layers on Al foil.

The areal density of ^{235}U is calculated from the total activity measured by alpha-particle counting at low geometry, the isotopic composition and the diameter of the deposit defined by the thin Al ring mounted on top of the substrate.

References

[1] C Ingelbrecht et al., Nuclear Instruments and Methods in Physics Research A 397 34-38, (1997)

Crystal structure and physical properties of the new $UCu_{7-x}Al_{4+x}$ (x = 0.32) phase

Yu Verbovytskyy[1], E Bauer[2], H Michor[2], A Gonçalves[1]

[1]*Chemistry Department, IST-ITN/CFMC-UL, Estrada Nacional 10, P-2686-953 Sacavém Codex, Portugal*
e-mail: apg@itn.pt
[2]*Institute of Solid State Physics, Vienna University of Technology, A-1040 Wien, Wiedner Hauptstrasse 8-10, Austria*

Uranium-based intermetallic compounds exhibit a great variety of unusual physical phenomena, such as exotic magnetism, spin-glass behaviour, Kondo effects, heavy fermion ground state, superconductivity, etc. These electronic features are mainly related to the degree of hybridisation between the 5*f* and *s*, *p* and *d* orbitals of neighbour ligands. The study of new uranium compounds can lead to a better understanding of such physical phenomena.

The present work is a part of systematic investigation of the phase diagrams, the crystal structure and physical properties characterisation of intermetallic compounds from the uranium, *d*-metal and *p*-metal systems. Herein, we focused our attention on the study of a new ternary uranium intermetallic, $UCu_{7-x}Al_{4+x}$ (x = 0.32), recently discovered by us during the U-Cu-Al phase diagram investigation [1].

Samples with xU:yCu:zAl general composition were prepared from the elements by arc-melting under argon atmosphere. The as-cast ingots were sealed in evacuated quartz tubes and annealed at 600°C for 30 days. X-ray phase and structural analyses were performed using a PANalytical X'Pert Pro diffractometer (Cu Kα-radiation, 2ϑ region 15-100°, step scan 0.03°, counting time per step 15 s). Rietveld refinements were performed using the FullProf program. Electrical resistivity, specific heat and magnetic susceptibility measurements were made below room temperature in order to derive the physical behaviour of this new ternary compound.

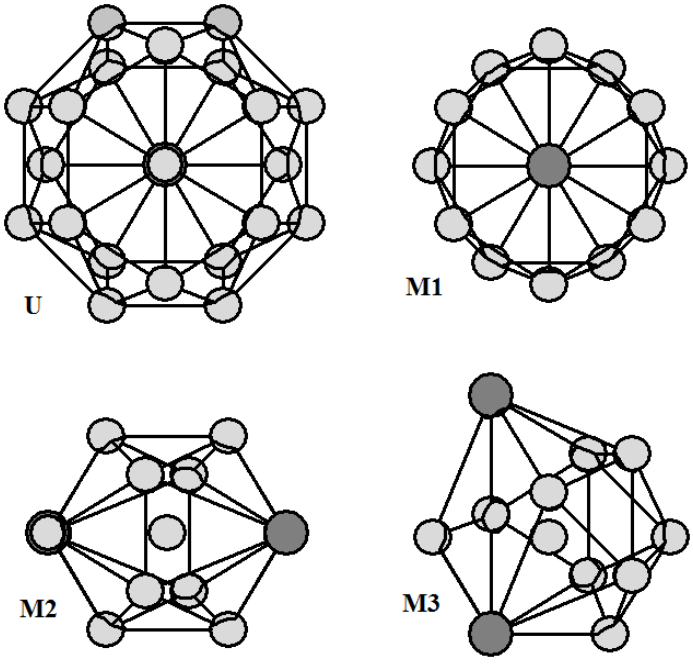

Figure 1. Nearest neighbours of the atoms (U, Cu and Al) in the structure of $UCu_{7-x}Al_{4+x}$.

Alloys from the annealed Cu-rich corner with compositions along the 8.3 at.% U cross-section show a new ternary $UCu_{7-x}Al_{4+x}$ phase, with small homogeneity range. The above mentioned phase belongs to the tetragonal $BaCd_{11}$ structure type (space group *I*4_1*/amd*, Pearson symbol *tI*48, *Z* = 4). Calculated lattice parameters for x = 0.32 are: *a* = 10.2471(4) Å, *c* = 6.5883(3) Å, *V* = 691.78(4) Å^3. Atomic parameters are: U in 4*b* 0 1/4 3/8; M1 in 4*a* 0 3/4 1/8; M2 in 8*c* 0 0 0; M3 in 32*i* 0.2039(2) 0.1277(2) 0.0677(3). Statistical mixtures are: M1 = 0.07Cu + 0.93Al; M2 = 0.86Cu + 0.14Al; M3 = 0.61Cu + 0.39Al. Residual factors are:

R_B = 4.87 %, R_F = 2.68 %. The U atoms are located inside of 22-vertex polyhedra (equatorially capped distorted hexagonal prism). The 14-vertex Frank-Kasper polyhedron is the coordination sphere for the M1 atoms. Nearest neighbours of the M2 and M3 atoms form the deformed icosahedra.

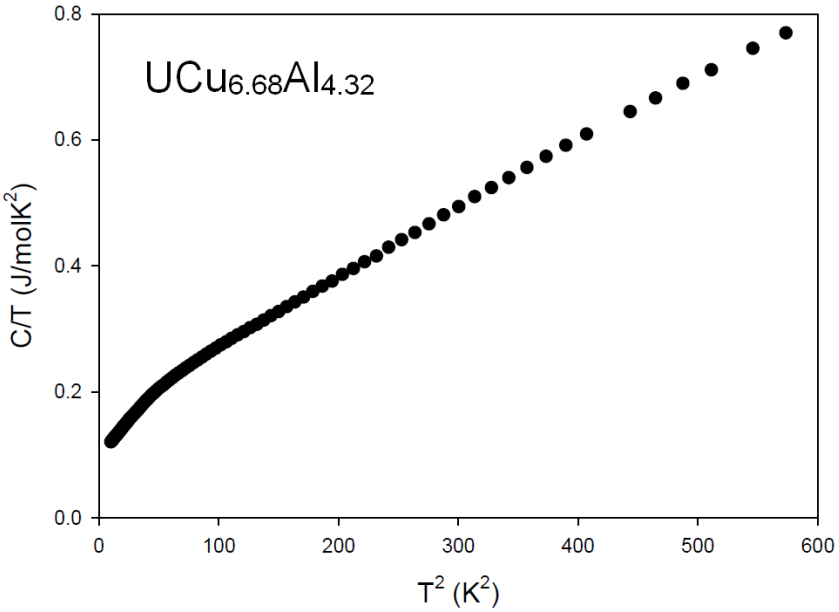

Figure 2. Specific heat *versus* temperature.

The electrical resistivity, specific heat and magnetic susceptibility measured down to about 3 K do not reveal any magnetic phase transition; consequently, the compound in stays in its paramagnetic state. The Sommerfeld value of the specific heat, γ ~ 100 mJ/molK^2, is well above the values derived for simple metallic systems. In the context with the overall shape of the temperature dependent electrical resistivity, spin fluctuations can be concluded, dominating the ground state behaviour in this U based compound, similar to the archetypal system UAl_2 which also displays a linear temperature dependence of the susceptibility at low temperatures [2].

References

[1] Yu Verbovytskyy, A Gonçalves, Workshop on strongly correlated electron and complex systems, ITN, Sacavém, Portugal, 10-11 November, 2011, 30

[2] S Foner et al., Phys. Rev. B **32**, 4768 (1985) and references therein

Investigating the structure of splat-cooled uranium and uranium-molybdenum alloys

A Warren, T Scott

Interface Analysis Centre, University of Bristol, Oldbury House, 121 St. Michaels Hill, Bristol, BS2 8BS, United Kingdom
e-mail: xander.warren@bristol.ac.uk

Splat cooled uranium has been used in a range of studies for around 50 years, coming into focus more recently as a source of 'glassy' or 'amorphous' uranium for super-conductor and electromagnetic experiments. Aside from cursory optical metallographic study in the early 60s [1,2], no detailed or more recent metallurgical characterisation work has ever been conducted.

The range of new techniques which have been developed since the initial study have significantly broadened the possible approaches, and have led to a truly novel study. Perhaps the most significant finding of the study has been the demonstration that using a splat cooling method with cooling rates of the order of 10^6 K/s it has been possible to preserve the high temperature gamma phase at room temperature in pure uranium, something which was hither-to considered impossible. The gamma phase observed using EBSD were both intra-granular micrograins (typically siting along sub-boundaries) and inter-granular micro-grains. This correlates with XRD measurements on the as-formed materials and, given the relative strength of the XRD signal; it is thought that the gamma phase is concentrated towards the outer surfaces of the splats - the zone of most rapid cooling. Unfortunately, the majority of this material was removed during sample preparation using electropolishing that was required to yield a surface of the required quality for electron backscattered diffraction (EBSD) analysis.

As part of the same study, the structure of a range of different uranium-molybdenum alloys (4, 11 and 15 wt%) have been splat cooled under similar conditions to ascertain the γ- phase stabilising effect of the alloying element. The XRD data show that the 4% Mo sample is a mix of α'+γ, with the 11% effectively γ^0 and the 15% the expected pure γ phase. Following characterisation, these samples will be thermally aged to study the spinoidal decomposition which is often associated with uranium shape-memory alloy systems.

References

[1] S Isserow; Early work on rapidly solidified uranium, Journal of Materials Science, 1981,16, 3214-3215
[2] A Kaufmann; Nuclear Metals Inc. (1963); Method and apparatus for making powder, US-3099041

Title Index

A

A comparison between the two novel polar intermetallics $Yb_3Pd_2Sn_2$ and $Eu_3Pd_2Sn_2$ 76
Actinide-ligand multiple bond linkages: Recent progress in uranium carbene and nitride chemistry 35
Atom probe in materials science research 71

B

Bristol-Oxford Nuclear Research Centre 10

C

Characterisation and recrystallisation of the surface over-layer of gadolinium following beam welding 89
Controlled conversion of uranium carbide fission targets using water vapour 18
Corrosion of uranium in mixed environments of water vapour and oxygen 20
Crystal structure and physical properties of RBeGe (R = La-Nd, Th, U) 26
Crystal structure and physical properties of the new $UCu_{7-x}Al_{4+x}$ (x = 0.32) phase 93

D

Development of new generation of radio-luminescence emitters based on durable actinide-doped crystals 46

E

Electrochemical properties of uranium in LiCl-KCl-CsCl eutectic melt 82

F

Focussed ion beams in actinides research 67

I

Investigating the structure of splat-cooled uranium and uranium-molybdenum alloys 95
Investigation of oxide growth and structure on the surface of uranium 21
Isothermal and isochronal ageing behaviour of dilute Al-Sc-AC (AC=Th,U) alloys 73

M

Magnetic and electronic properties of NpCoGe 23
Magnetic properties of epitaxial UO_2 thin films 14
Mikro-kopter, chopper and mini UAV system for monitoring a radioactive dispersion scene in RDD scenario 61
Mine waters radioactive decontamination using p-hexasulfonated calix[6] arene acid as delivery vehicle in a liquid membrane. 86
Modelling of uranium hydride reaction site initiation 17
Mössbauer and SQUID under high pressure in actinides research 69

N

Nanoscale zero-valent iron particles for the remediation of uranium contaminated groundwater 39
New ammonium thorium oxalates 41
New aspects in nuclear forensics 58
Nuclear forensics analytical approaches and simulations 60

Nuclear terrorism: A brief review of threats and responses **63**

O

On the structural distortion of UFeGe **80**

P

Plenary lecture **51**
Polymorphism in salts of tetraalkylammoniumhexanitratothorium **36**
Preparation and characterisation of thin actinide layers **19**
Preparation of ^{235}U targets by molecular plating **91**
Progress in the magnetic study of Np_2Co_{17} **30**
Progress in the magnetic study of Np_2Ni_{17} and $NpNi_5$ **32**

S

Solubility of uranium in gallium-indium eutectic alloy **84**
Sorption preconcentration of radionuclides using detonation nanodiamonds **37**
Stabilisation of cubic γ-phase uranium molybdenum alloys by splat-cooling technique **52**
Strengthening of magnetic interactions in UGa_2 under pressure **28**
Studies on the UFe_3B_2 uranium boride **24**
Superconductivity in the cubic γ-phase uranium molybdenum alloys synthesised by ultrafast cooling **44**
Suppression of magnetic order in $U_2(Ni_{1-x}Fe_x)_2Sn$ **65**

T

The bulk hydriding kinetics of cerium **88**
The corrosion of uranium niobium alloys **75**
The influence of transitional metal in Al-T-Th system on stability of ternary intermetallic phases formed **74**
The study of thermal cycling effect on the stability of a δ-stabilised Pu-Ga alloy **56**
Thermodynamic investigations of the (Th, U)O_2 solid solution **54**
Time-resolved laser induced chemiluminescence spectroscopy and detection of actinides in solutions **48**

U

Uranium carbide material investigations at CERN-ISOLDE and at the Swiss Light Source **78**

V

Variations of actinide magnetism in uranium-base hydrides **12**

X

XMCD in magnetic properties research **68**

Author Index

A

Abraham, F 36, 41
Adamska, A 12
Aleksandrov, D 82
Allen, G 51
Andreev, A 12, 28, 65
Andrighetto, A 78

B

Bao, Z 14
Bauer, E 93
Bazley, S 17
Beeri, O 71, 73
Beneš, O 54
Blanchard, F 41
Borrmann, H 26
Boublil, E 61
Bram, A 73, 74
Bricault, P 78
Buchatskaya, Y 37
Burakov, B 46
Burkhardt, U 26

C

Caciuffo, R 14, 30, 32
Cadogan, J 76
Carvalho, P 24
Catherall, R 18, 78
Coe, C 75
Colineau, E 23, 30, 32
Crane, R 39
Čurlik, I 76

D

Degueldre, C 78
Dias, M 24
Dunand, D 73

E

Eloirdi, R 23, 30, 32
Eykens, R 19, 91

F

Firsin, N 48
Frånberg-Delahaye, H 78

G

Gaczyński, P 23, 30, 32
Ghelman, M 61
Giovannini, M 76
Glascott, J 17, 20, 21, 75
Gonçalves, A 24, 80, 93
Gorshkov, N 48
Gottberg, A 78
Gouder, T 14
Grandjean, S 36, 41
Grin, Yu 26
Griveau, J-C 23, 30, 32
Grolimund, D 78
Gumeniuk, R 26
Günther-Leopold, I 78

H

Hablot, I 41
Halevy, I 30, 32, 58, 60, 61, 63, 68, 69
Hallam, K 18, 20, 21, 39
Harker, N 18, 20
Havela, L 12, 28, 44, 52, 65, 80
Heard, P 18, 20, 21, 67
Hen, A 30, 32, 58, 60, 61, 63, 68, 69
Henriques, M 80
Hone, N 76
Humelnicu, D 86
Humelnicu, I 86

I

Ipatova, J 46
Izosimov, I 48

J

Jones, C 17, 18, 20, 21, 67

K

Kalmykov, S 37
Kim-Ngan, N-T 44, 52
Klimczuk, T 80
Knowles, J 88
Kolomiets, A 28, 65
Konings, R 54
Kormilitsyn, M 84
Kulakova, I 37
Kuznetsova, Y 46

L

Lander, G 14

Langridge, S 14
Lau, C 78
Leithe-Jasper, A 26
Lemoine, P 76
Liddle, S 35
Likhachyov, P 82
Ling, M 56

M

Magnani, N 30, 32
Maltsev, D 82, 84
Mašková, S 44, 52, 65, 80
Mateescu, M 86
Meshi, L 74
Michor, H 93
Mikhalev, V 48
Miliyanchuk, K 65
Moens, A 19, 91
Morrall, P 75

N

Nakotte, H 65
Nekhoroshkov, S 48
Nisbet, G 14

O

Orion, I 30, 32
Osipenko, A 84

P

Pasternak, M 69
Pereira, L 24
Peterson, J 65
Petherbridge, J 17, 20, 21
Petrova, M 46
Polovov, I 82
Popescu, I-C 39, 86
Prchal, J 28

R

Raspopin, S 84
Reiffers, M 76
Renard, C 36
Ridnik, T 61
Rivenet, M 41
Rogalev, A 30
Romanchuk, A 37
Rudajevová, A 80
Rule, G 88
Ryan, D 76

S

Saccone, A 76
Sanchez, J-P 30
Santos, I 24
Schnelle, W 26
Scott, T 17, 18, 20, 21, 39, 44, 52, 67, 75, 89, 95
Seidman, D 73
Shandalov, M 73
Sharon, A 58, 60, 61, 63
Shick, A 23, 30, 32
Shiryaev, A 37
Sibbens, G 19, 91
Skourski, Y 12
Smith, D 10
Soldani, G 36
Solokha, P 76
Springell, R 14
Stitt, C 44, 52, 89
Stora, T 78

T

Tkach, I 44, 52
Tougait, O 24, 80
Tran, V 24
Trifonov, Yu 48

V

Vălu, O 54
Vanleeuw, D 19, 91
Vasin, B 82
Venkert, A 74
Verbovytskyy, Yu 93
Vigier, N 41
Vilar, R 80
Vladykin, E 82
Volkovich, V 82, 84

W

Warren, A 44, 52, 95
Welcomme, E 36
Wilhelm, F 30
Winterrose, M 30, 32

Y

Yaar, I 61
Yamschikov, L 84

Z

Zamoryanskaya, M 46
Zirlin, V 46